Fall 2014

Thermal efficiency and emission analysis of advanced thermodynamic strategies in a multi-cylinder diesel engine utilizing valve-train flexibility

Chuan Ding
Purdue University

Graduate School ETD Form 9
(Revised 01/14)

PURDUE UNIVERSITY
GRADUATE SCHOOL
Thesis/Dissertation Acceptance

This is to certify that the thesis/dissertation prepared

By Chuan Ding

Entitled
Thermal Efficiency and Emission Analysis of Advanced Thermodynamic Strategies in a Multi-cylinder Diesel Engine Utilizing Valve-train Flexibility

For the degree of Doctor of Philosophy

Is approved by the final examining committee:

GREGORY M. SHAVER

JOHN H. LUMKES

PETER H. MECKL

ROBERT P. LUCHT

To the best of my knowledge and as understood by the student in the *Thesis/Dissertation Agreement. Publication Delay, and Certification/Disclaimer (Graduate School Form 32)*, this thesis/dissertation adheres to the provisions of Purdue University's "Policy on Integrity in Research" and the use of copyrighted material.

GREGORY M. SHAVER

Approved by Major Professor(s): _____

_____

Approved by: Ganesh Subbarayan 10/06/2014

Head of the Department Graduate Program Date

THERMAL EFFICIENCY AND EMISSION ANALYSIS OF ADVANCED THERMODYNAMIC STRATEGIES IN A MULTI-CYLINDER DIESEL ENGINE UTILIZING VALVE-TRAIN FLEXIBILITY

A Dissertation

Submitted to the Faculty

of

Purdue University

by

Chuan Ding

In Partial Fulfillment of the

Requirements for the Degree

of

Doctor of Philosophy

December 2014

Purdue University

West Lafayette, Indiana

To my parents and my uncle who have inspired me in academic.

ACKNOWLEDGMENTS

I would like to thank my advisor, Dr. Gregory M. Shaver, for the opportunity to work with him as part of his research team. His passion and enthusiasm for this research has inspired me. I also thank my other committee members, Dr. Peter H. Meckl, Dr. Robert P. Lucht and Dr. John Lumkes as well as project manager Eric A. Holloway for their additional involvement and feedback. This work would not be possible without financial support and technical advise from our industry partner and for that I gratefully acknowledge Cummins Inc. and Eaton Corp.

Good research usually involves cooperation and my work would not be possible without this excellent team of fellow researchers. Deepest thanks to David Fain, Leighton Roberts, Akash Garg, Mark Magee and Aswin Ramesh who have endured with me the challenges and joys of experimental testing.

Special thanks to the Herrick Laboratories administrative staff including Judy Hanks and Donna Cackley for their assistance in this research. Most of all, I am grateful to my family and friends for their love and confidence in me.

TABLE OF CONTENTS

Page

Page

LIST OF TABLES

LIST OF FIGURES

SYMBOLS

$P-V$	Pressure-Volume
V_{ivceff}	Effective Volume at Intake Valve Closure
V_{tdc}	Volume at TDC (clearance volume)
$\eta_{\text{closed cycle}}$	Closed Cycle Efficiency
$\eta_{\text{open cycle}}$	Open Cycle Efficiency
$\eta_{\text{mechanical}}$	Mechanical Efficiency
q	Convective Heat Transfer Rate
h	Convective Heat Transfer Coefficient
$A_{surface}$	Surface Area of the Tube
T_{bed}	Temperature of the Bed of Catalyst
N_{u_D}	Nussel Number
k	Thermal Conductivity
D	Diameter of the Pipe
R_{e_D}	Reynold Number
Pr	Prandtl Number
ρ	Density
v	Mean Fluid Velocity
μ	Dynamic Viscosity
$\dot{m}$	Mass Flow Rate
A	Cross Section Area of the Pipe
Cp	Specific Heat

ABBREVIATIONS

AFR	Air Fuel Ratio
$ATDC$	After Top Dead Center (firing)
BDC	Bottom Dead Center
$BMEP$	Brake Mean Effective Pressure
$BSFC$	Brake Specific Fuel Consumption
$BSNOx$	Brake Specific NOx
BTE	Brake Thermal Efficiency
CAC	Charge Air Cooler
CAD	Crank Angle Degrees
CDA	Cylinder Deactivation
CFD	Computational Fluid Dynamic
DOC	Diesel Oxidation Catalyst
DOE	Design of Experiment
DPF	Diesel Particulate Filter
ECR	Effective Compression Ratio
EGR	Exhaust Gas Recirculation
$EIVC$	Early Intake Valve Closure
EPA	Environmental Protection Agency
EVC	Exhaust Valve Closure
EVO	Exhaust Valve Open
$FHRR$	Fixed Heat Release Rate
$FMEP$	Friction Mean Effective Pressure
$GIMEP$	Gross Indicated Mean Effective Pressure
GCR	Geometric Compression Ratio
HC	Hydrocarbon

$HCCI$	Homogeneous Charge Compression Ignition
$iEGR$	Internal EGR
IVC	Intake Valve Closure
IVO	Intake Valve Open
$kRPM$	Thousand Revolutions per Minute
LFE	Laminar Flow Element
$LIVC$	Late Intake Valve Closure
$LVDT$	Linear Variable Differential Transformers
$NIMEP$	Net Indicated Mean Effective Pressure
NVO	Negative Valve Overlap
NO_x	Nitrogen Oxides
PCP	Peak Cylinder Pressure
$PMEP$	Pumping Mean Effective Pressure
PM	Particulate Matter
RPM	Revolutions per Minute
SCR	Selective Catalytic Reduction
SI	Spark Ignition
SOI	Start of Injection
TDC	Top Dead Center
TIT	Turbine Inlet Temperature
TOT	Turbine Outlet Temperature
TPA	Three Pressure Analysis
UHC	Unburned Hydrocarbon
VCR	Variable Compression Ratio
VGT	Variable Geometry Turbocharger
VVA	Variable Valve Actuation

ABSTRACT

Ding, Chuan Ph.D., Purdue University, December 2014. Thermal Efficiency and Emission Analysis of Advanced Thermodynamic Strategies in a Multi-cylinder Diesel Engine Utilizing Valve-train Flexibility . Major Professor: Dr. Gregory M. Shaver, School of Mechanical Engineering.

Stringent emission regulations and a growing demand for fossil fuel drive the development of new technologies for internal combustion engines. Diesel engines are thermally efficient but require complex aftertreatment systems to reduce tailpipe emissions of unburned hydrocarbons (UHC), particulate matter (PM), and nitrogen oxides (NOx). These challenges require research into advanced thermodynamic strategies to improve thermal efficiency, control emission formation and manage exhaust temperature for downstream aftertreatment. The optimal performance for different on-road conditions is analyzed using a fully flexible valve-train on a modern diesel engine. The experimental investigation focuses on thermal management during idling and high-way cruise conditions. In addition, simulation are used to explore the fuel efficiency of Miller cycling at elevated geometric compression ratios.

Thermal management of diesel engine aftertreatment is a significant challenge, particularly during cold start and extended idle operation. For instance, to be effective, NOx-mitigating selective catalytic reduction (SCR) systems require bed and gas inlet temperatures of at least 200°C, and diesel oxidation catalysts coupled with upstream fuel injection require inlet temperatures of at least 300°C in order to raise diesel particulate filter inlet temperatures to at least 500°C for active regeneration. However, during peak engine efficiency idle operation, the exhaust temperatures only reach 120 and 200°C for unloaded (800 rpm/ 0.26 bar BMEP) and loaded (800 rpm/ 2.5 bar BMEP) idle, respectively, for a typical modern-day diesel engine. For this and other engines like it, late injections or throttling (for instance via an over-closed

variable geometry turbocharger) can be used to increase exhaust temperatures above 200°C (unloaded idle) and 300°C (loaded idle), but result in fuel consumption increases in excess of 100% and 67%, respectively. Fortunately, and as this thesis describes, cylinder deactivation can be used to increase exhaust temperatures above 300°C at the loaded idle condition without increasing fuel consumption. Further, at the unloaded idle condition, the combination of cylinder deactivation and flexible valve actuation on the activated cylinders allows 200°C exhaust temperatures without a fuel consumption penalty. At both operating conditions the primary benefits are realized by reducing the airflow through the engine, directly resulting in higher exhaust temperatures; and as good, or better, open cycle efficiencies compared with conventional 6 cylinder operation. In all cases, comparisons are made with strict limits on engine out NOx, unburned hydrocarbons, and particulate matter emissions.

Internal exhaust gas recirculation (iEGR), late intake valve closure (LIVC) and cylinder deactivation (CDA) were experimentally investigated as methods for fuel economy and thermal management at 1200 RPM and 7.58 bar brake mean effective pressure (BMEP), which corresponds to the highway cruise condition for over the road trucks. These strategies were compared with conventional operation on the basis of optimized fuel consumption, exhaust temperature, and exhaust power at three NOx targets. Physical constraints and emission limits were set to ensure realistic engine operation and emission regulations. The results show that conventional valve profiles lead to the best fuel economy, but iEGR, LIVC and CDA increase achievable exhaust temperature by 57-216 °C. iEGR increases exhaust temperatures by eliminating the heat rejection that occurs when using external EGR. Both LIVC and CDA increase combustion temperature by reducing the air to fuel ratio.

Advanced thermodynamic strategies such as the Miller cycle and Atkinson cycles have been realized on production spark ignition engine through variable valve timing. However, fewer efforts have been directed to compression ignition engines. Increases in geometric compression ratio typically lead to increased thermal efficiency, but the application is constrained by physical limits including peak cylinder pressure and tur-

bine inlet temperature. An experimentally validated model was used to obtain the trade-off between fuel economy and NOx emissions in order to thoroughly investigate Miller cycling at elevated geometric compression ratio. The results demonstrate the expected improvement in thermal efficiency, however, as expected, the maximum in-cylinder pressure and temperature violate the physical constraints at elevated power conditions. These challenges can be addressed through the use of Miller cycling via a reduced effective compression ratio through the modulation of intake valve closure. Miller cycling enables the engine operation with elevated geometric compression ratio at maximum power condition and further improves fuel economy by advancing combustion. The results present a 5% fuel economy improvement at operating conditions without EGR and equivalent fuel consumption when EGR is incorporated. Brake thermal efficiency (BTE) is improved by 0.1%-2% using Miller cycle at elevated GCR. Although EGR was able to achieve very low NOx emissions, fuel economy was sacrificed at medium load condition. Moreover peak cylinder pressure (PCP) and turbine inlet temperature (TIT) exceeded the upper limits at maximum power condition using EGR with elevated geometric compression ratio.

1. INTRODUCTION

1.1 Motivation

Stringent emission regulations and a growing demand for fossil fuel drive the development of new technologies for internal combustion engines. Diesel engines are thermally efficient but require complex aftertreatment systems to reduce engine-out emissions including unburned hydrocarbons (UHC), particulate matter (PM), and nitrogen oxides (NOx). Strategies such as diesel oxidation catalysts (DOC) for UHC, diesel particulate filters (DPF) for PM, and selective catalytic reduction (SCR) for NOx have been developed and implemented to convert harmful emissions to innocuous species [1]. The efficiencies of these aftertreatment systems are heavily temperature dependent and generally require temperatures between 250 °C and 450 °C to provide required performance. Moreover, periodic passive DPF regenerations require temperature in excess of 500 °C [2]. Therefore it is critical to manage the temperature and power of exhaust gases and to do so in a fuel efficient way [3, 4].

Current regulations for heavy duty diesel engines after 2010 require BS (Brake specific) NOx $\leq$ 0.2 g/hp-hr, UHC $\leq$ 1.3 g/hp-hr, idle CO $\leq$ 0.5 % of exhaust flow and PM $\leq$ 0.01 g/hp-hr by Environmental Protection Agency (EPA). In 2014 new regulations for the green house gas decrease the CO_2 limit below 502 g/hp-hr [5]. The strict emission regulations necessitate the investigation for new technologies which continuously make diesel engine efficient and clean. The following section introduces several strategies to improve engine performance and emission reduction.

1.2 Internal Exhaust Gas Recirculation

Exhaust gas recirculation (EGR) systems are widely used to reduce NOx emissions in diesel engines. When burned gases are recirculated into the intake manifold, the

primarily inert species of exhaust gases serve to displace excess oxygen, decreasing flame temperatures and NOx production. However, EGR requires a pressure differential between the exhaust manifold and intake manifold which can result in pumping penalty losses and reduced engine efficiency [6]. In addition, heat rejected from the EGR loop decreases turbine out temperatures [7].

An alternative to external EGR is internal EGR (iEGR), which can be achieved by trapping or re-inducting burned gases via off-nominal valve events. These methods do not require, or allow, an external cooling system. Compared with external EGR, iEGR usually results in higher exhaust temperatures which could be beneficial in thermal management of aftertreatment systems. Fessler et al. investigated iEGR during engine warm-up and concluded that iEGR can globally reduce emissions and quickly increase the temperature dependent efficiency of aftertreatment system [7]. Trajkovic et al. explored iEGR via negative valve overlap (NVO) and utilized it to stabilize combustion and reduce hydrocarbon (HC) and CO emissions [8–11]. In addition, iEGR was widely used in the research of Homogeneous charge compression ignition (HCCI) for high efficient combustion and emission reduction on gasoline engine [12–14].

iEGR can be realized by opening the intake valves during a portion of the exhaust stroke (per Fig. 1.1), exhaust re-induction by opening the exhaust valve during a intake stroke [15, 16] (per Fig. 1.2) and NVO [8, 17, 18] (per Fig. 1.3). NVO and exhaust re-induction were used to introduce iEGR for NOx control at idle and cruise conditions in Chapters 3 and 4.

1.3 Cylinder Deactivation

Cylinder deactivation (CDA) is a method to increase exhaust temperatures by reducing the air-fuel ratio (AFR), and in some cases can also result in improved brake thermal efficiency (BTE). An lean-burn engine operating with deactivated cylinders must inject more fuel per activated cylinder relative to an engine operating at the

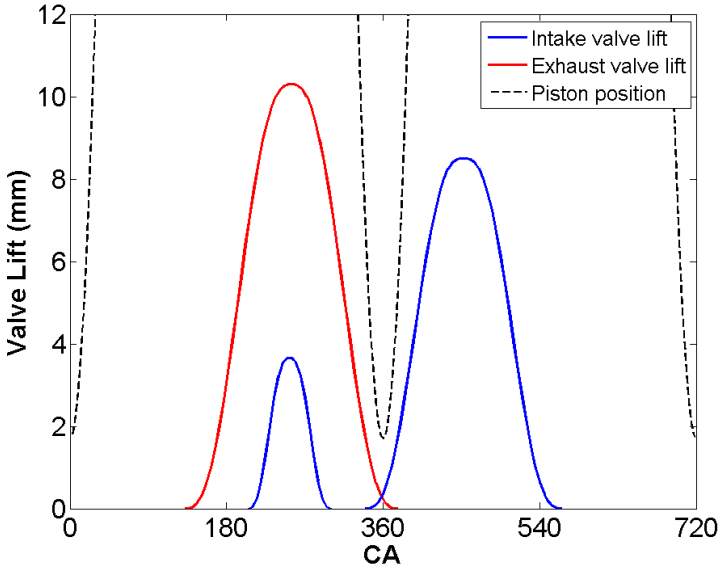

Figure 1.1. Valve profiles with re-induction (IV reopen).

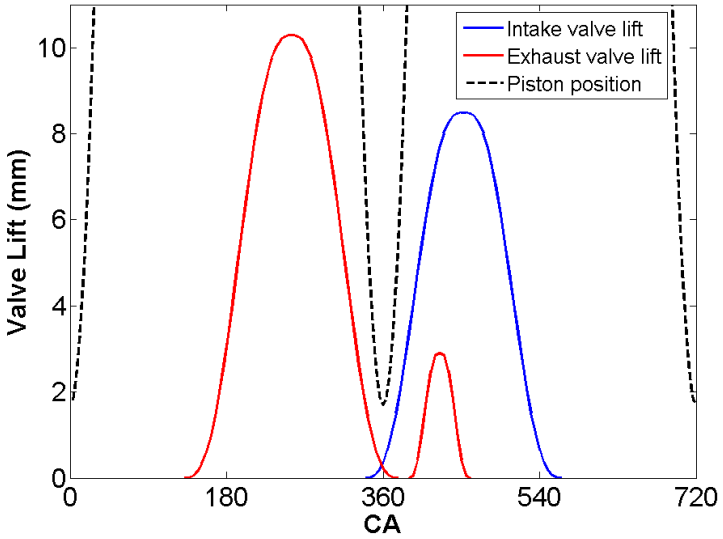

Figure 1.2. Valve profiles with re-induction (EV reopen).

same load with all cylinders activated. The displaced volume is reduced by half when half of the cylinders are deactivated, resulting in a reduction in the AFR. Cylinder

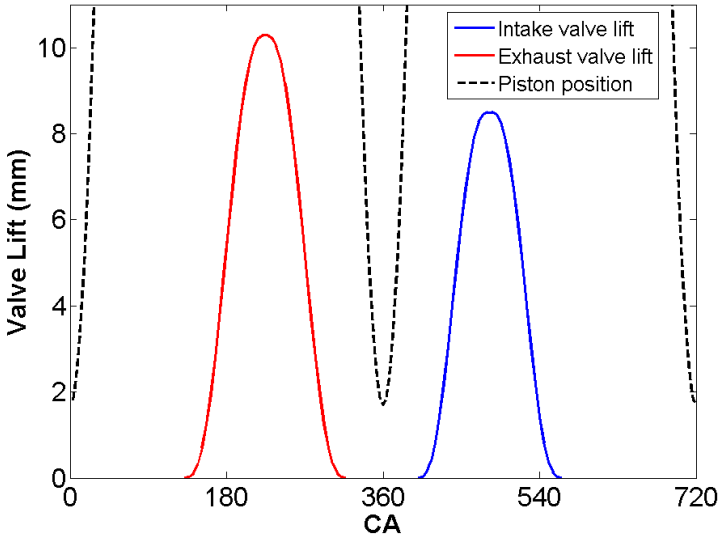

Figure 1.3. Valve profiles with negative valve overlap.

deactivation has been studied as a method for efficiency improvement in spark ignited (SI) engines and is implemented in several production vehicles equipped with SI engines. In SI engines, CDA reduces the amount of throttling required at low loads to stay at stoichiometric conditions, enabling a reduction in pumping penalty [19]. However, few studies have been conducted regarding the use of CDA in diesel engines [20] as a method for improving fuel economy or aftertreatment thermal management.

The analytical study of light-duty diesel engine conducted by K. Edwards et al. [21] simulated cylinder deactivation in a GM 1.9-L four-cylinder, light duty diesel engine in GT-Power. Only one cylinder was deactivated and the intake valves remained open throughout the cycle while the exhaust valves remained closed. The exhaust temperature increased by only 15°C while brake specific fuel consumption (BSFC) increased by 14 g/kw-hr. The increase in fuel consumption was attributed to increased heat transfer and residual friction losses in the deactivated cylinder.

Foster et al. [22] simulated CDA using a model of a 6 cylinder compression ignition engine equipped with a turbocharger operating at 1800 rpm and a brake mean effective

pressure (BMEP) of 9 bar. The results showed that deactivating three of the six cylinders increased exhaust gas temperatures at the exit of the turbocharger by 320°C. The authors concluded that these increased temperatures could be used to improve NOx absorption, NOx reduction, diesel particulate trap purging, and desulfation of the NOx absorber.

1.4 Miller Cycle

The Miller Cycle is a thermodynamic cycles patented by Ralph Miller in 1957. More research focused on the application of Miller Cycling on a spark ignition engine equipped with supercharger of turbo-charging [23–26] and showed efficiency improvement. Relevant research has extended to compression ignition engine recently.

Miller Cycling utilizes late or early intake valve closure (IVC) to reduce the amount of piston motion induced compression resulting in a lower effective compression ratio (ECR). Fig. 1.7 and 1.5 show late IVC (LIVC) and early IVC (EIVC) strategies to achieve Miller Cycling. These valve profiles also reduce the volumetric efficiency of the engine, increasing exhaust temperatures due to the reduction in airflow. Gehrke et al. showed that LIVC enabled exhaust temperature increase at a relatively low fuel consumption on a single cylinder heavy-duty engine [27]. Murata et al. demonstrated elevated exhaust gas temperature with reduced flow rate via LIVC on a single cylinder light-duty engine [28].

Previous research explored LIVC on diesel engines in 1-D and 3-D simulations. Deng and Stobart investigated BSFC benefit in simulation and reported 2% to 6% BSFC benefit with LIVC on a Caterpillar C6.6 heavy duty diesel engine [29].

Besides fuel economy, LIVC reduces NOx via reduced in-cylinder pressure and temperature by lower piston-motion induced compression [30, 31]. Bo and Philip analyzed fuel economy and NOx emission of a diesel engine in simulation and found 24% NOx reduction and 1% fuel economy benefit from LIVC with variable geometry turbocharger (VGT) [32]. Munnannur et al. used KIVA-3V to optimize a heavy duty

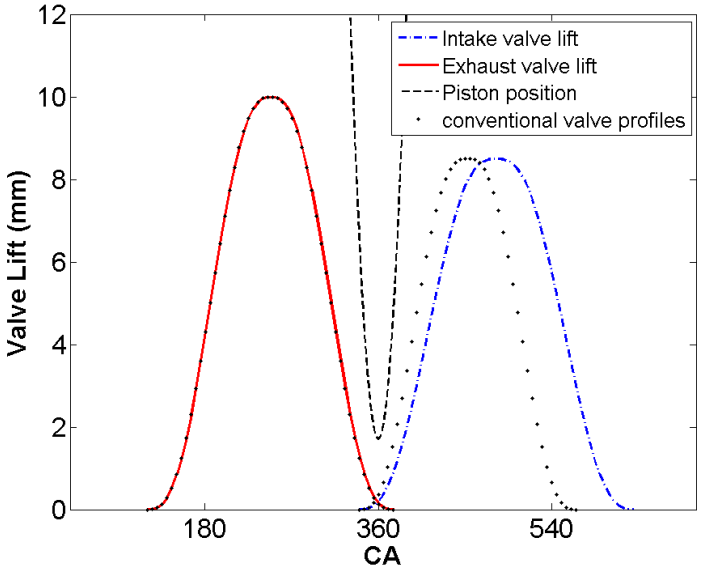

Figure 1.4. Valve profiles with late intake valve closure.

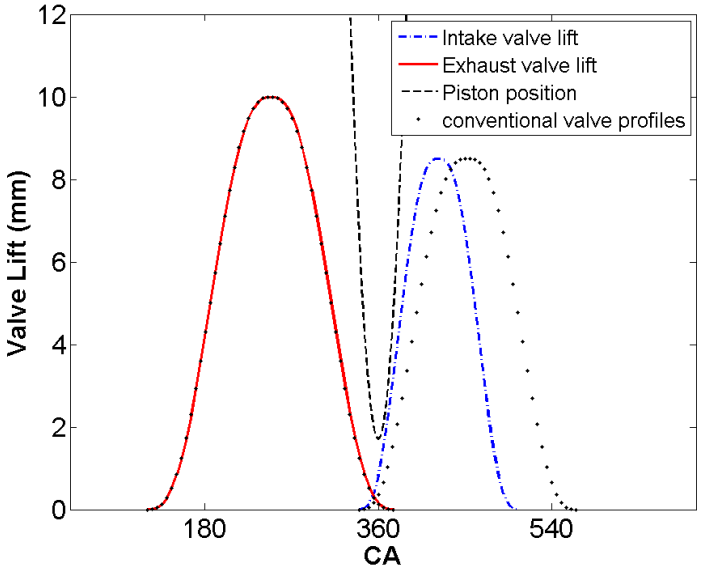

Figure 1.5. Valve profiles with early intake valve closure.

diesel engine and demonstrated a 82% reduction in NOx and HC, 48% reduction of soot and 7.4% better fuel efficiency with LIVC [33]. Murata et al. showed that LIVC coupled with EGR and supercharging reduced NOx and smoke emissions, but with penalties on CO and HC in computational fluid dynamics (CFD) simulations [34] [28]. Su et al. showed the concept of low temperature combustion with LIVC and controlled NOx and PM emissions with less usage of EGR using CFD model [35]. Fessler and Genova experimentally demonstrated 6% BSFC improvement on a 3.0L diesel engine with EIVC [7]. He et al. presented that a single cylinder engine with LIVC satisfied Tier 2 Bin 5 regulation without aftertreatment systems [36]. Gurney et al. tested LIVC on a 2.0L diesel engine and showed soot reduction at low speed and load conditions [37].

Compared with simulation based efforts, experimental investigations of LIVC have just begun. In general, previous efforts have focused on fuel economy and raw emission reduction but not thermal management of aftertreatment systems. Moreover, the previous experimental efforts were limited to small displacement multi-cylinder diesel engines (2 to 3 liters) or single cylinder engines.

1.5 Elevated Geometric Compression Ratio

Geometric compression ratio (GCR) is one of the key factors of combustion efficiency and is usually fixed when engine is produced. Elevated GCR increases the combustion efficiency with longer expansion ratio reducing the fuel consumption [26, 38]. However the elevated GCRs increases the pressures and temperatures at the end of the compression stroke resulting in auto-ignition on spark ignition engines. Previous research used the variable compression ratio (VCR) technique to improve efficiency without causing auto-ignition on gasoline engines [39]. One way to vary the compression ratio is using additional mechanism [40, 41], such as adjustable stroke length [42]. Another way to realize VCR is adjusting the amount of charged air by valve motions on an elevated GCR engine [16, 43]. Akihisa et al. varied the effective compression

ratio using EIVC on an elevated GCR (24.8) engine. It resulted in a 5.3% improvement in thermal efficiency on a 4 cylinder SI engine [44]. In addition the production gasoline engine on Pruis produced by Toyota has applied the VCR technique, which is 12 % to 14 % more efficient than normal Otto cycle engine.

In comparison, research on diesel engines have not been thoroughly investigated due to the concern over physical constraints such as in-cylinder peak pressure and temperature. Miller cycling is investigated to enable elevated GCR on a diesel engine within physical constraints at high load conditions and improve thermal efficiency at medium load under simulation environment in Chapter 5.

1.6 Variable Valve Lift and Open Timing

Variable valve profiles provide flexibility in AFR control which is beneficial in thermal management. The reduction in AFR are consistent with higher exhaust temperature because of aggressive combustion. One of the AFR control strategies is reduced intake valve lift (Fig. 1.6). The intake valve lift is largely reduced to throttle the engine resulting in lower AFR.

Another strategy of AFR control is "over shutting" the variable geometry turbocharger (VGT) which results in an increase in the pumping penalty as a result of increased exhaust manifold pressure. Higher pumping penalties increase the required fueling to maintain the same torque decreasing the AFR. Similarly, delayed exhaust valve open (EVO) and reduced valve lift (Fig. 1.7) throttle the exhaust process increasing the pumping penalties, which result in lower AFR.

1.7 Contributions

The work presented here seeks to understand thermal efficiency and thermal management benefit of valve-train flexibility including iEGR, CDA and Miller cycling on a multi-cylinder diesel engine. Contributions include:

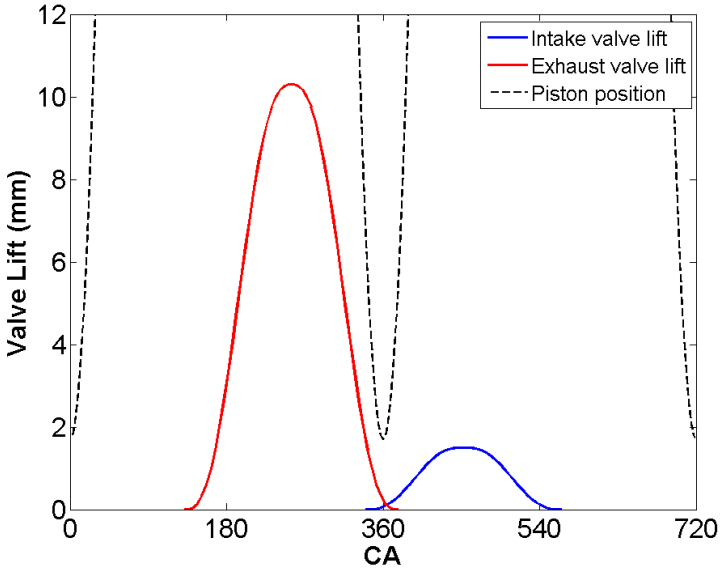

Figure 1.6. Valve profiles with reduced intake valve lift.

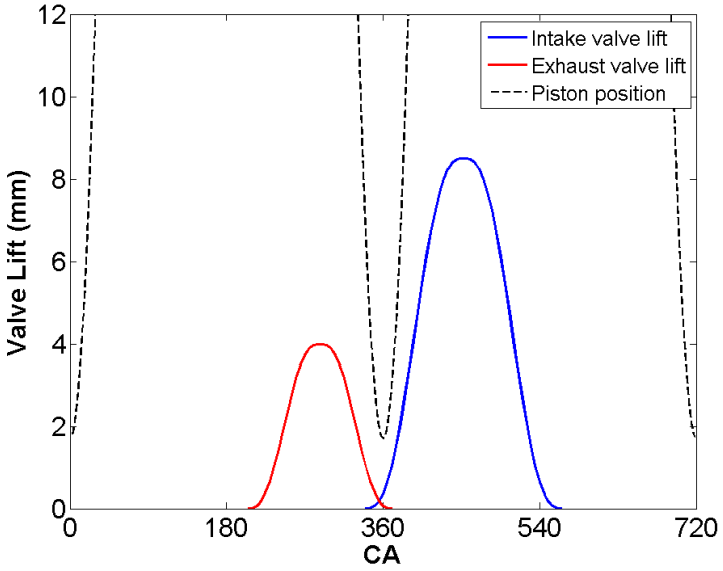

Figure 1.7. Valve profiles with small exhaust valve profile.

1.7.1 Model Calibration and Variable Valve Actuation (VVA) Function Implementation

A GT-power engine model was carefully calibrated to predict the gas exchange and combustion processes with support from Mark Magee, Leighton Roberts and Akash Garg. It provided a simulation platform to explore the impact of valve motion, optimal gas exchange process and different strategies to improve efficiency and emission control. A valve control algorithm was implemented to realize exhaust re-induction using a dSPACE system with support from David Fain.

1.7.2 Thermal Management Analysis using CDA and VVA Functions at Idle Conditions

CDA and flexible valve profiles were investigated to enables engine operating with elevated turbine outlet temperature (TOT) at unloaded and loaded idle conditions. During peak engine efficiency idle operation, the exhaust temperatures only reach 120 and 200°C for unloaded (800 rpm/ 0.26 bar BMEP) and loaded (800 rpm/ 2.5 bar BMEP) conditions, respectively, for a typical modern-day diesel engine. For this and other engines like it, late injections or throttling (for instance via an over-closed variable geometry turbocharger) can be used to increase exhaust temperatures above 200°C (unloaded idle) and 300°C (loaded idle), but result in fuel consumption increases in excess of 100% and 67%, respectively. Fortunately, and as this paper describes, cylinder deactivation can be used to increase exhaust temperatures above 300°C at the loaded idle condition without increasing fuel consumption. Further, at the unloaded idle condition, the combination of cylinder deactivation and flexible valve actuation on the activated cylinders allows 200°C exhaust temperatures without fuel consumption penalty. At both operating conditions the primary benefits are realized by reducing the airflow through the engine, directly resulting in higher exhaust temperatures; and as good, or better, open cycle efficiencies compared to conventional 6 cylinder operation. The increased exhaust temperatures offset exhaust flow

reductions, resulting in higher exhaust gas-to-catalyst heat transfer rates, resulting in superior aftertreatment warm-up performance with CDA in comparison to no-CDA operation. In all cases, comparisons are made with strict limits on engine-out emissions.

1.7.3 Fuel Economy and Thermal Management Analysis using CDA and VVA Functions at Cruise Condition

The cruise condition is critical for fuel economy and thermal management. iEGR, LIVC and CDA were experimentally investigated as methods for aftertreatment thermal management and fuel economy improvement. Optimization-targeted fuel economy, TOT results at three selected NOx levels were determined using a calibrated model. The analysis shows that iEGR, LIVC and CDA bring no benefit in engine-specific fuel economy over conventional valve profiles at 1.5, 3 and 4 g/hp-h BSNOx levels. The valve profiles of iEGR and LIVC are optimized back to conventional valve profiles and fuel economy is worse with CDA due to higher heat losses and delayed combustion. This result is not surprising as efficiency maximized at "highway cruise" conditions is a primary focus of conventional engine design. Conventional operation increases TOT from 350°C to 450°C with delayed SOI resulting in a 23% increase of fuel consumption. iEGR via re-induction or NVO reduces the fuel consumption by 10% at same TOT due to lower total heat losses and AFR. LIVC increase TOT up to 550°C with 5% less fuel used compared with conventional valve profiles at 450°C. CDA further maximizes TOT above 550°C with additional 3% fuel used due to lower AFR. iEGR via re-induction and NVO will warm-up the catalysts more quickly, and can sustain bed temperatures of $\sim$450°C, whereas the baseline case will cool down the catalysts when above $\sim$350°C. LIVC and CDA promote a better heat transfer rate at bed temperature above 150°C for 1.5 g/hp-hr BSNOx compared with the highest heat transfer rate with conventional valve profiles using delayed SOI. Both LIVC and

CDA can keep catalyst bed temperature of ∼550°C and LIVC has relatively lower fuel cost.

1.7.4 Simulation Investigation of Miller Cycling with Elevated GCR

Elevated GCR increases thermal efficiency with higher in-cylinder pressure, however, the application is constrained by physical limits including peak cylinder pressure (PCP) and turbine inlet temperature (TIT). Simulation investigations were conducted to enable engine operating at elevated GCR with Miller cycling using GT-power. The investigation incorporated constrained optimization considering the physical limit of engine operation as well as emission control. Trade-offs between fuel economy and NOx emission were analyzed at five operating conditions. Miller cycling reduces piston-motion induced compression which allows advanced combustion to improve thermal efficiency. Elevated GCR generates more power and increases brake thermal efficiency due to longer expansion and higher closed cycle efficiency. Miller cycling enables engine operating at rated condition (maximum power) without physical constraints violated although the solutions are limited. It also allows the usage of elevated GCR at low-moderate loads for efficiency improvement. EIVC with GCR of 23 reduces fuel consumption by 0.7%∼5% corresponding to 0.1%∼2% increase of BTE at medium speed and low-moderate load conditions.

1.8 Thesis Outline

The previous section outlines the author's primary contributions to the research groups' overall goal of investigating fuel economy and emission reduction in a modern diesel engine. The following chapters detail the efforts in which the author is the lead investigator.

Chapter 2: METHODOLOGY details the methods in model based optimization, 1-D engine simulation and experimental work. This preparation work provides

a foundation for future analytical and experimental work of optimized engine performance with flexible valve profiles.

Chapter 3: FUEL EFFICIENT EXHAUST THERMAL MANAGEMENT AT IDLE details the potential strategies to increase exhaust temperature with valve train flexibility at 800 RPM 0.26 bar and 2.5 bar BMEP conditions.

Chapter 4: FUEL ECONOMY AND THERMAL MANAGEMENT AT HIGH WAY CRUISE CONDITION details the analysis of optimized results using analytical model as well as experimental validation with valve train flexibility at 1200 RPM 7.58 bar BMEP condition.

Chapter 5: SIMULATION EXPLORATION OF MILLER CYCLE WITH ELEVATED GCR details the analysis of optimized results from analytical models for miller cycling with elevated GCR. Five operating conditions have been analyzed including the maximum power condition.

Chapter 6: SUMMARY AND FUTURE WORK revisits conclusions from the previous chapters and presents possibilities for future work.

2. METHODOLOGY

2.1 BSFC vs BSNOx Trade-off

BSFC is used to evaluate fuel consumption per unit brake power as shown in Eq. (2.1).

$$\text{Brake Specific Fuel Consumption} = \frac{\text{Engine Fuel Rate}}{\text{Brake Power}}. \tag{2.1}$$

BSNOx presents the NOx emission per unit brake power as shown in Eq. (2.2).

$$\text{Brake Specific NOx} = \frac{\text{NOx production}}{\text{Brake Power}}. \tag{2.2}$$

Fuel consumption and NOx usually cannot be optimized at the same time [7, 32, 45]. An example trade-off curve between BSFC and BSNOx is shown in Fig. 2.1. BSFC increases when the NOx constraint is low and decreases when NOx emission is high.

2.2 TOT vs BSFC Trade-off and Thermal Management

Thermal management is another key issue to be addressed in advanced powertrains. Besides normal fuel injection into the cylinders, extra fuel can be dosed ahead of the DOC and DPF to increase exhaust temperature to improve emission conversion efficiencies [46]. It is beneficial to improve the exhaust temperature at a specific fuel consumption, which reduces the fuel or urea usage in the aftertreatment system. An example of a TOT/BSFC trade-off is shown in Fig. 2.2. The increases of TOT usually require more fuel energy resulting in less fuel efficient operation.

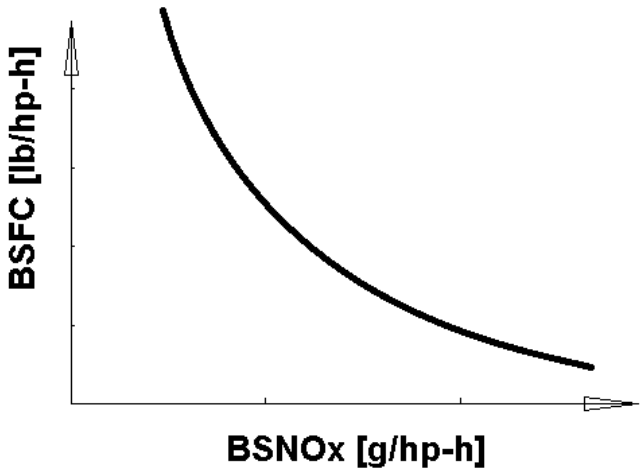

Figure 2.1. BSFC vs BSNOx trade-off.

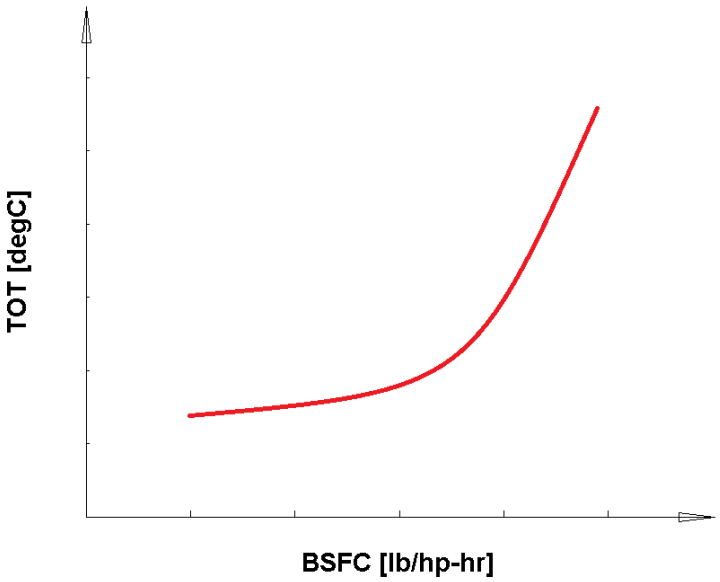

Figure 2.2. TOT vs BSFC trade-off.

2.3 BTE Analysis

Brake thermal efficiency (BTE) is another measure for fuel economy. BTE and BSFC have an inverse relationship for a specific type of fuel (i.e., diesel). as shown in Eq. (2.3).

$$\text{Brake Thermal Efficiency} = \frac{1}{\text{BSFC}} \times \frac{\text{Unit Diesel Fuel Mass}}{\text{Lower Heating Value}} = \frac{0.1375}{\text{BSFC}}. \tag{2.3}$$

Cycle efficiency analysis was used to understand the impact of CDA and valvetrain flexibility. The brake thermal efficiency of the engine can be decomposed into closed cycle efficiency, open cycle efficiency, and mechanical efficiency (per Eq. (2.4)-Eq. (2.7)). The calculations of mean effective pressure (MEP) including gross indicated MEP (GIMEP), net indicated MEP (NIMEP) and brake MEP (BMEP) are based on in-cylinder pressure [38]. Closed cycle efficiency is impacted by combustion completeness, piston expansion work, and heat transfer. Open cycle efficiency quantifies the efficiency of the gas exchange and is impacted by turbine and compressor efficiencies, and pressure differences between the intake and exhaust manifold. Mechanical efficiency captures losses from friction and parasitic loads.

$$\text{BTE} = \eta_{\text{closed cycle}} \times \eta_{\text{open cycle}} \times \eta_{\text{mechanical}}. \tag{2.4}$$

$$\eta_{\text{closed cycle}} = \frac{\text{GIMEP}}{\text{Fuel Equivalent Work}}. \tag{2.5}$$

$$\eta_{\text{open cycle}} = \frac{\text{GIMEP+PMEP}}{\text{GIMEP}} = \frac{\text{NIMEP}}{\text{GIMEP}}. \tag{2.6}$$

$$\eta_{\text{mechanical}} = \frac{\text{BMEP}}{\text{BMEP+FMEP}} = \frac{\text{BMEP}}{\text{NIMEP}}. \tag{2.7}$$

2.4 Experimental Setup

The experimental test bed used in this study is a multi-cylinder direct injection diesel engine with a static geometric compression ratio of 17.3:1 outfitted with high pressure, cooled EGR regulated with an electronically-controlled EGR valve, a sliding nozzle type variable geometry turbocharger (VGT), an air-to-water charge air cooler (CAC), and a common rail injection system as shown in Fig. 2.3. Kistler 6067C and AVL QC34C in-cylinder pressure transducers in tandem with an AVL 365C crankshaft position encoder are used with an AVL 621 Indicom module for high-speed indicating data acquisition. Fresh air flow is measured with a laminar flow element (LFE). Two channels of a Cambustion NDIR Fast CO/CO_2 analyzer are utilized, with one in the intake manifold and the other in the exhaust pipe. Also used are California Analytical Instruments NDIR, and HFID analyzers for exhaust CO_2, and total unburned hydrocarbons, respectively. A wide-band O_2 sensor is also present in the exhaust, as is an AVL 483 photo-acoustic transient particulate matter analyzer [47–49].

In addition, the multi-cylinder test bed is outfitted with a fully flexible electro-hydraulic variable valve actuation (VVA) system that enables cylinder-independent, cycle-to-cycle control of the engine's valve events. Figure 2.4 presents a schematic of the VVA system for a given intake or exhaust valve pair. Currently both the intake and exhaust valve pairs are driven by the VVA system, such that it is possible to change the valve opening timing, valve closing timing, valve lift, and the ramp rates/velocity of the profile on a cycle-to-cycle basis. High pressure hydraulic fluid powers the system. The servo valve position determines the pressure difference between the upper and lower face of the piston actuator. The piston actuator acts directly on the crosshead and actuates a valve pair. Linear variable differential transformers (LVDT) are integrated into the piston actuator and are used to provide feedback signals which allow the valves to be controlled to a desired profile.

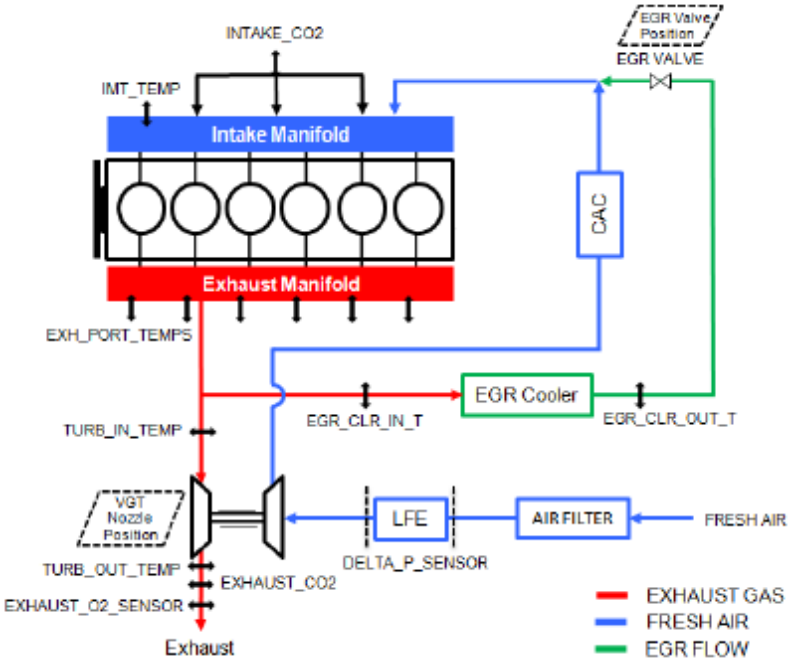

Figure 2.3. Schematic of engine.

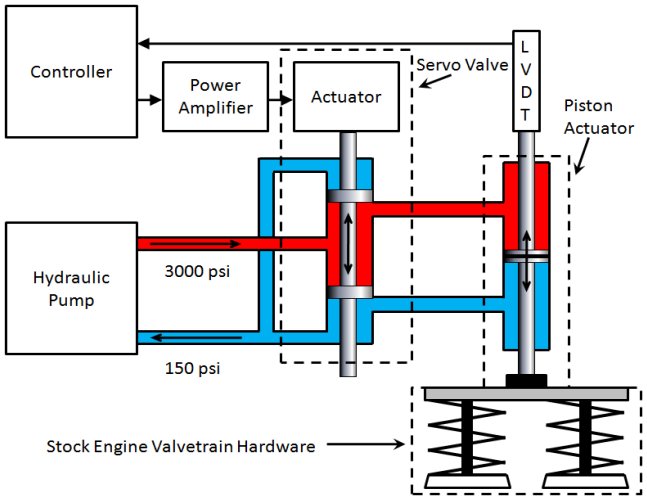

Figure 2.4. Schematic of variable valve actuation system.

To realize iEGR, LIVC, and CDA, valve control algorithms were developed in SIMULINK/MATLAB and communicated to the VVA system through dSPACE in

real time. The motion of valves were monitored during the engine test. An example of iEGR via re-induction is shown in Fig. 2.5. Besides the nominal valve profiles the exhaust valve reopened during the intake stroke. The measured profiles closely match the desired profiles.

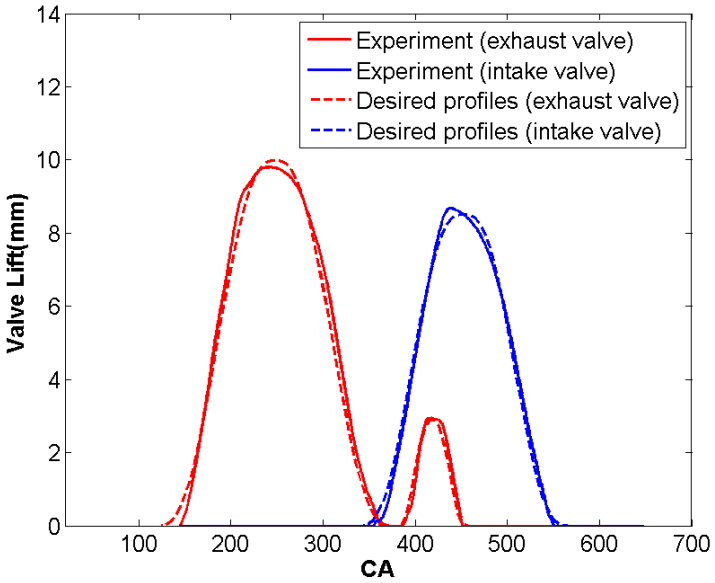

Figure 2.5. Control of intake and exhaust valve profiles (re-induction).

In the experimental testing, CDA is realized by using the VVA system to deactivate the valve-train for half of the cylinders. The fueling to these cylinders is also deactivated. The intake valve is opened every 100 cycles to recharge the cylinders in order to minimize the amount of oil drawn into the cylinders.

2.5 Analytical Model Calibration in GT-power

Engine testing is a time consuming way to evaluate combustion recipes and control techniques. Moreover, the results can be affected by fuel quality, sensor and actuator accuracy. Engine simulation tests provide an efficient and low cost way for new strategy exploration. Especially simulation supports data analysis with informations

which cannot be measured on the test bed such as residuals inside the cylinder. Furthermore, models provide the theoretical basis for hypothesis development and guide the experimental work.

Common 1-dimensional simulation tools for engine research include GT-power, Simulink by MATLAB or in-house codes [32,50]. Others use code generated based on thermodynamic principles with 3-D models to describe particular physical processes, such as KIVA and Simulink+FLUENT [28,34,35].

2.5.1 Gas Exchange Model

The model is built based on the Cummins diesel engine in Ray W. Herrick Laboratories. The calibration included two major stages: the air handling system and the combustion model. The air path includes (in order): the compressor, charge air cooler, intake manifold, cylinders, exhaust manifold, turbine and exhaust pipes. Part of the exhaust gases recirculate from exhaust manifold to intake manifold through the EGR loop.

The intake and exhaust manifold models were built to correspond to the 3-D CAD models (i.e., exhaust manifold model in Fig. 2.6). The flow area in the 3-D model was separated into small flow sections based on the changes of flow direction and cross section area. Each small flow area was transformed into 1-D model distinguished as a pipe, bend pipe or flow split (the basis of the engine model) as shown in Fig. 2.7. In addition the long pipes could be further discretized to improve the accuracy in predicting the physical process.

The intake and exhaust valves were calibrated using the flow bench data. The flow rate was calculated using forward and reverse flow coefficients with swirl numbers to capture the turbulence effect. The cylinders were modeled based on engine physical geometry. Turbine and compressor maps from the turbo manufacturer were implemented to capture the pressure drop and flow rate. A tabulated data of turbo shaft friction was used to capture the non-linear relationship between friction and turbo

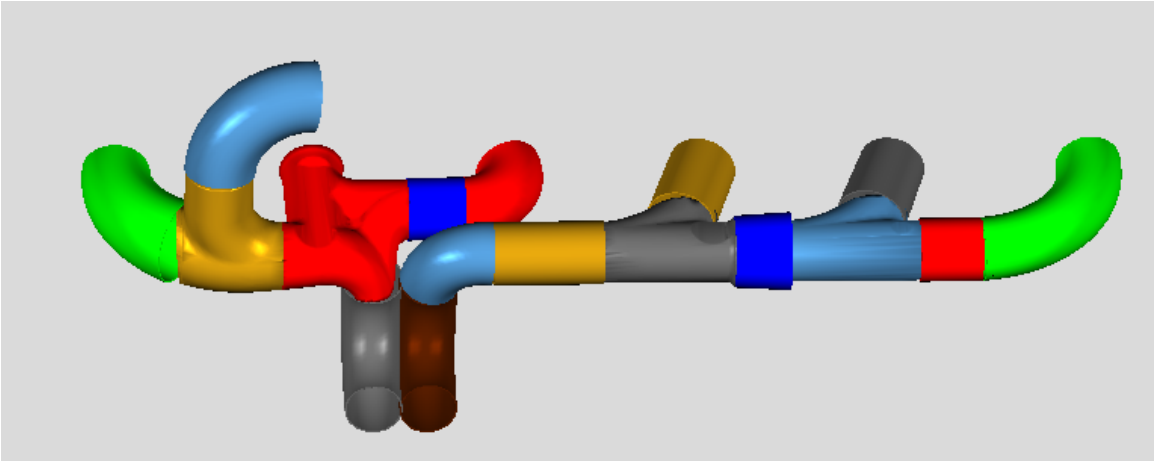

Figure 2.6. Flow area separation (exhaust manifold).

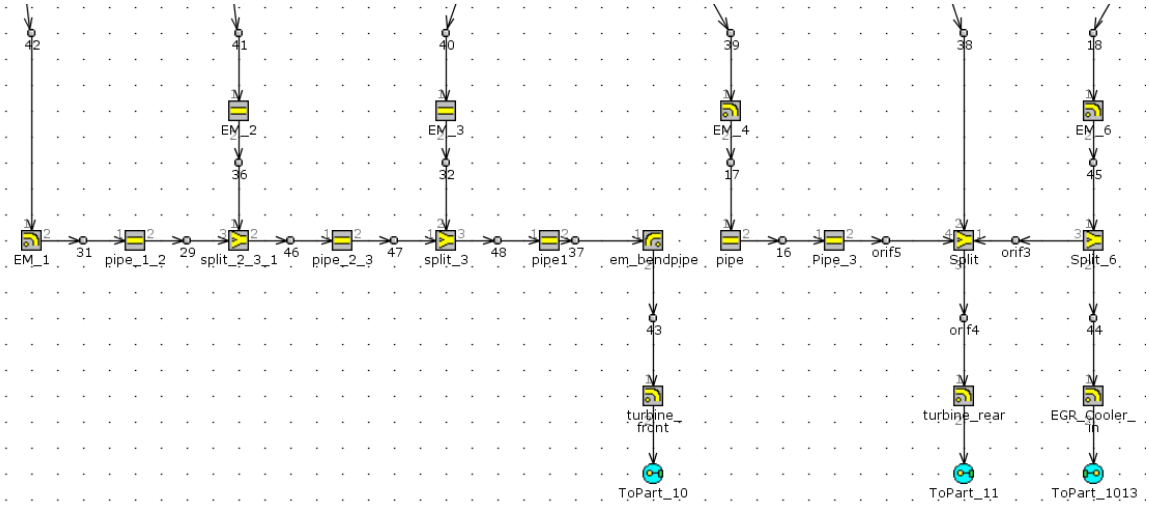

Figure 2.7. Exhaust manifold model in GT-power.

speed. EGR cooler and charge air cooler were discretized into 600 and 300 identical small pipes based on the physical structure.

Above all, the air handling system was built based on physical geometries of different components.

2.5.2 Combustion Model

The combustion model chosen in this study was the DIpulse model framework [51]. This combustion model predicts the instantaneous burned rate of injected fuel based on estimated in-cylinder pressure and temperature. The model characterize the combustion process with four parameters including entrainment rate of fuel spray, ignition delay, premixed combustion rate and diffusion combustion rate. Coupled with the combustion model, the fuel injector was modeled using interpolation of injection maps with corresponding rail pressure and engine speed. The hydraulic delay and electric delay of the injectors were calibrated using a previous effort [52] for this specific engine.

2.5.3 Parameter Calibration

Detailed parameter calibration was performed based on experimental data. The calibration procedure is:

- Data screening
- Three pressure analysis (TPA)
- Single cylinder model
- Adding intake and exhaust manifold
- Adding CAC and EGR loop
- Adding turbine and compressor
- Complete gas exchange model calibration
- Combustion model calibration

The first step is data screening, which guarantees the quality of data used for model calibration, eliminating incomplete data or non-steady state data. The carbon balance was calculated for each case comparing the carbon atoms before and after the combustion. A reasonable assumption is made such that the fuel has been completely consumed. Carbon balance error within 5% was considered as good quality data in this step. In addition data were selected widely spread on the engine speed and load map to capture various operating conditions.

The calibration of the air handling system was performed in fixed heat release rate (FHRR) mode when the fuel burned rate is calculated from the experimental in-cylinder pressure traces. The in-cylinder heat transfer model and compression ratio were calibrated in three pressure analysis (TPA) which uses in-cylinder, intake and exhaust manifold pressures to predict the engine operation. The burned rate was generated in the single cylinder model with necessary in-cylinder information from TPA including volumetric efficiency, residual fraction, wall temperatures in different zones and swirl number. In addition, another round of data screening was proceed in this step to remove cases with noisy in-cylinder pressure trace.

The engine model was assembled part by part from single cylinder to the complete model in the FHRR mode. The friction model of the crankshaft was calibrated in multi-cylinders model with intake and exhaust manifolds added. A check was performed here to guarantee pressures and temperatures within 3 % error and air flows within 5 % error. Then CAC, EGR and turbocharger were added to the model, one component at a time. The calibrated parameters included pipe numbers inside the EGR cooler, heat transfer coefficient, turbine and compressor coefficients. Model check is performed every time when new component was integrated. The last step is combustion model calibration in the single cylinder mode. Four parameters were calibrated using design of experiment (DOE) to match the experimental P-V diagram. A final check of model accuracy was completed when the combustion model was integrated into the air handling system model.

A well-calibrated GT-power model of a multi-cylinder diesel engine is obtained, which can predict BSFC within 5%, BSNOx within 25%, charge flow within 5%, temperatures and pressures within 3%.

2.6 Optimization

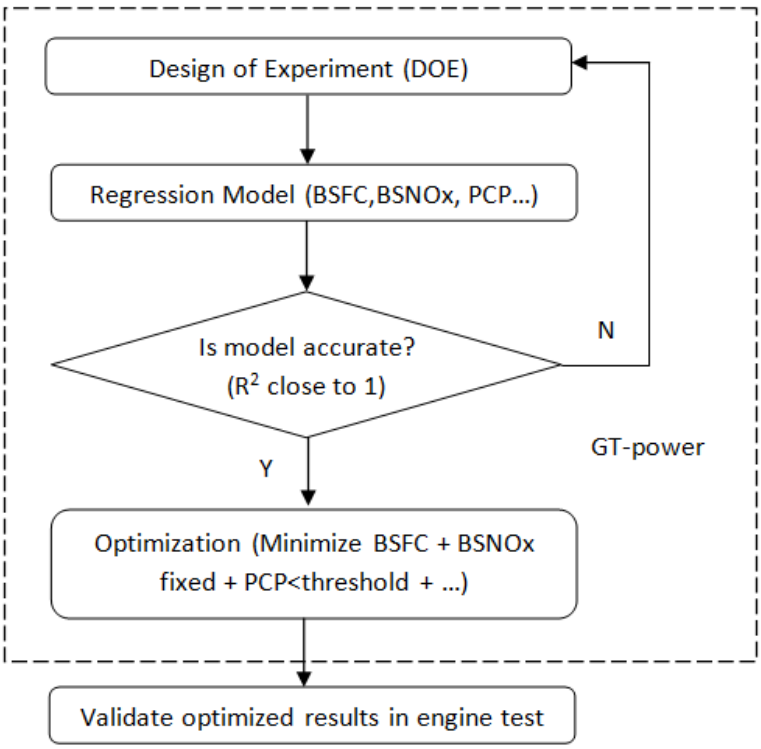

Figure 2.8. Optimization method.

Systematic optimization was performed to find optimal BSFC and TOT values using the GT-power model or experimental results (Fig. 2.8). The optimization process started with a design of experiment (DOE) with independent variables of valve timing, EGR valve diameter, the rack position of the VGT, start of injection, and rail pressure. The identified independent variables varied in a reasonably wide range. For instance, EGR valve diameter was varied from fully closed to fully open

in order to explore all the possible operating conditions. The DOE can be generated using a fully factorial with all the possible combinations or central composite design with reduced number of cases. A trade-off of model accuracy and computing time exists in different methods to creat a DOE.

DOE results include engine informations such as pressure, temperature and flow rate which can be used to generate regression models including BSFC, BSNOx, AFR, as well as the mechanical and emission constraints. Iteration is necessary to improve the accuracy of the regression models compared with simulation results. The regression models are used in the optimization of the minimum BSFC and maximum TOT, at specific BSNOx targets. The optimization uses the multi-start constrained nonlinear multivariable function in Matlab to obtain a global minimum value. Finally the optimized results were validated in the experiment.

The uncertain analysis at high-way cruise condition is based on the daily repeated cases with conventional valve profiles. This analysis provides the error bars on all the plots of one standard deviation of each variable measured.

2.7 Emission Constraints

The emission and mechanical constraints used for all optimizations and analysis in this thesis are shown in Table 2.1 and 2.2, respectively. These emission constraints were set such that tail pipe regulations could reasonably be met with current aftertreatment technology. In simulation the lowest AFR allowed was 18 as a proxy for meeting UHC and PM constraints. The mechanical engine constraints (Table 2.2) were provided by Cummins.

2.8 Summary

In this chapter the analysis methods for fuel economy, thermal management and emission control are introduced. 1-D engine simulation, model based optimization, and experiment setup are detailed. The analysis in the following chapters will mainly

Table 2.1. Emission Limit.

Operating Condition	**NOx**	**UHC**	**PM**
Unloaded Idle (800 RPM, 0.26 bar BMEP)	$\leq$ 20 g/hr	$\leq$ 15 g/hr	$\leq$ 1 FSN
Loaded Idle (800 RPM, 2.5 bar BMEP)	$\leq$ 1.5 g/hp-hr	$\leq$ 15 g/hr	$\leq$ 1 FSN
Cruise Condition (1200 RPM, 7.58 bar)	$\leq$ 1.5, 3, 4 g/hp-hr	$\leq$ 100 ppm	$\leq$ 1.5 FSN

Table 2.2. Mechanical constraints.

Mechanical Parameter	Unit	**Limit**
Turbine Inlet Temperature	°C	760
Compressor Outlet Temperature	°C	230
Turbo Speed	kRPM	193
Peak Cylinder Pressure	psi	2500
Exhaust Manifold Pressure	kPa	500
Pressure Rise Rate	bar/sec	100
Air-fuel Ratio	–	18

focus on BSFC vs BSNOx trade-off and TOT vs BSFC trade-offs at various operating conditions.

3. FUEL EFFICIENT EXHAUST THERMAL MANAGEMENT AT IDLE

The experimental efforts described in this chapter focus on fuel economy and exhaust thermal management of a turbocharged multi-cylinder diesel engine utilizing cylinder deactivation and variable valve actuation at both "unloaded" idle (800 RPM, 0.26 BMEP) and "loaded" idle (800 RPM 2.5 bar BMEP) conditions. The emphasis is on the idle conditions given the low engine exhaust temperatures for, and significant amount of time spent at, these conditions. Traditional strategies, such as late injection, over-closing a variable geometry turbocharger or intake throttling can increase exhaust temperatures but lead to significant increase in fuel consumption. The effort described here will demonstrate how CDA and valve-train flexibility can be used to achieve thermal management in a more efficient manner.

3.1 CDA at Unloaded Idle

The results of turbine outlet temperature (TOT) and fuel consumption are shown in Fig. 3.1. CDA improves the trade-off between TOT and fuel consumption as less fuel is needed to achieve a particular TOT. Different valve profiles coupled with CDA (labeled as "CDA + VVA" in Fig. 3.1) have also been investigated to further increase TOT and reduce fuel consumption. Three consecutive cases were taken for each operating condition (loaded and unloaded idle) and each operation (no-CDA and CDA), which is used in measurement uncertainty analysis. This analysis provides the error bars on all the plots of one standard deviation of each variable measured. The results discussed in this chapter are all from engine test.

The baseline condition (a black square in all figures) corresponds to the lowest fuel consumption of the engine with all cylinders activated (i.e., "no-CDA"). As shown, the TOT at this condition is only 120°C. No-CDA engine operation can achieve TOTs

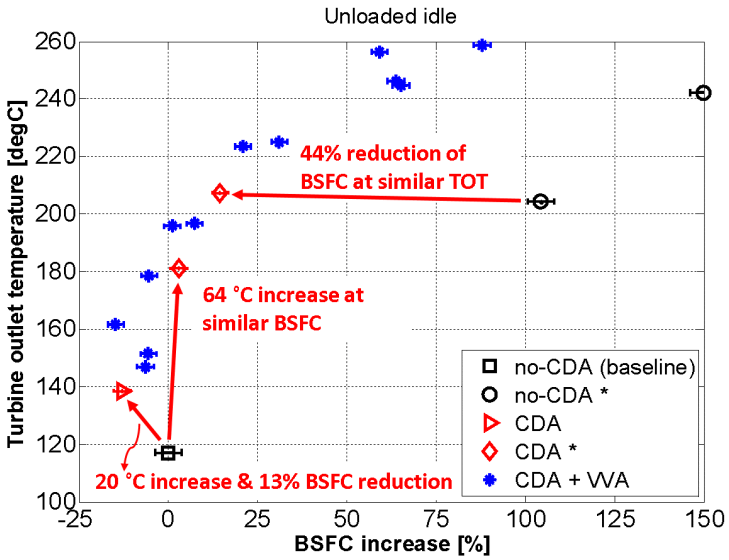

Figure 3.1. Turbine outlet temperature vs fuel consumption at unloaded idle (* labels cases with over-closed VGT and delayed fuel injection).

above 200°C at the cost of a 100% increase in fuel consumption with late injections and throttling via an over-closed VGT (black circles in all figures). Over-closing the VGT significantly decreases the open cycle efficiency as shown in Fig. 3.2 (due to an increase in pumping work brought on by restricting flow through the turbine), necessitating an increase in fueling to maintain brake torque. This increase in fueling decreases the AFR as shown in Fig. 3.3, resulting in the increase in TOT. For these cases the start of injection (SOI) is delayed to stay within the NOx constraint.

The lowest fuel consumption during CDA with conventional valve profiles used for the activated cylinders is shown as a red, rightward pointing triangle in all the plots. This operating mode results in a 13% reduction in fuel consumption and a 20°C increase of TOT relative to the baseline, as shown in Fig. 3.1. TOT increases as a result of a decrease in the AFR (per Fig. 3.3) brought on by a reduction in the air flow (Fig. 3.4) caused by cylinder deactivation. CDA increases closed cycle efficiency (combustion efficiency) and open cycle efficiency (less pumping work) resulting in a

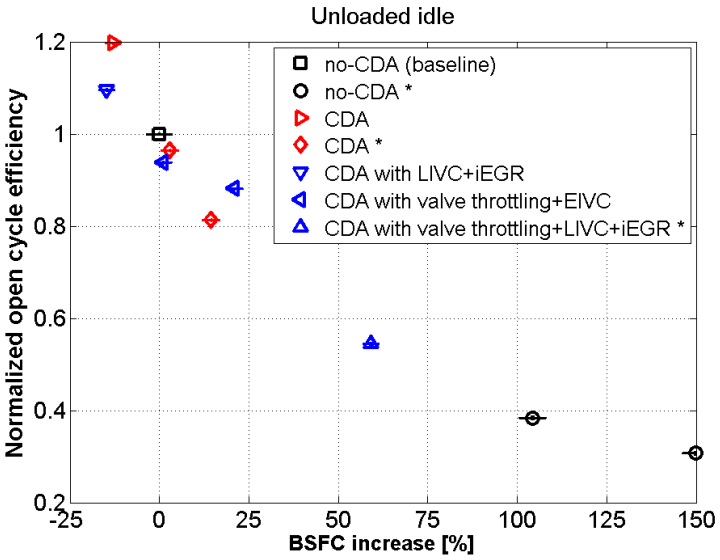

Figure 3.2. Normalized open cycle efficiency vs fuel consumption at unloaded idle (* labels cases with over-closed VGT and delayed fuel injection).

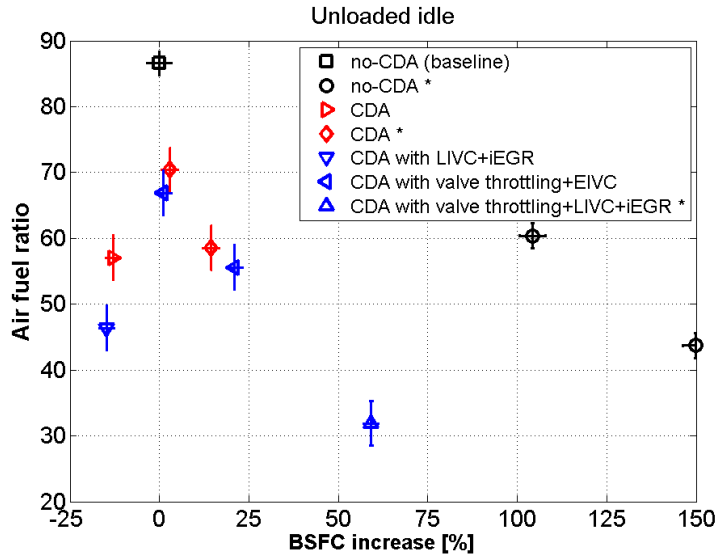

Figure 3.3. Air-fuel ratio vs fuel consumption at unloaded idle (* labels cases with over-closed VGT and delayed fuel injection).

reduction of fuel consumption. The closed cycle efficiency (Fig. 3.5) increase is due to aggressive combustion with almost doubled fueling per activated cylinder in the CDA mode. Open cycle efficiency (Fig. 3.2) increases as the air flow is lower when half of the cylinders are deactivated. Mechanical efficiency decreases by 15% with CDA as shown in Fig. 3.6 due to the higher in-cylinder pressure. Taken together, the increases in open and closed cycle efficiencies and reduction in mechanical efficiency lead to an increase in brake thermal efficiency (per Fig. 3.7).

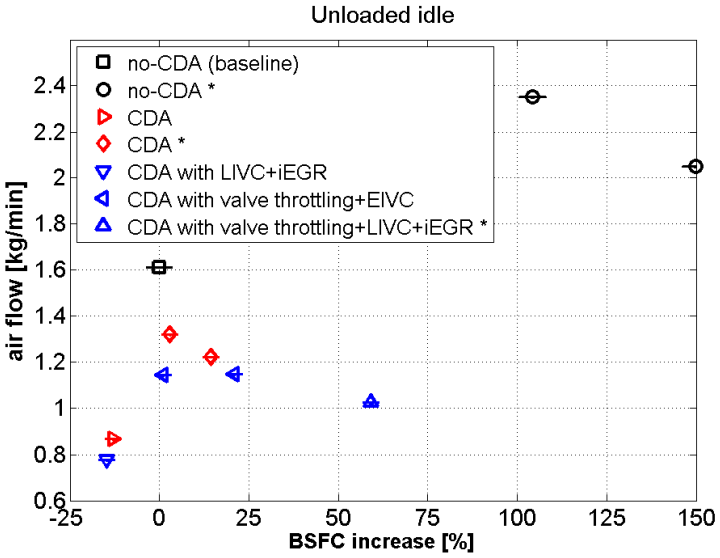

Figure 3.4. Air flow vs fuel consumption at unloaded idle (* labels cases with over-closed VGT and delayed fuel injection).

As expected, over-closing the VGT and delaying SOI while in the CDA mode increases TOT and fuel consumption relative to the best efficiency CDA point, as shown with red diamonds in Fig. 3.1. Furthermore this combination allows a TOT of ∼180°C (a 63°C increase) with a 3% fuel consumption increase relative to the no-CDA baseline (again, the black square in Fig. 3.1). A further increase to a TOT of 207°C is possible while realizing only a 14% fuel consumption increase relative to the no-CDA baseline. In addition, as shown in Fig. 3.1, the CDA point at 207°C has

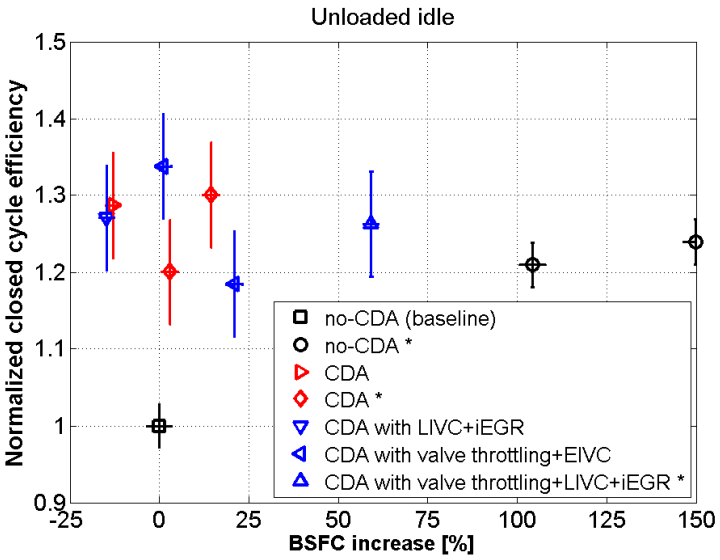

Figure 3.5. Normalized closed cycle efficiency vs fuel consumption at unloaded idle (* labels cases with over-closed VGT and delayed fuel injection).

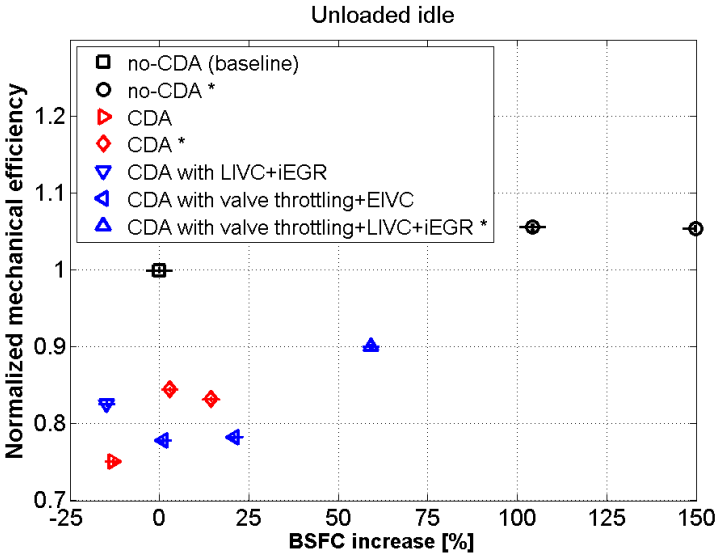

Figure 3.6. Normalized mechanical efficiency vs fuel consumption at unloaded idle (* labels cases with over-closed VGT and delayed fuel injection).

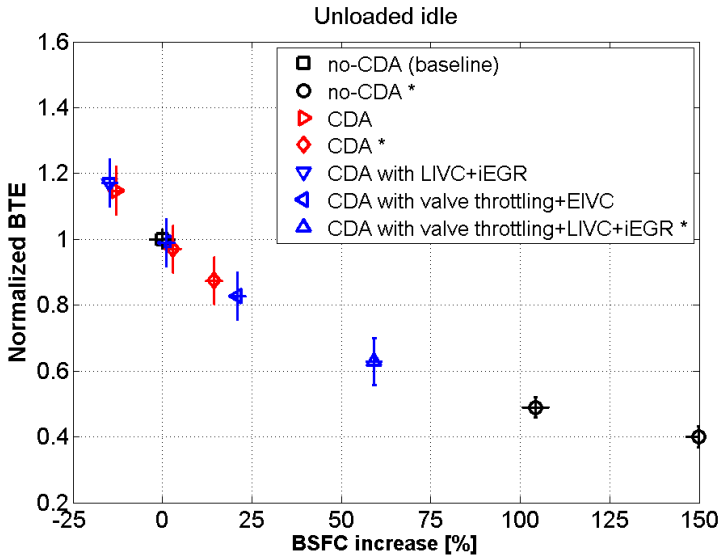

Figure 3.7. Normalized brake thermal efficiency vs fuel consumption at unloaded idle (* labels cases with over-closed VGT and delayed fuel injection).

a 44% lower fuel consumption than that achieved by the no-CDA case achieving a similar TOT.

3.2 CDA with Variable Valve Profiles at Unloaded Idle

As described previously, and shown in Fig. 3.1, the combination of CDA with valve-train flexibility (i.e., CDA+VVA) improves the TOT/fuel consumption trade-off and allows higher TOTs. A subset (the most promising) of these points in Fig.3.1 are shown in Fig. 3.8, and will now be discussed in more detail. These cases are shown as blue triangles: downward pointing for the "LIVC+iEGR" case, leftward pointing for the "valve throttling+EIVC" cases, and upward pointing for the "valve throttling+LIVC+iEGR" case.

CDA with LIVC+iEGR increases TOT to 160 °C with 15% less fuel consumption compared with the baseline, and exhibits a ∼20°C TOT increase compared with the CDA only case at a similar BSFC (the open, mechanical and closed cycle efficiencies

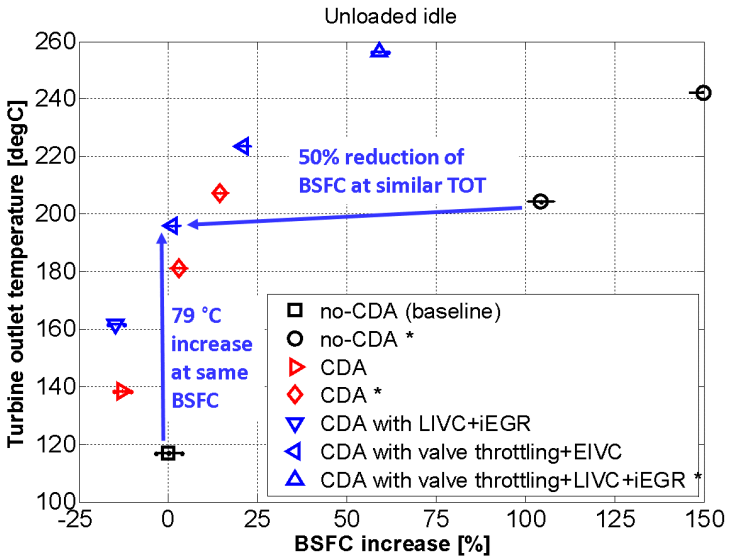

Figure 3.8. Turbine outlet temperature vs fuel consumption at unloaded idle (selected cases) (* labels cases with over-closed VGT and delayed fuel injection).

are similar resulting in a similar BTE and BSFC). Fig. 3.9 show the valve profiles for this case, which includes: (i.) negative valve overlap (NVO) to generate "internal EGR" (iEGR) by trapping a portion of the combustion gases, and (ii.) late intake valve closure (LIVC) to further reduce the amount of air inducted from the intake manifold, and to reduce the amount of in-cylinder compression. Relative to the CDA only point (which uses cooled external EGR and conventional valve profiles for the activated cylinders), the implementation of LIVC allows further reduction in the air flow (Fig. 3.4), resulting in a decrease in AFR (per Fig. 3.3) which causes an additional increase in TOT.

"CDA with valve throttling+EIVC" results in a ~200°C TOT with nearly equivalent fuel consumption compared with the no-CDA baseline and CDA* cases as shown in Fig. 3.8. The smaller intake and exhaust valve profiles (per Fig. 3.10) effectively throttle the engine, resulting in a reduction in the air flow (per Fig. 3.4) compared with the other two cases at similar BSFC. The reduced air flow results in lower AFR

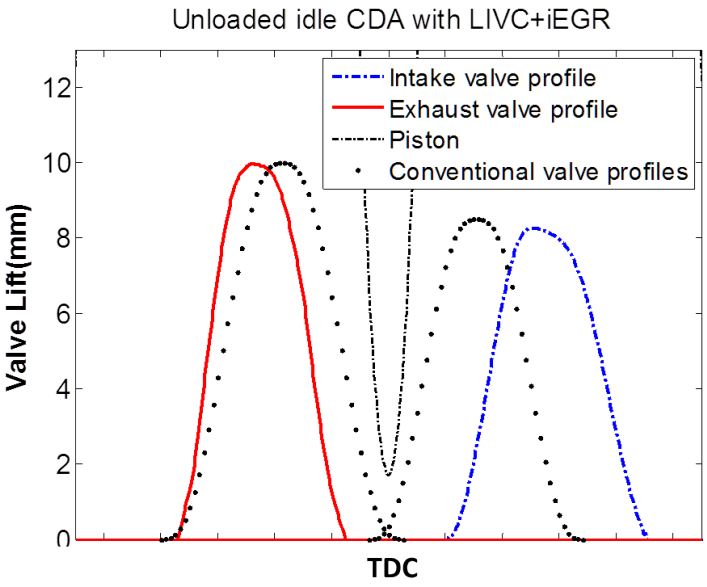

Figure 3.9. Valve profiles of CDA with LIVC+iEGR.

(per Fig. 3.3), increasing TOT to 200°C (per Fig.3.8). This operating condition also corresponds to a 50% reduction of fuel consumption compared with the non-CDA case with late SOI and over-closed VGT that has a similar TOT of ∼200°C.

Early IVC reduces the amount of in-cylinder compression (a NOx reducer) allowing earlier injection timing leading to earlier heat release (per Fig. 3.11) compared with the CDA* case, which causes (i.) an increase in closed cycle efficiency (Fig. 3.5), and (ii.) a decrease in mechanical efficiency (Fig. 3.6) from higher in-cylinder pressure. Together these changes result in similar BTE/BSFC.

"CDA with valve throttling+LIVC+iEGR" (Fig. 3.12) increases TOT up to 260°C, the maximum TOT at the unloaded idle condition, with an over-closed VGT and delayed SOI. NVO enables iEGR instead of cooled external EGR. Together with the LIVC, which reduces the amount of in-cylinder compression, this results in less heat rejected from the engine in comparison to the high TOT no-CDA case (Fig. 3.13). LIVC also reduces the volumetric efficiency of the engine, decreasing airflow (Fig. 3.4) and AFR (Fig. 3.3). Reduced heat losses and lower AFR increases the

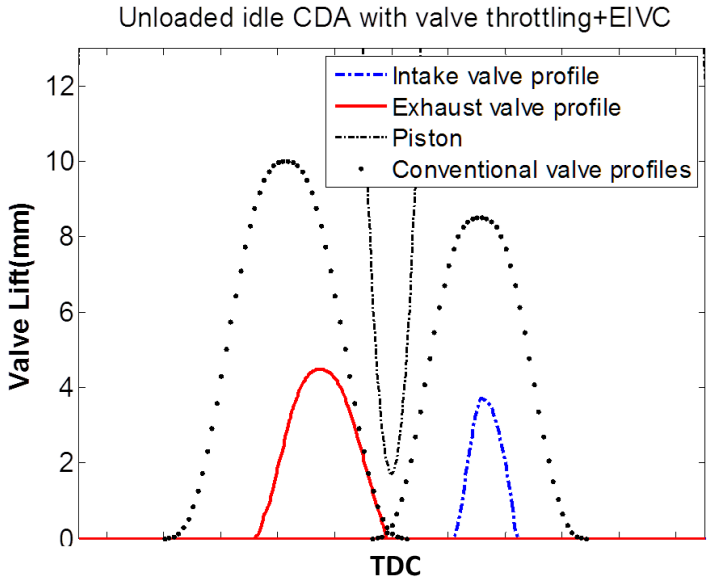

Figure 3.10. Valve profiles of CDA with valve throttling+EIVC.

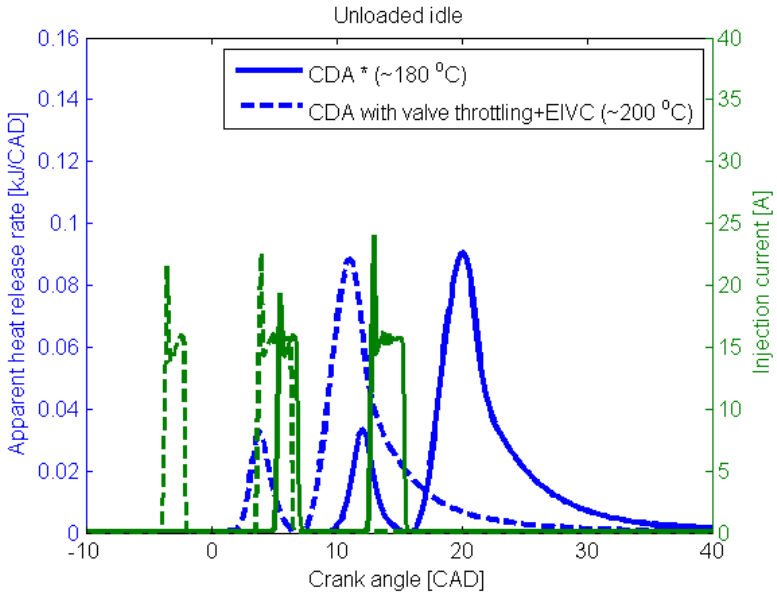

Figure 3.11. Heat release rate for selected three cases at unloaded idle.

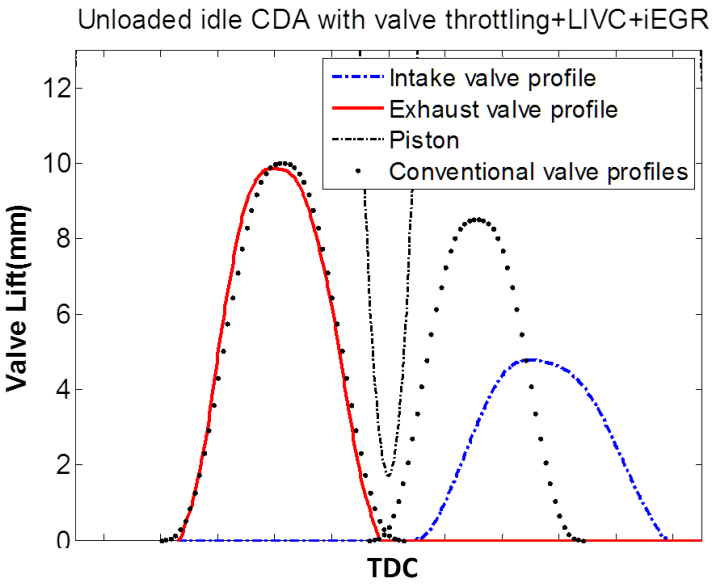

Figure 3.12. Valve profiles of CDA with valve throttling+LIVC+iEGR.

TOT. An additional benefit of the reduction in heat losses and AFR is that a less aggressive decrease in open cycle efficiency is required for AFR reduction (Fig. 3.2), allowing a lower BSFC with slightly higher TOT compared with the high TOT, no-CDA case (Fig. 3.8).

3.3 Impact of Results for Thermal Management at Unloaded Idle

Sections 3.1 and 3.2 have focused on improving the trade-off between exhaust temperature and fuel consumption for thermal management considerations. However, the heat transfer between the exhaust gas and catalyst beds is a more complex process, which does not only rely on TOT, but also the exhaust flow rate. As an approximation, consider the heat transfer rate within round pipes - which is determined by a convective heat transfer coefficient, geometric structure of the pipes (constant) and the temperature difference between the bed and the exhaust gas as shown in eqn. 3.1 [53]. The convective heat transfer coefficient is determined by the Nusselt number

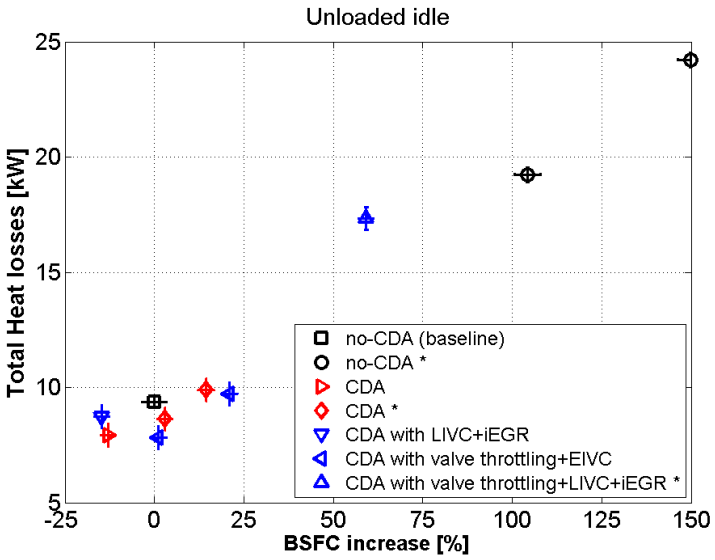

Figure 3.13. Total engine heat losses vs fuel consumption at unloaded idle (* labels cases with over-closed VGT and delayed fuel injection).

Nu, the diameter of the pipe (constant) and thermal conductivity. The Nusselt number can be calculated using the Prandtl number Pr (assumed constant) and Reynolds number which is determined by the mass flow rate and dynamic viscosity. The convective heat transfer can be simplified (Eq. (3.2)) depending on the exhaust flow rate and difference between turbine out and bed temperatures, and a coefficient C. Both thermal conductivity and dynamic viscosity slightly increases with temperature resulting in little variation of C at specific engine speed and load condition. Assuming C is constant the normalized heat transfer rate can be estimated using measured turbine outlet temperature and exhaust flow rate at different bed temperature using this simplified heat transfer model of aftertreatment system.

$$
\begin{aligned}
q &= h \times A_{surface} \times (TOT - T_{bed}), \\
h &= N_{u_D} \times k/D, \\
N_{u_D} &= 0.023 \times {R_{e_D}}^{4/5} \times Pr^n, \\
R_{e_D} &= \rho \times v \times D/\mu = \dot{m} \times D/(\mu \times A), \\
Pr &= \mu \times Cp/k.
\end{aligned} \tag{3.1}
$$

$$
\begin{aligned}
q &= C \times \dot{m}^{4/5} \times (TOT - T_{bed}), \\
C &= 0.023 \times A_{surface} \times 1/D^{1/5} \times 1/A^{4/5} \times Pr^n \times k/\mu^{4/5}.
\end{aligned} \tag{3.2}
$$

As shown in Fig. 3.14, the estimated exhaust gas-to-catalyst heat transfer, calculated using eqn. 3.2, is given for different bed temperatures for the three cases with similar BSFCs corresponding to the "no-CDA (baseline)", "CDA*" and "CDA with valve throttling+EIVC" conditions. Of greatest importance, note that the CDA conditions outperform the no-CDA case for the entire range of relevant catalyst bed temperatures. In other words, CDA operation will warm-up the catalysts more quickly, and sustain higher temperatures (120 vs. ∼180 or ∼200°C).

3.4 Summary of Results at Unloaded Idle

Key findings at unloaded idle, presented in Sections 3.1-3.3, demonstrate that CDA enables a 64°C increase in TOT with only a 3% increase in fuel consumption compared with the most efficient no-CDA operation (Fig. 3.1). The TOT can further be increased to 196°C with no fuel economy penalty (Fig. 3.8) by combining CDA with intake/exhaust valve-based throttling and early IVC through valve-train flexibility. This strategy also allows for a 50% reduction in fuel consumption compared with conventional no-CDA strategies at a similar TOT of ∼200°C (Fig. 3.8). The thermal management potential of CDA is also directly demonstrated in Figure 3.14, which shows that for all catalyst bed temperatures of interest, CDA will out perform no-CDA operation at the same fuel consumption levels. As such, there is a significant

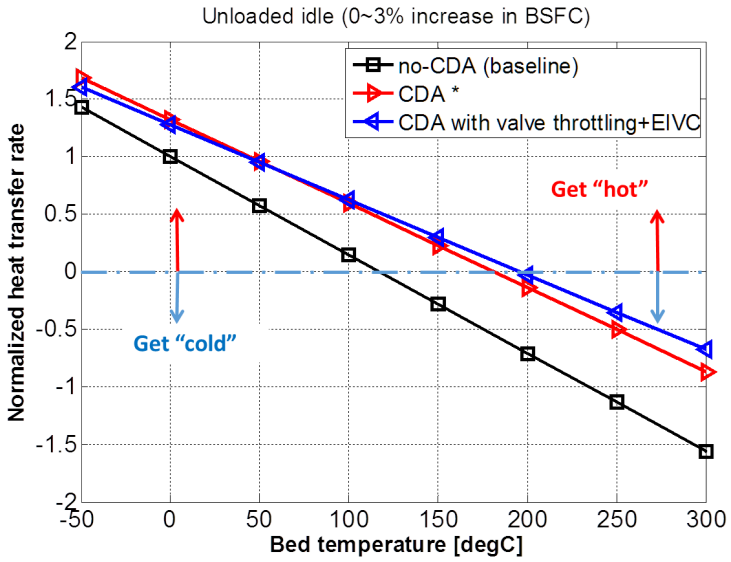

Figure 3.14. Estimated exhaust gas-to-catalyst heat transfer rate (equal BSFC) at unloaded idle (* labels cases with over-closed VGT and delayed fuel injection).

thermal management and efficiency benefit of both CDA and valve-train flexibility at the unloaded idle condition.

3.5 CDA at Loaded Idle

The no-CDA baseline condition corresponds to the lowest fuel consumption at loaded idle, with a TOT of 190°C (black square in Fig. 3.15). Relative to the baseline, no-CDA engine operation with delayed SOI and an over-closed VGT can increase TOT to 320 °C at the cost of a 67% increase in fuel consumption as shown in Fig. 3.15. As was also the case for the unloaded idle case, the over-closed VGT decreases the open cycle efficiency, requiring more fuel to maintain the same torque. This increased fueling decreases the AFR (per Fig. 3.16) resulting in the increase of TOT to 320°C (Fig. 3.15). SOI is delayed to maintain the NOx target.

The lowest fuel consumption during CDA with conventional valve profiles used for the activated cylinders leads to a TOT increase of 118°C (to 308°C) with only a

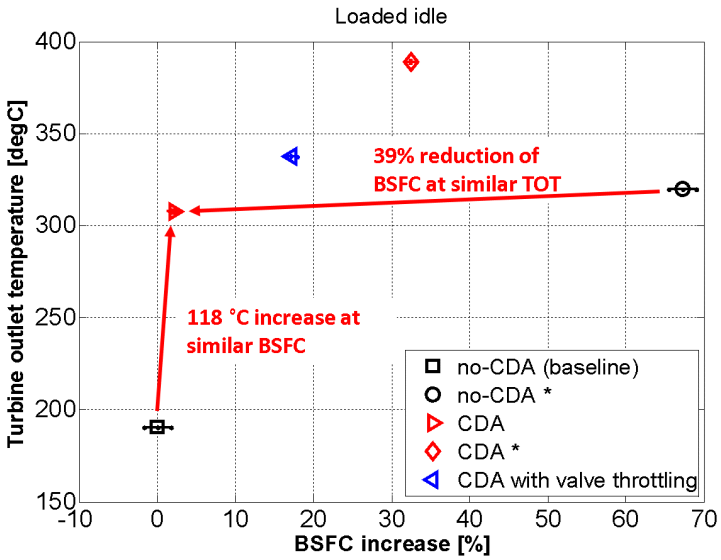

Figure 3.15. Turbine outlet temperature vs fuel consumption at loaded idle (1.5 g/hp-hr NOx) (* labels cases with over-closed VGT and delayed fuel injection).

2% fuel consumption increase relative to the baseline, as shown in Fig. 3.15. TOT increases as a result of a decrease in the air flow (per Fig.3.17) and AFR (per Fig. 3.16) as a result of CDA. The fuel consumption slightly increases due to lower mechanical efficiency (Fig. 3.18) with higher in-cylinder pressure from the aggressive combustion. The closed cycle efficiency (Fig. 3.19) increases only slightly, by 2.5%, due to efficiency canceling effects of more aggressive heat release (Fig. 3.20) (due to more fuel injected per activated cylinder) and later heat release (to maintain the NOx constraint). Open cycle efficiency (Fig. 3.21) increases as the air flow is lower when half of the cylinders are deactivated. The open cycle efficiency of the no-CDA operation was already quite high, such that there was little improvement possible with CDA at this speed/load point. Taken together, the small increases in open and closed cycle efficiencies and reduction in mechanical efficiency lead to slightly lower brake thermal efficiency (per Fig. 3.22).

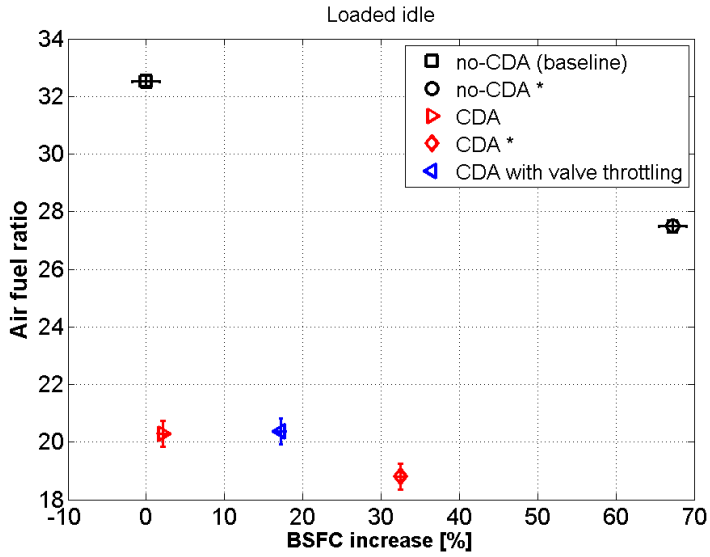

Figure 3.16. Air-fuel ratio vs fuel consumption at loaded idle (* labels cases with over-closed VGT and delayed fuel injection).

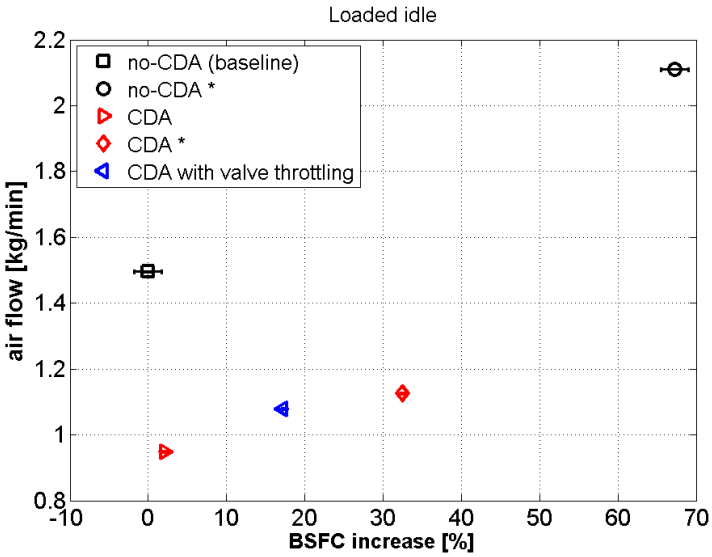

Figure 3.17. Air flow vs fuel consumption at loaded idle (* labels cases with over-closed VGT and delayed fuel injection).

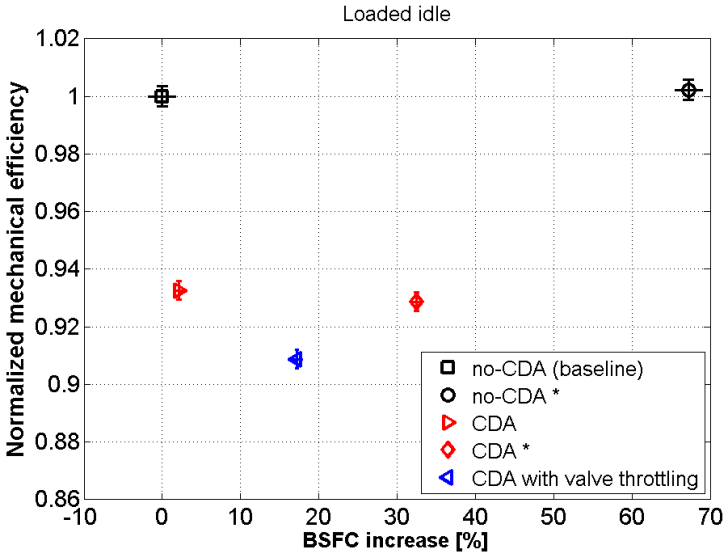

Figure 3.18. Normalized mechanical efficiency vs fuel consumption at loaded idle (* labels cases with over-closed VGT and delayed fuel injection).

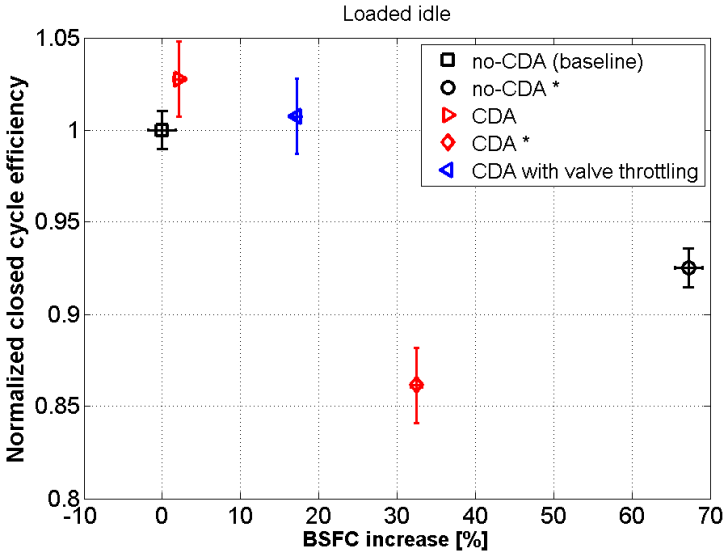

Figure 3.19. Normalized closed cycle efficiency vs fuel consumption at loaded idle (* labels cases with over-closed VGT and delayed fuel injection).

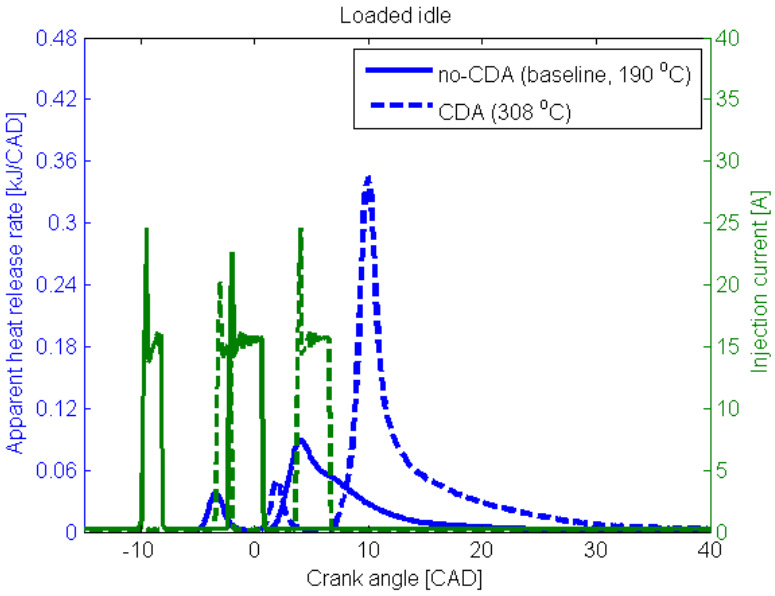

Figure 3.20. Heat release rate for selected two cases at loaded idle.

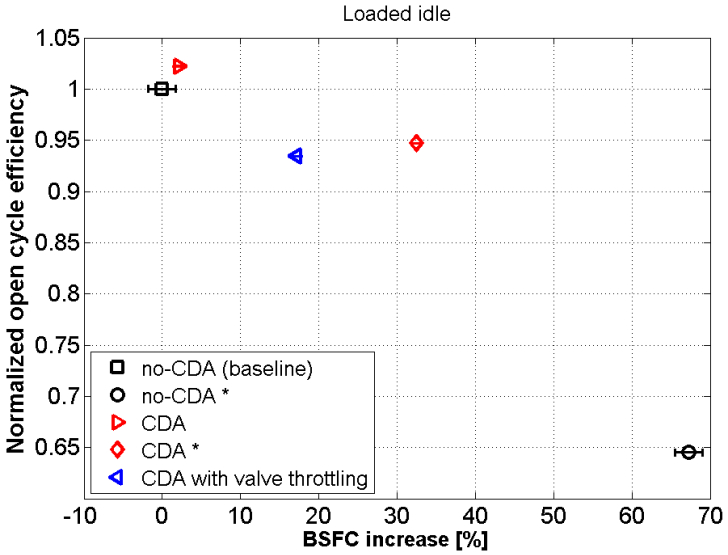

Figure 3.21. Normalized open cycle efficiency vs fuel consumption at loaded idle (* labels cases with over-closed VGT and delayed fuel injection).

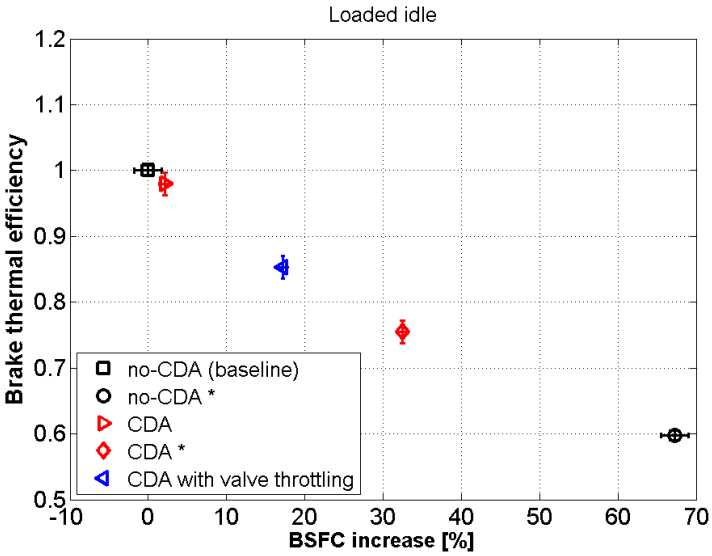

Figure 3.22. Normalized brake thermal efficiency vs fuel consumption at loaded idle (* labels cases with over-closed VGT and delayed fuel injection).

Over-closing the VGT and delaying SOI in CDA mode increases TOT to 390°C (as shown with a red diamond in Fig. 3.15), the highest temperature realized during loaded idle conditions. This increase of TOT corresponds to the lowest AFR, close to the stoichiometric condition, per Fig. 3.16. This low AFR results in higher combustion temperature and heat losses as shown in Fig. 3.23. Higher in-cylinder heat losses decrease the closed cycle efficiency as shown in Fig. 3.19. Moreover SOI is delayed to balance the NOx emission increase with elevated combustion temperature, also reducing the closed cycle efficiency. Open cycle efficiency decreases with over-closed VGT as the engine is throttled (per Fig. 3.21). Mechanical efficiency is 7% lower than the baseline (per Fig. 3.18) due to higher in-cylinder pressure from the aggressive heat release with CDA. In short, CDA with delayed SOI and an over-closed VGT allows an increase in TOT to 390°C (exceeding what is possible with no-CDA operation, which also has a higher fuel consumption, per Fig. 3.15). This could be

considered as a short term strategy to quickly warm up the aftertreatment system, if required, during loaded idle operation.

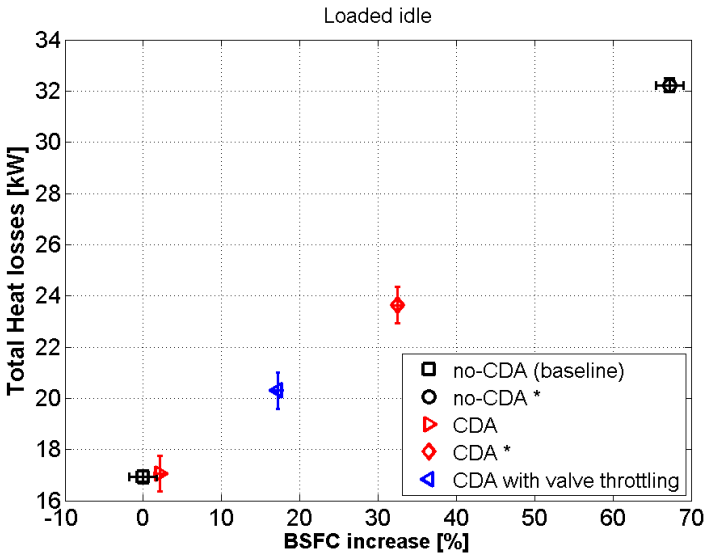

Figure 3.23. Total engine heat losses vs fuel consumption at loaded idle (* labels cases with over-closed VGT and delayed fuel injection).

3.6 CDA with Variable Valve Profiles at Loaded Idle

Flexible valve profile utilization during CDA operation does not further improve the trade-off between TOT and fuel consumption due to the low AFR (close to stoichiometric) that occurs during CDA at loaded idle (Fig. 3.16). In other words, unlike CDA operation during unloaded idle operation which still has elevated AFRs (Fig. 3.3), there is no more "margin" to reduce AFRs at loaded idle.

3.7 Impact of Results for Thermal Management at Loaded Idle

The normalized heat transfer rate (per Fig. 3.24) is calculated using eqn. 3.2 at different bed temperatures for the "no-CDA (baseline)" and "CDA*" cases. As was also the case at unloaded idle, CDA operation outperforms no-CDA operation

for all relevant catalyst bed temperatures. Specifically, CDA operation will warm-up the catalysts more quickly, and can sustain bed temperatures of 300°C, whereas no-CDA operation will cool down the catalysts when above ~200°C. Also note that the disparity in the warm-up benefit of CDA increases as the bed temperatures increase. For instance, the heat transfer rates for CDA are ~60% and ~180% higher than no-CDA operation for bed temperatures of 100 and 150°C, respectively.

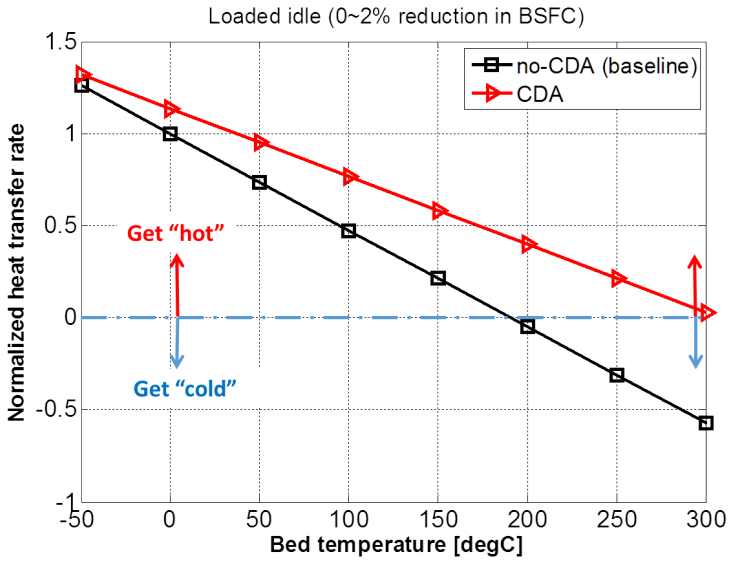

Figure 3.24. Estimated exhaust gas-to-catalyst heat transfer rate (equal BSFC) at loaded idle.

3.8 Summary of Results at Loaded Idle

CDA enables a TOT increase of 118°C (to 308°C) with a minor increase in BSFC compared with the no-CDA baseline (Fig. 3.15). This operating condition also exhibits a 39% fuel consumption reduction in comparison to a no-CDA condition at a similar TOT (Fig.3.15). As shown in Figure 3.24, CDA outperforms no-CDA operation, from a catalyst warm-up point of view, across all relevant catalyst bed temperatures. Due to the low AFR achieved during CDA at loaded idle (Fig.3.16), there is

much less merit relative to unloaded idle to combine CDA with valve-train flexibility on the activated cylinders. In short, there is a significant thermal management and efficiency benefit of CDA at loaded idle condition.

3.9 NOx, UHC and PM

The NOx, UHC and PM emissions of the cases analyzed in this chapter are shown in Fig. 3.25-3.30. UHC and PM are within the 15 g/hr and 1 FSN limit separately. NOx is between 18 g/hr and 23 g/hr beside one "no-CDA*" case at unloaded idle. BSNOx is between 0.9 g/hp-hr and 1.5 g/hp-hr at loaded idle.

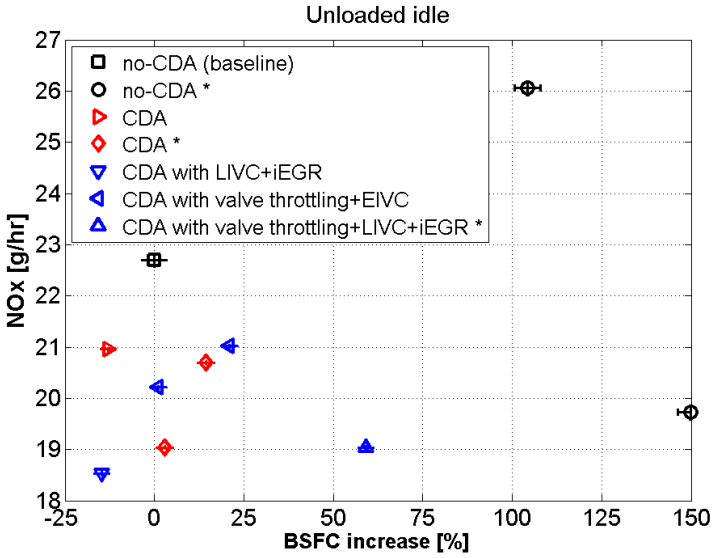

Figure 3.25. NOx vs fuel consumption at unloaded idle (* labels cases with over-closed VGT and delayed fuel injection).

3.10 Summary

The effort described above concentrated on determining the trade-off between exhaust temperature and fuel consumption of cylinder deactivation (CDA) and valve-train flexibility at unloaded and loaded idle conditions. These results would be useful

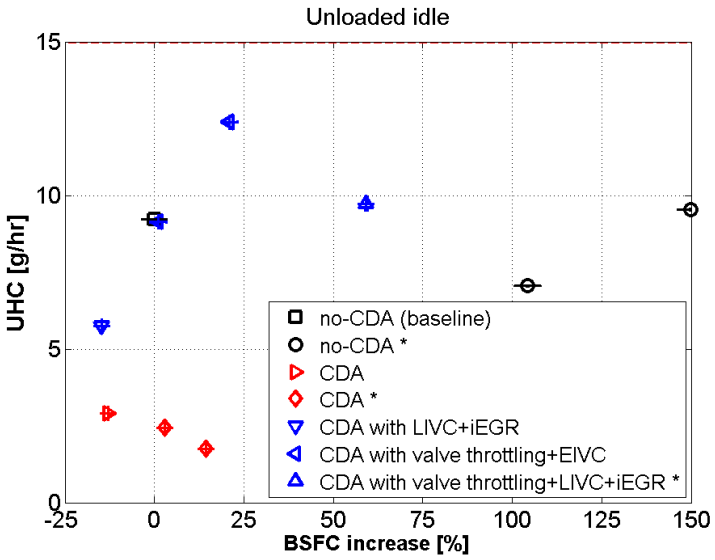

Figure 3.26. UHC vs fuel consumption at unloaded idle (* labels cases with over-closed VGT and delayed fuel injection).

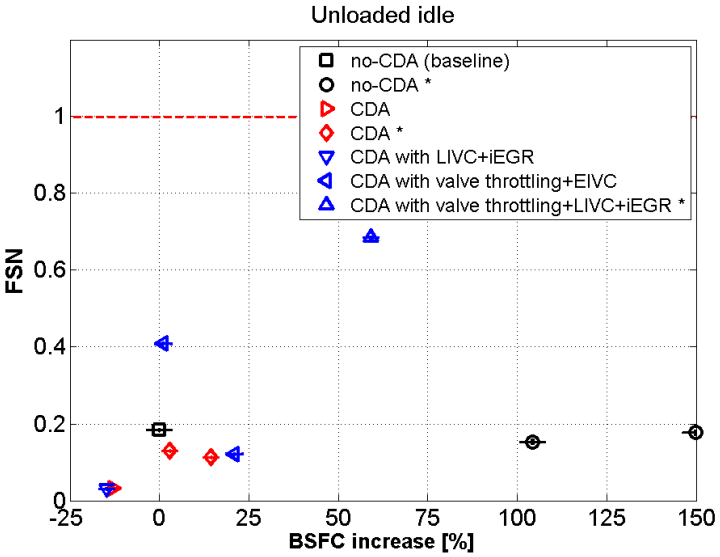

Figure 3.27. PM vs fuel consumption at unloaded idle (* labels cases with over-closed VGT and delayed fuel injection).

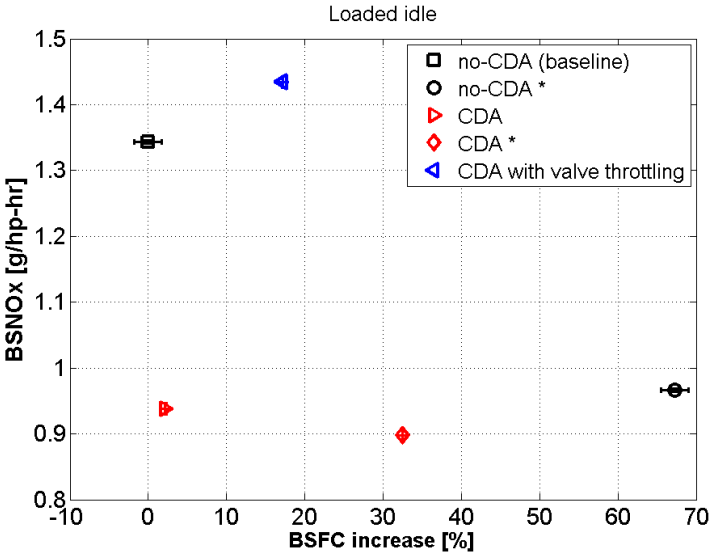

Figure 3.28. BSNOx vs fuel consumption at loaded idle (* labels cases with over-closed VGT and delayed fuel injection).

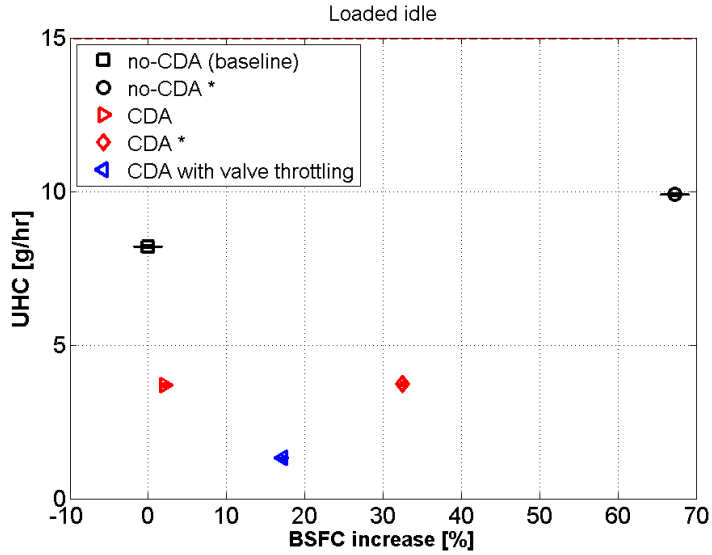

Figure 3.29. UHC vs fuel consumption at loaded idle (* labels cases with over-closed VGT and delayed fuel injection).

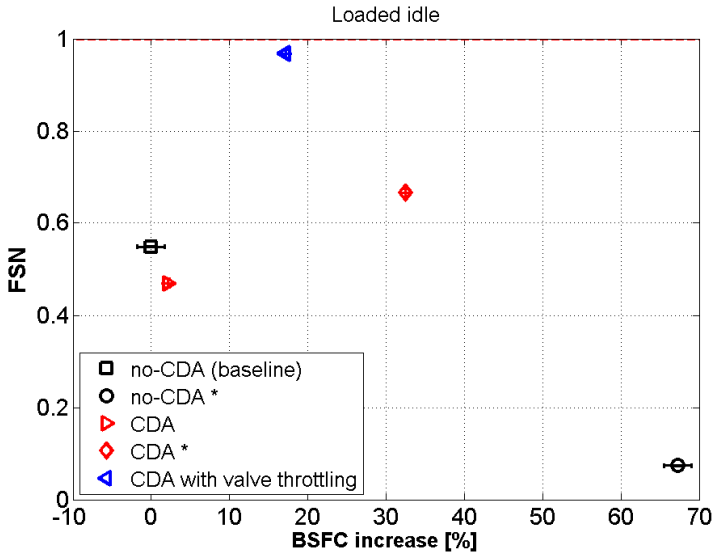

Figure 3.30. PM vs fuel consumption at loaded idle (* labels cases with over-closed VGT and delayed fuel injection).

in the thermal management of aftertreatment system as the efficiencies of DOC, DPF and SCR are heavily temperature dependent and generally require temperatures between 250°C and 450°C to provide required performance. Specifically the lowest exhaust gas temperature required to activate SCR is 200°C to avoid urea deposit.

The key observations are:

Unloaded idle (800 RPM, 0.26bar BMEP)

1. CDA enables a 64°C increase in TOT (to 180°C) with only 3% fuel consumption increase compared with the most efficient no-CDA operation;

2. Valve-train flexibility enables a TOT of ∼200°C with no fuel economy penalties by combining CDA with intake/exhaust valve based throttling and EIVC;

3. CDA with valve throttling, LIVC and iEGR maximize TOT up to 260°C at unloaded idle.

Loaded idle (800 RPM, 2.5 bar BMEP)

4. CDA enables TOT to 308°C with 39% lower fuel consumption than that achieved with no-CDA operation at same TOT. This corresponds to a 118°C TOT

increase and nearly no fuel penalty compared with the most efficient no-CDA operation;

5. CDA coupled with an over-closed VGT and delayed fuel injection maximizes TOT up to 390°C at loaded idle.

Both conditions

6. The exhaust gas-to-catalyst heat transfer for CDA operation outperforms no-CDA operation across all relevant catalyst bed temperatures. As such, there is a significant thermal management impact of CDA at both conditions.

4. FUEL ECONOMY AND THERMAL MANAGEMENT AT HIGH-WAY CRUISE CONDITION

The analytical and experimental efforts described here focus on fuel economy and exhaust thermal management at 1200 rpm, 7.58 bar BMEP, a speed and load consistent with cruise conditions for over the road trucks. With conventional valve-train operation the exhaust temperature at the turbine exit is 350 °C . Higher exhaust temperatures are necessary to more quickly heat up the SCR and periodically regenerate the DPF. Three strategies enabled by flexible actuation are investigated to increase exhaust gas temperature and power.

4.1 BSFC vs BSNOx Trade-offs

Constrained optimization and experimental validation were conducted to find the minimum fuel consumption that each variable valve actuation (VVA) strategy could provide. Optimization and validation was also performed with conventional operation to provide a baseline for comparison. The trade-off between fuel consumption and NOx emissions with conventional operation, iEGR via re-induction, LIVC, and CDA are shown in Fig. 4.1. Engine operation with CDA has an increase in BSFC while operation with iEGR and LIVC has fuel consumption levels comparable to conventional operation. The results discussed in this chapter are all from experimental validation of optimized results.

The durations of the re-induction profiles for the exhaust valves were optimized to a value of 2-3 crank angle degrees (CAD), a very short duration. This indicates that hot, re-inducted, burned gases bring essentially no benefit to fuel efficiency relative to cooled external EGR at the highway cruise condition. As the profiles are close to the nominal operation of the exhaust valves, it is not surprising that fuel consumption

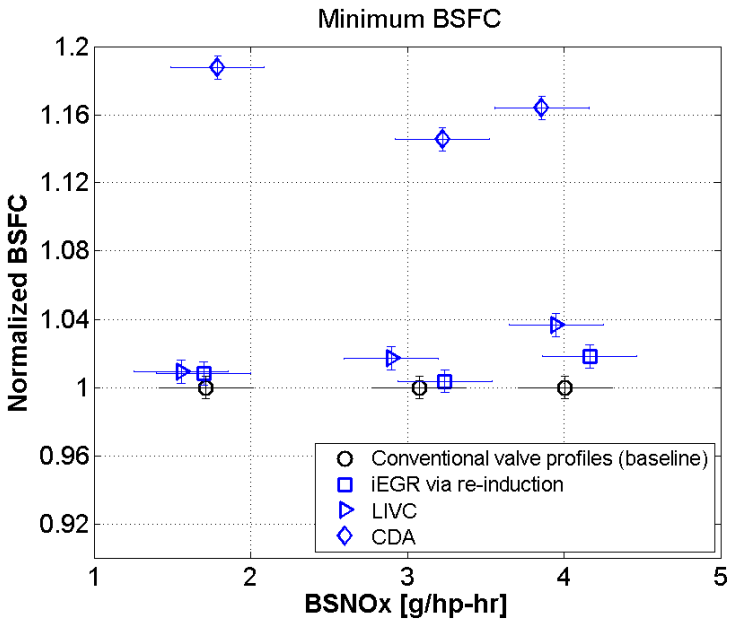

Figure 4.1. BSFC vs BSNOx trade-offs between conventional valve profiles and VVA functions.

remains comparable to that of baseline operation. Similarly, for the optimization of the LIVC function the intake valve closing timing was only retarded by around 10 CAD for the three BSNOx targets. This change in duration of intake valve opening had very little impact on the gas exchange and fuel consumption relative to baseline operation. In short, from a BSFC minimization point of view there is no reason to implement iEGR, LIVC or CDA at the 1200 RPM, 7.58 bar BMEP operating condition for this engine. In general, it is not necessarily surprising that VVA enabled functions did not improve fuel efficiency at this operating condition, since highly efficient operation at the "cruise" point is a direct focus of engine design.

4.1.1 Closed Cycle Efficiency

The fuel consumption for CDA is approximately 16 % worse than baseline operation, as shown in Fig. 4.1, which is consistent with lower BTE as shown in Fig.

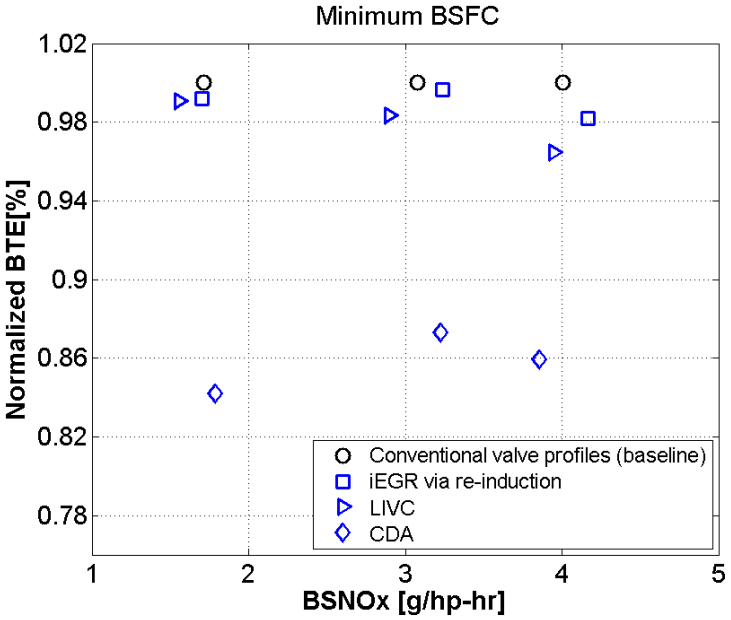

Figure 4.2. Normalized BTE vs BSNOx.

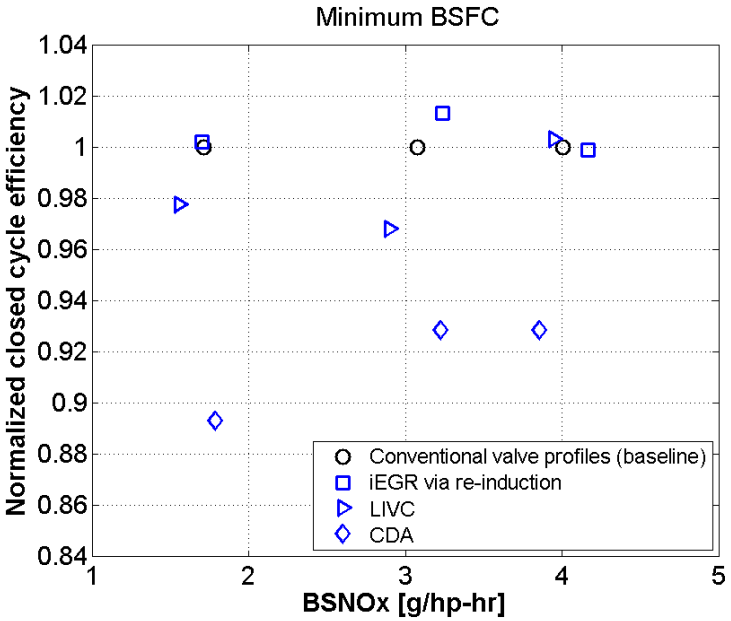

Figure 4.3. Normalized closed cycle efficiency vs BSNOx.

4.2. BTE can be broken down into cycle efficiencies to understand the losses in fuel efficiency associated with the operation of CDA. Fig. 4.3 shows the closed cycle efficiency and NOx emissions for the four functions. CDA has a reduced closed cycle efficiency which is the major cause of lower BTE.

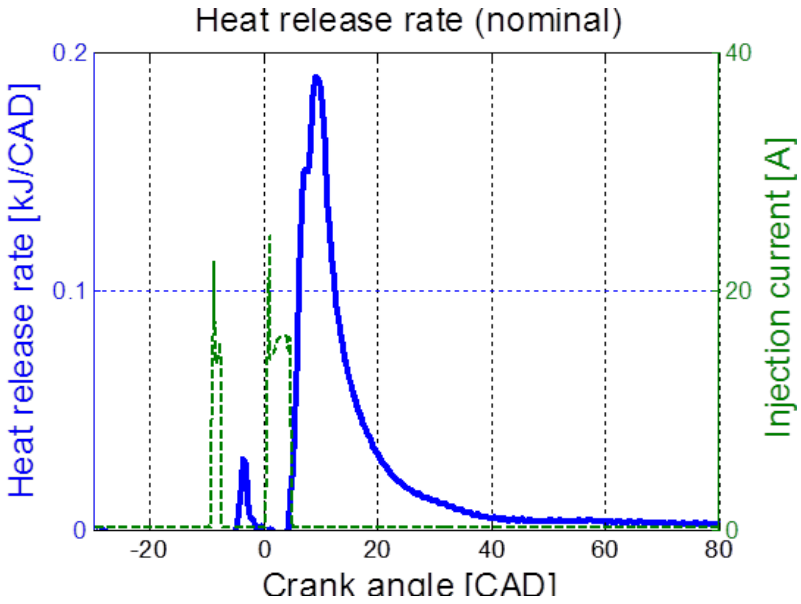

Figure 4.4. Heat release rate with conventional valve profiles.

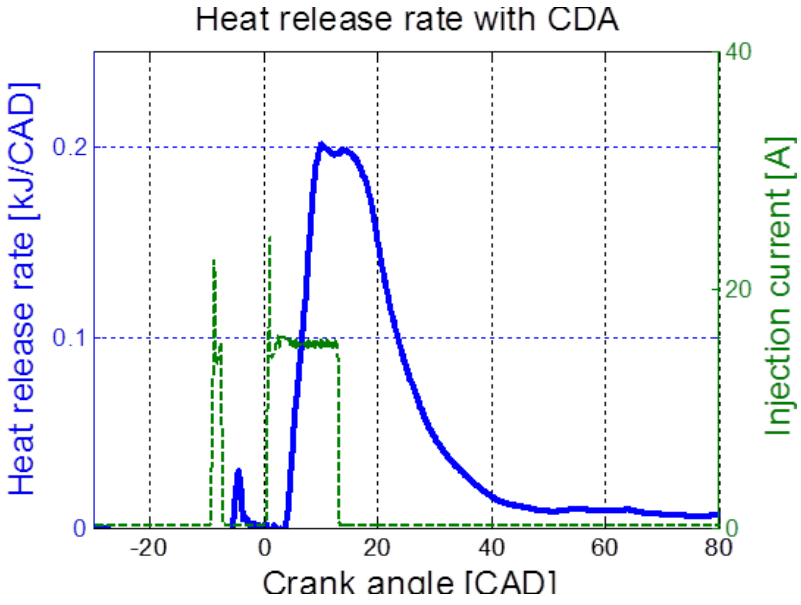

Figure 4.5. Heat release rate with CDA.

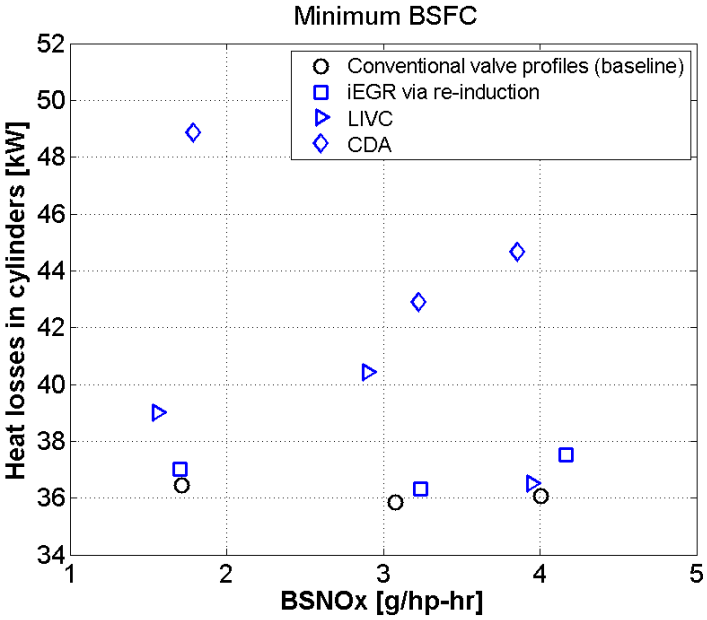

Figure 4.6. In-cylinder heat losses vs BSNOx.

Cylinder deactivation studied in this work is realized by deactivating half of the cylinders based on firing order. The fueling amount per active cylinder in CDA cases are nearly doubled to maintain the same 7.58 bar BMEP relative to nominal operation. As a result, combustion duration is longer and the centroid of heat release is further after TDC than nominal operation as shown in Figs. 4.4 and 4.5. The centroid of heat release is approximately 10 ATDC with conventional valve profiles and 15 ATDC with CDA. This heat release delay causes a reduction in power during the expansion stroke and results in lower closed cycle efficiency. In addition, the longer combustion duration with CDA increases heat losses through the cylinder walls and combustion chamber as shown in Fig. 4.6. The longer combustion process per cylinder increases temperature and residence time of hot burned gases resulting in higher convective heat losses.

4.1.2 Open Cycle and Mechanical Efficiency

As shown in Fig. 4.7 iEGR via re-induction and LIVC have very similar open cycle efficiency as the baseline since the optimizations identify the baseline to be the optimal fuel efficient operation. CDA slightly reduces open cycle efficiency by 1 % ~2 % as the compressor is operating less efficiently. The AFR at the cruise condition is usually close to 25 as shown in Fig. 4.8. CDA reduces engine displacement by 50% resulting in lower AFR close to stoichiometric. The VGT is set to maximize the air flow and the compressor is operating close to the surge line. It results in lower compressor efficiency as well as open cycle efficiency.

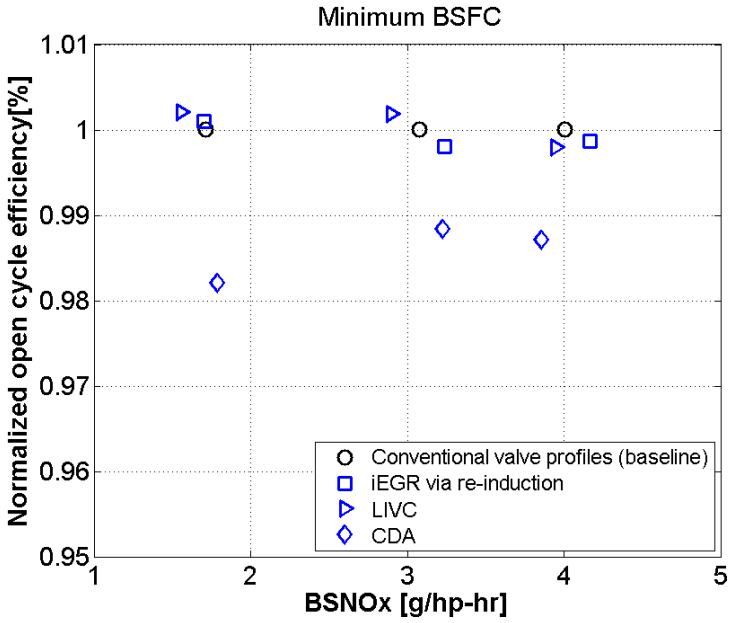

Figure 4.7. Normalized open efficiency vs BSNOx.

The mechanical efficiency of iEGR via re-induction and LIVC are very similar with the baseline as shown in Fig.4.9. The major reason is that the valve motions are driven by external hydraulic power. The valve profiles have no direct influence in mechanical efficiency. The mechanical efficiency is largely depend on in-cylinder pressure and parasitic losses such as high pressure fuel pump. Operations with CDA

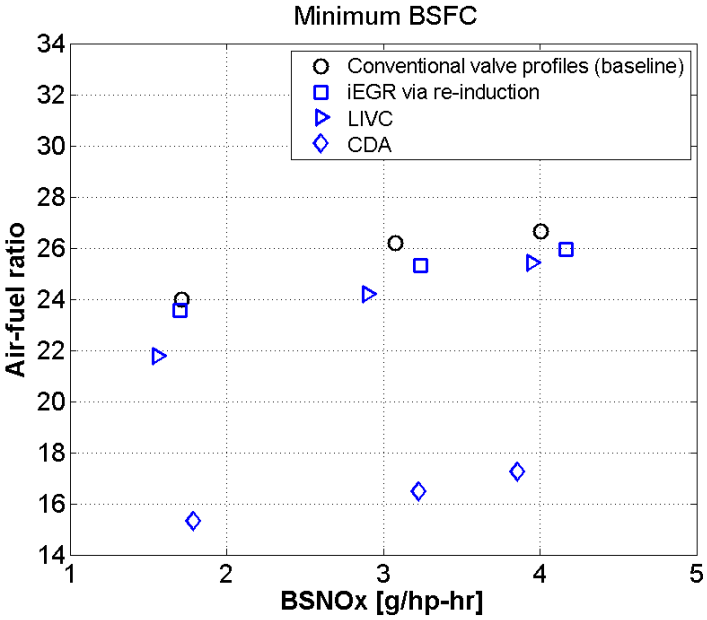

Figure 4.8. Air-fuel ratio vs BSNOx.

generally have longer combustion process and higher in-cylinder pressure, which result in greater frictional losses.

Above all, flexible valve train does not reduce the fuel consumption at cruise condition due to the fact that the engine is calibrated very efficient. However the well calibrated operation focuses on fuel consumption and may not necessarily consider the thermal mangement for aftertreatment system.

4.2 Maximum TOT vs BSNOx Trade-offs

Elevated exhaust temperatures are important for aftertreatment efficiencies. Constrained optimization and experimental validation were conducted to find the maximum TOT that each strategy could provide at three BSNOx levels.

Figure 4.10 presents the trade-off between TOT and BSNOx for conventional operation, iEGR via re-induction, iEGR via NVO, LIVC, and CDA. The TOT achieved with conventional valve profiles optimized for BSFC, indicative of what temperatures

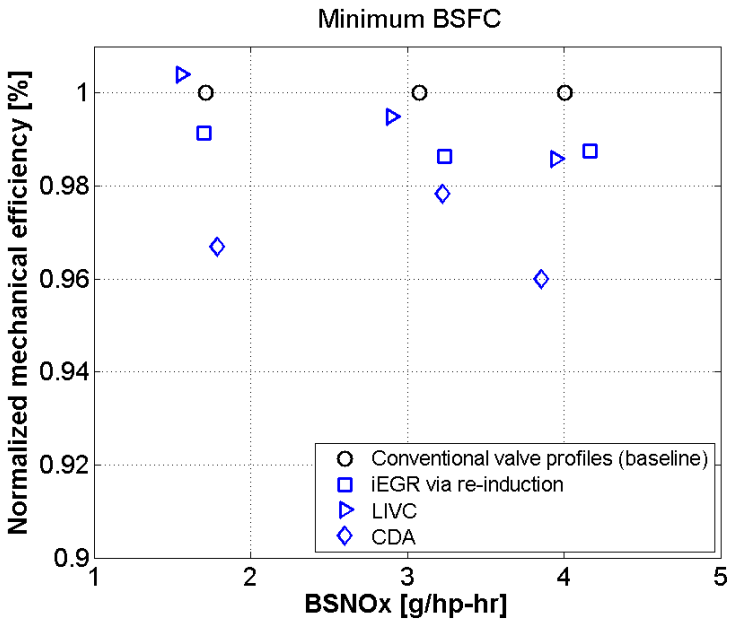

Figure 4.9. Normalized mechanical efficiency vs BSNOx.

would result from normal operation, are shown as a point of reference, the "baseline" in Figs. 4.10 - 4.16.

With conventional valve profiles, the TOT can be increased up to 400°C with retarded combustion as shown in Fig. 4.10. The main injection pulse is delayed from 1.5 to 6.5 ATDC corresponding to a 50°C increase relative to conventional operation optimized to minimize BSFC. Further delaying SOI to 15 ATDC results in higher TOT ∼450°C which is the maximum TOT achieved with conventional valve profiles. Delaying SOI increases exhaust temperature, however, it results in a ∼23% additional fuel cost as shown in Fig. 4.11.

The increase of fuel consumption is mainly due to reduced closed cycle efficiency (per Fig. 4.12) with the delayed fuel injection from baseline (the best BSFC), conventional valve profiles (SOI = 5 ATDC) and conventional valve profiles (SOI = 15 ATDC). Open cycle and mechanical efficiencies (Fig. 4.13 and 4.14) have little variation in these cases.

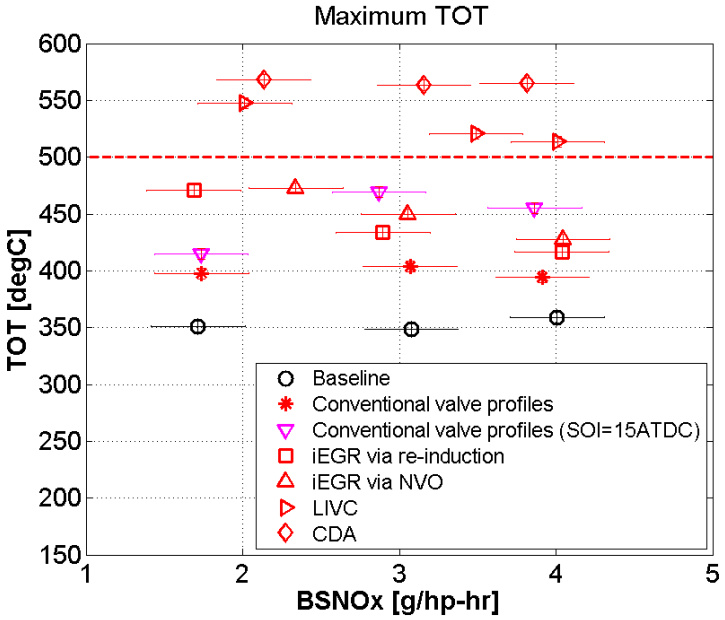

Figure 4.10. Maximum TOT vs BSNOx (500°C represent the minimum temperature for DPF active regeneration).

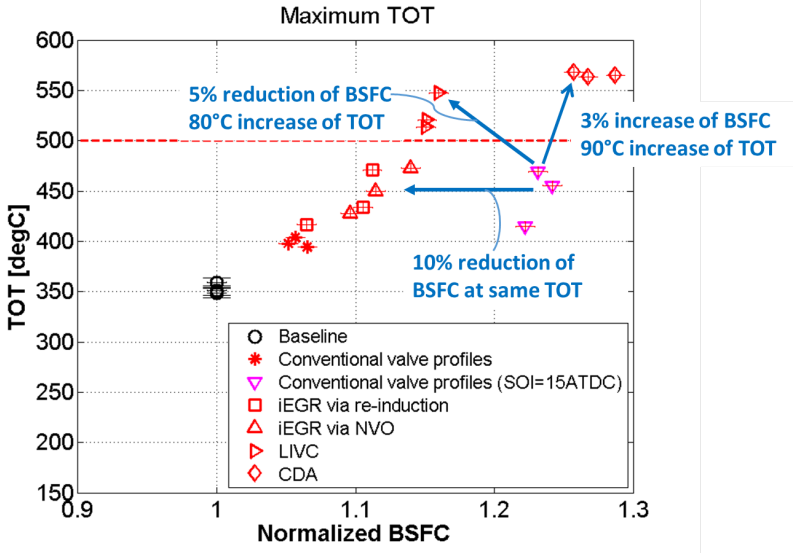

Figure 4.11. Maximum TOT vs BSFC (500°C represent the minimum temperature for DPF active regeneration).

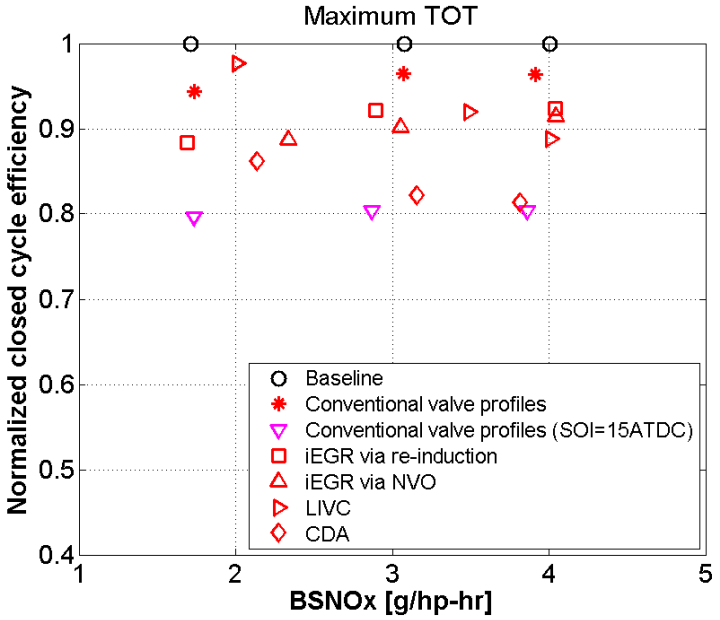

Figure 4.12. Closed cycle efficiency (max TOT).

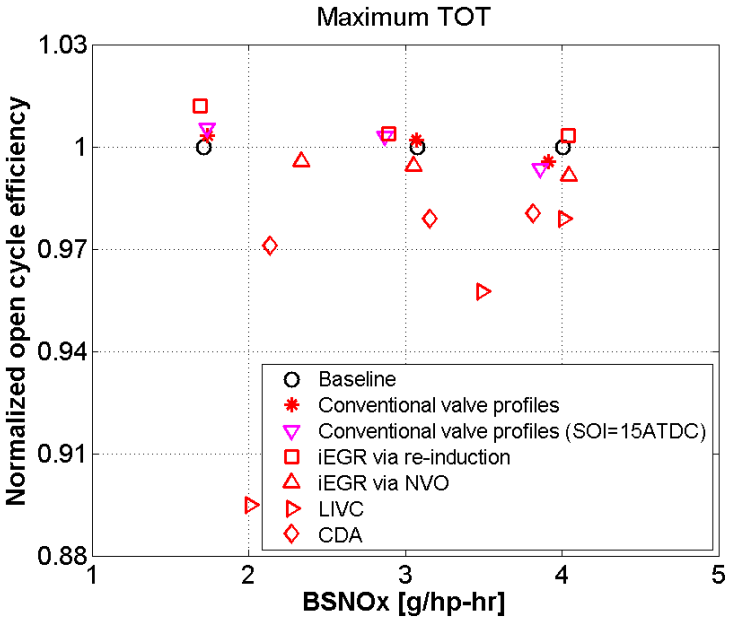

Figure 4.13. Open cycle efficiency (max TOT).

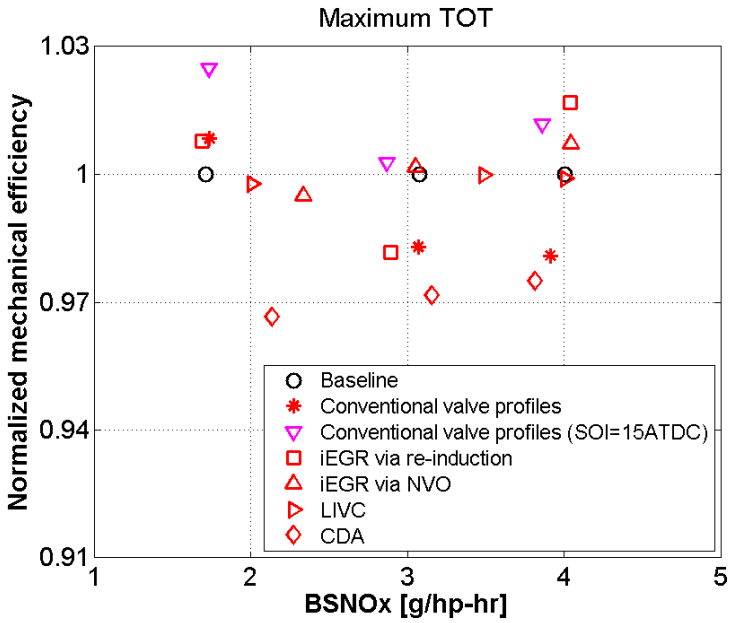

Figure 4.14. Mechanical efficiency (max TOT).

Internal EGR sufficiently meets NOx targets with the external EGR loop shut, except for the NVO case at the 1.5 g/hp-hr BSNOx due to a safety threshold set to limit the amount by which the duration of the intake and exhaust valve profiles could be reduced. This threshold prevented the required amount of residual burned gases from being trapped.

iEGR via re-induction and trapping (NVO) increases TOT to the 450°C corresponding to a ∼10% reduction in fuel consumption (Fig. 4.11) compared with the same temperature achieved by conventional valve profiles and delayed SOI (15 ATDC). iEGR reduces the fuel consumption to achieve the same 450°C due to less heat losses (Fig. 4.15) and higher closed cycle efficiency (Fig. 4.12). iEGR reduces NOx using hot burned gases instead of cooled EGR and delayed SOI. Relative early SOI allows heat release closer to TDC resulting in higher closed cycle efficiency than conventional valve profiles (SOI = 15ATDC). Open cycle efficiency and mechanical

efficiencies (Fig.4.13 and 4.14) are close to the cases using conventional valve profiles. Together iEGR reduces the fuel cost required to achieve 450°C by 10%.

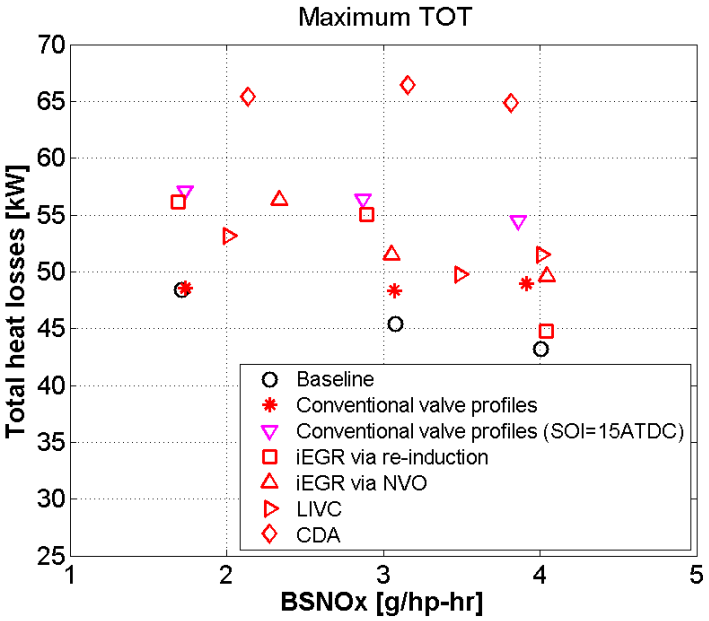

Figure 4.15. Total heat losses vs BSNOx.

LIVC increases TOT by 80°C (above 550°C) with 5% less fuel compared with conventional valve profiles (SOI=15ATDC) as shown in Fig. 4.11. The elevated TOT is due to reduced volumetric efficiency and AFR (per Fig. 4.16). LIVC also decreases the ECR, lowering the in-cylinder pressure and combustion temperature which reduces NOx emission. As such, LIVC allows a selectively early heat release resulting in higher closed cycle efficiency (Fig. 4.12). LIVC throttles the engine by pushing part of the inducted gases pushed back into the intake manifold which leads to slightly lower open cycle efficiency (Fig. 4.13). In addition open cycle efficiency decreases at low NOx levels as IVC timing is further delayed to reduce NOx emission with lower ECR. Mechanical efficiency changes little with IVC modulation (Fig. 4.14). Together these changes result in lower fuel consumption, but higher TOT, exceeding the passive DPF regeneration threshold at approximately 500°C (Fig. 4.10). In

short, LIVC provides another way to reduce NOx and improves the TOT/FC trade-off relative to late injection with conventional operation and the iEGR strategies.

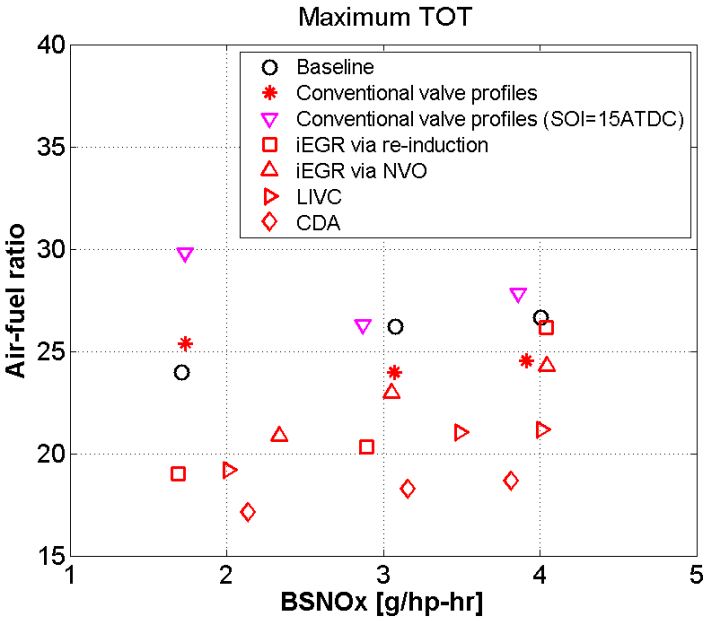

Figure 4.16. Air-fuel ratio vs BSNOx (max TOT).

Similar to LIVC, CDA results in an increase in TOT, which, in general, is above the temperature to start passive DPF regeneration [2]. Using only half of the cylinders reduces the displaced volume as well as AFR (Fig. 4.16) resulting in TOTs up to 560°C (90°C TOT increase) with only ~3% more fuel compared with conventional valve profiles with delayed SOI (per Fig. 4.11). Compared with LIVC, CDA has relatively lower closed cycle efficiency (Fig. 4.12) due to longer combustion process and higher heat losses (Fig. 4.15). Both open cycle and mechanical efficiencies are slightly reduced (Fig. 4.13 and 4.14) due to lower compressor efficiency and increased in-cylinder pressure and friction. Previous optimized BSFC with CDA actually has TOTs around 540°C (Fig. 4.1) with 5% less fuel used compared with conventional valve profiles and delayed SOI. This indicates that the TOT benefit is diminishing with losses in fuel efficiency at elevated TOT.

4.3 Estimated exhaust gas-to-catalyst heat transfer rate

Elevated turbine outlet temperature (TOT), as discussed in Section 4.2, are important for keeping aftertreatment devices hot. However it is convective heat transfer between the exhaust gas and catalyst beds to be the main driver for "heating up" the catalyst material. Using Eq. (3.2) the normalized heat transfer can be plotted as a function of catalyst temperature.

The normalized heat transfer rate increases as the fuel injection is delayed with conventional valve profiles at 1.5 g/hp-hr BSNOx as shown in Fig. 4.17. Case with delayed SOI will warm-up the catalysts more quickly, and can sustain bed temperatures of 400°C, whereas the baseline case will cool down the catalysts when above ∼350°C. This increase of heat transfer rate is consistent with the increased fuel consumption. The heat transfer rates for "conventional valve profiles (SOI = 15 ATDC)" are ∼75% and ∼200% higher than the baseline operation for bed temperatures of 100 and 300°C, respectively.

The normalized heat transfer rate is also calculated at different bed temperatures for the "iEGR via re-induction", "iEGR via NVO", "LIVC" and "CDA" cases as shown in Fig. 4.18. Cases with iEGR will warm-up the catalysts more quickly, and can sustain bed temperatures of 450°C. The increase of heat transfer rate corresponds to an 11%-14% increase of fuel consumption. LIVC further increases the heat transfer rate across different catalyst bed temperature and can sustain temperature of 550°C. The heat transfer rates for "LIVC" are ∼65% and ∼240% higher than the baseline operation for bed temperatures of 100 and 300°C, respectively. "CDA" slightly improves the heat transfer rate but the fuel consumption increases by 9% with this diminishing return compared with LIVC case.

A comparison is made in cases of "conventional valve profiles (SOI = 15 ATDC)", "LIVC" and "CDA", which have relatively high heat transfer rates with different bed temperatures. The delayed fuel injection strategy without VVA functions allows higher heat transfer rate at bed temperature below 150°C (Fig. 4.19). Both LIVC and

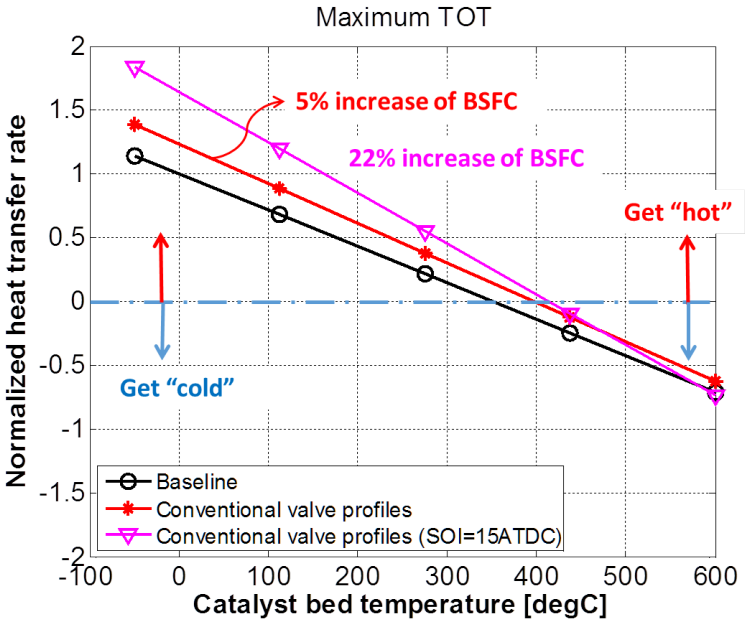

Figure 4.17. Estimated exhaust gas-to-catalyst heat transfer rate with conventional valve profiles (1.5 g/hp-hr BSNOx).

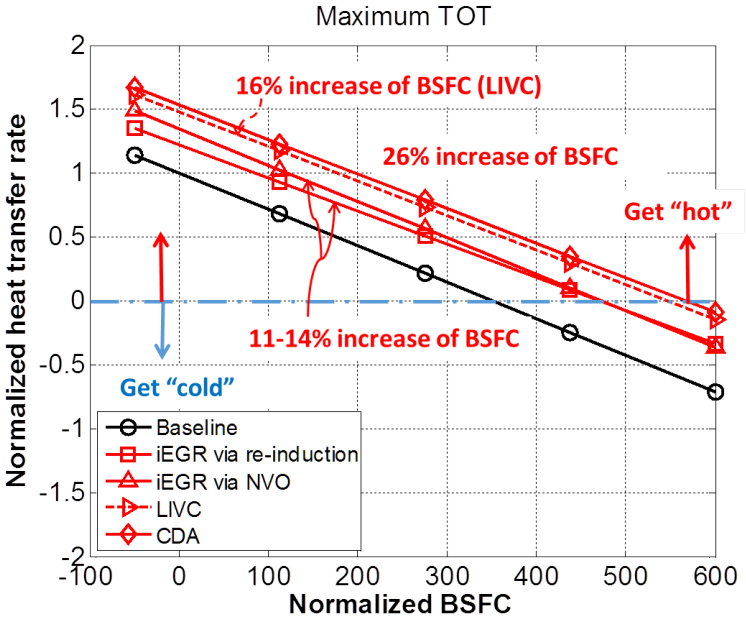

Figure 4.18. Estimated exhaust gas-to-catalyst heat transfer rate with VVA functions (1.5 g/hp-hr BSNOx).

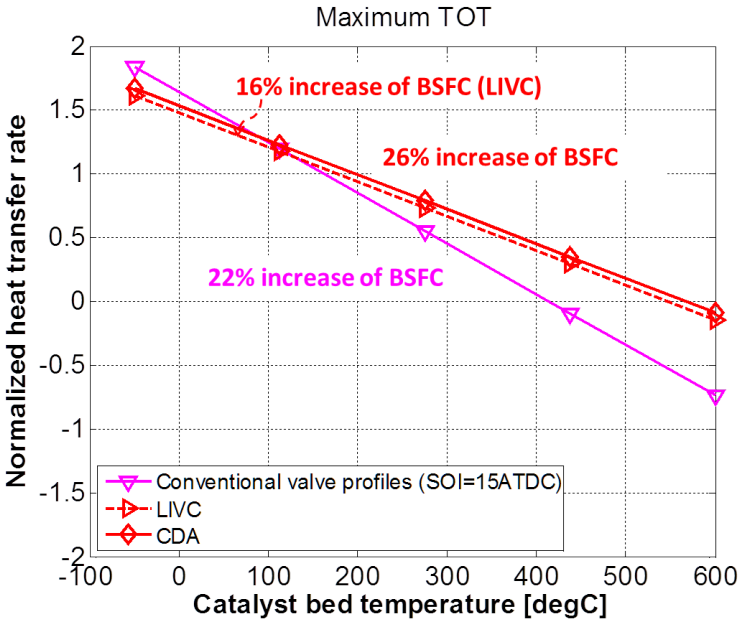

Figure 4.19. Estimated exhaust gas-to-catalyst heat transfer rate with LIVC and CDA (1.5 g/hp-hr BSNOx).

CDA promote a better heat transfer rate at bed temperature above 150°C. The heat transfer rates for LIVC are ~50% and ~560% higher than the delayed SOI strategy for bed temperatures of 300 and 400°C, respectively. Similarly the heat transfer rates for CDA are ~60% and ~650% higher than the delayed SOI strategy for bed temperatures of 300 and 400°C, respectively. In addition the fuel consumption using LIVC is lower than CDA and conventional valve profiles with delayed SOI. And as such, the LIVC based strategy is the most effective way to "warm-up" the aftertreatment at the "high-way cruise" operating condition.

Cases at 3 and 4 g/hp-hr BSNOx generally follow the same trend of 1.5 g/hp-hr case as shown in Fig. 4.20-4.23. iEGR via re-induction and NVO will warm-up the catalysts more quickly, and can sustain bed temperatures of ~450°C, whereas the baseline case will cool down the catalysts when above ~350°C. LIVC and CDA further increase the heat transfer rate and can keep bed temperature of ~550°C.

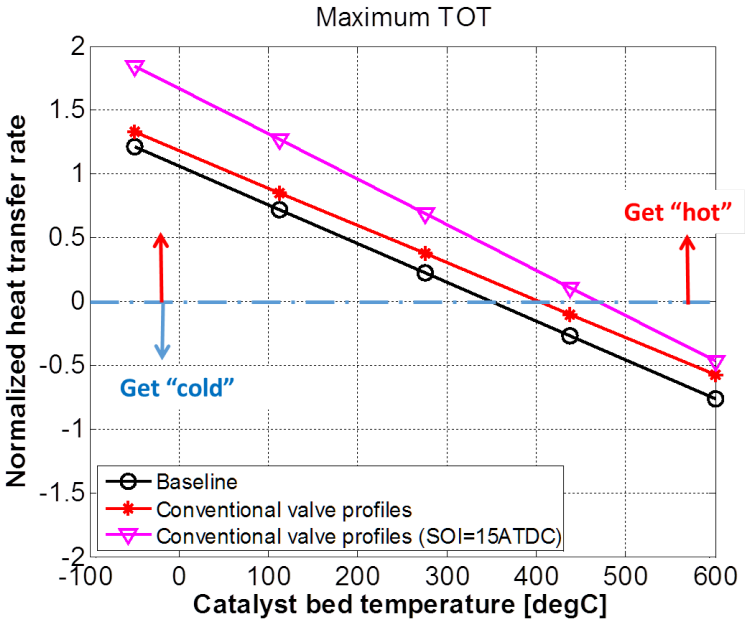

Figure 4.20. Estimated exhaust gas-to-catalyst heat transfer rate with conventional valve profiles (3 g/hp-hr BSNOx).

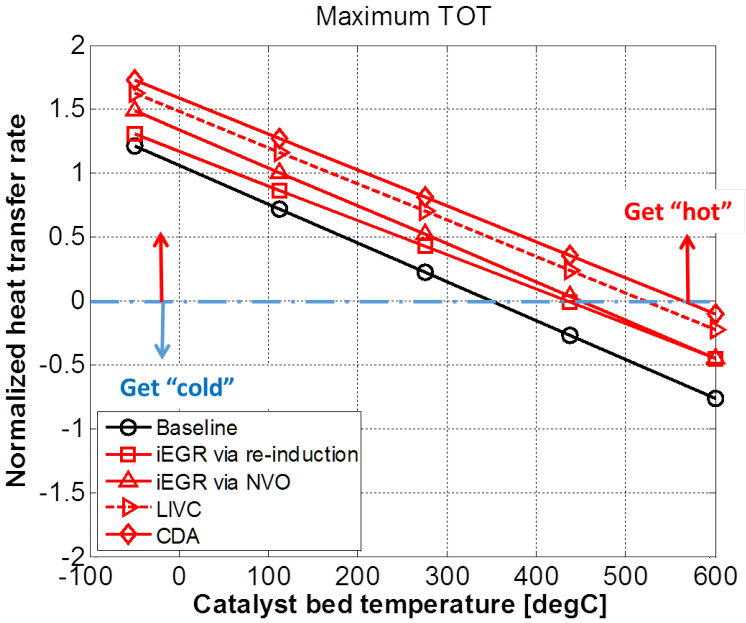

Figure 4.21. Estimated exhaust gas-to-catalyst heat transfer rate with VVA functions (3 g/hp-hr BSNOx).

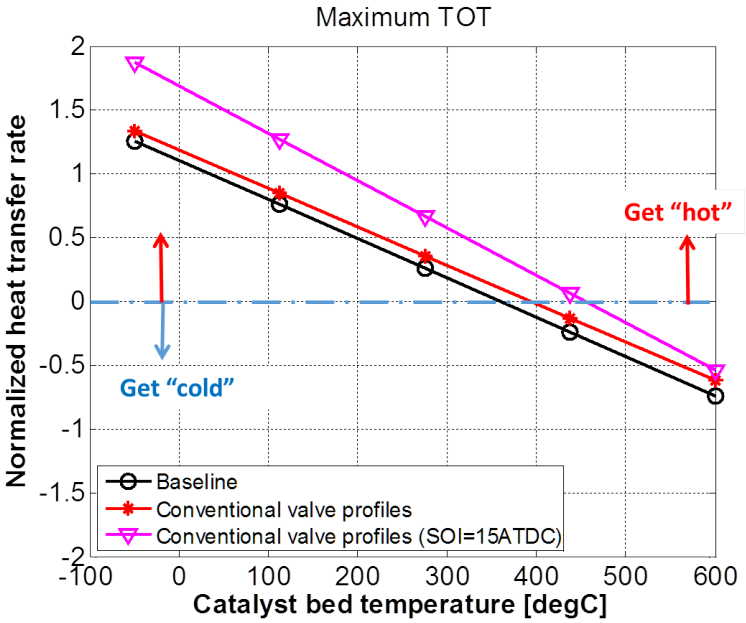

Figure 4.22. Estimated exhaust gas-to-catalyst heat transfer rate with conventional valve profiles (4 g/hp-hr BSNOx).

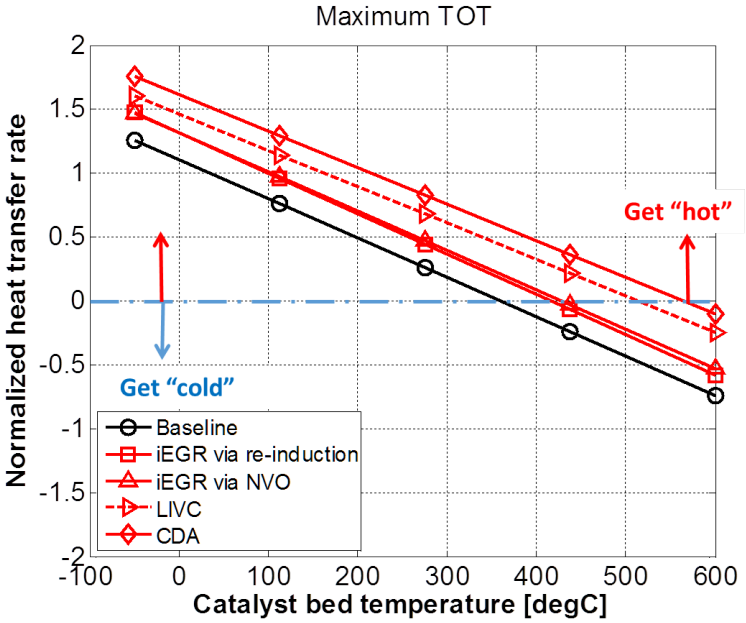

Figure 4.23. Estimated exhaust gas-to-catalyst heat transfer rate with VVA functions (4 g/hp-hr BSNOx).

4.4 UHC and PM

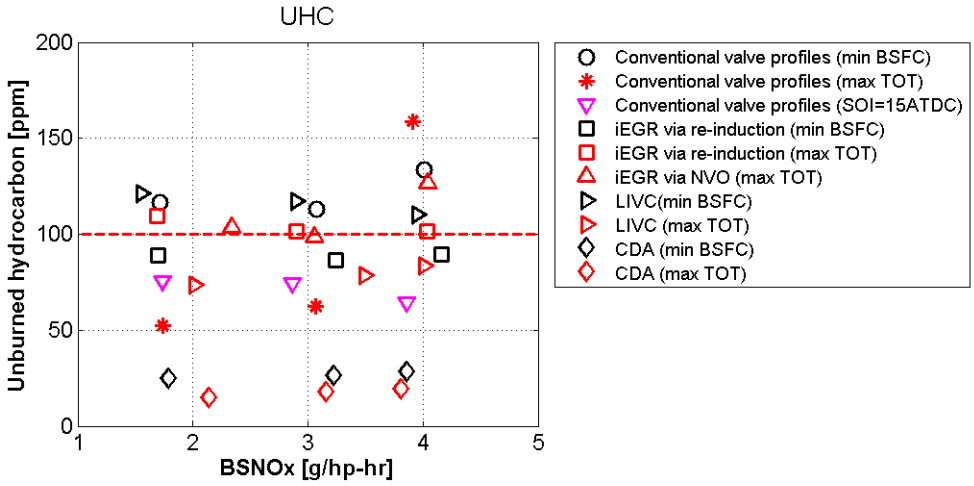

Figure 4.24. Unburned hydrocarbon.

The limit of UHC is 100 ppm and most of the cases especially those using flexible valve train are below or close to 100 ppm as shown in Fig.4.24.

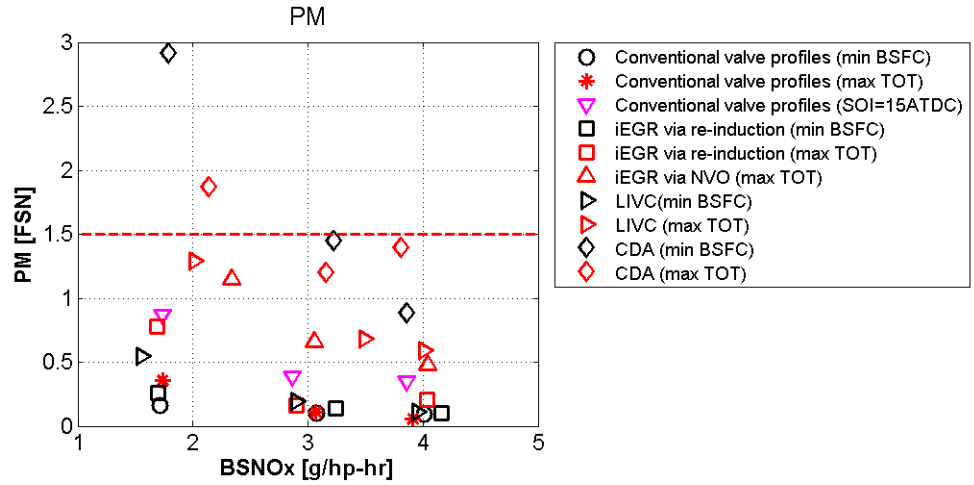

Figure 4.25. Particulate matter.

The constraint for PM measured from AVL analyzer is 1.5 FSN. Most of the cases satisfy this emission constraint with the exception of the 1.5 g/hp-hr BSNOx point in CDA operation as shown in Fig.4.25. The AFR with CDA is significantly lower than points where all cylinders are used. AFR is even lower for the 1.5 g/hp-hr BSNOx case where more EGR is required for NOx reduction as shown in Fig. 4.8 and 4.16. Soot is a big issue at low AFR conditions. Even with VGT, AFR is still around 16 with CDA at lowest NOx cases. With priority given to BSNOx the EGR valve and VGT actuators could not be set such that 1.5 FSN limit for PM could be met with CDA at 1.5 g/hp-hr BSNOx.

4.5 Model and Experiment Comparison

The experimental work in this chapter was guided from optimization using the simulation tools. The model was calibrated to predict the steady state engine operation on the test bed. The comparison between simulation and experiment results are shown in Fig. 4.26. The horizontal error bars represent error observed in repeat points taken at the beginning and end of each experiment. Generally the model is consistent with experimental results in fuel economy (BSFC), BSNOx and exhaust temperature (TOT). The model provides a convenient and efficient way to find the optimal operation with different strategies using flexible valve-train. The experimental validations demonstrate the solid proof of optimized results and support the analysis in this chapter.

4.6 Summary

This chapter investigated potential benefits of utilizing flexible valve actuation on a diesel engine at an operating condition consistent with highway cruise. The key findings include:

1. iEGR, LIVC and CDA bring no benefit in engine-specific fuel economy over conventional valve profiles at 1.5, 3 and 4 g/hp-h BSNOx levels. The valve profiles of

iEGR and LIVC are optimized back to conventional valve profiles and fuel economy is worse with CDA due to higher heat losses and delayed combustion. This result is not surprising as efficiency maximized at "highway cruise" conditions is a primary focus of conventional engine design.

2. Conventional operation increases TOT from 350°C to 450°C with delayed SOI resulting in a 23% increase of fuel consumption. iEGR via re-induction or NVO reduces the fuel consumption by 10% at same TOT due to lower total heat losses and AFR. LIVC increase TOT up to 550°C with 5% less fuel used compared with conventional valve profiles at 450°C. CDA further maximizes TOT above 550°C with additional 3% fuel used due to lower AFR.

3. iEGR via re-induction and NVO will warm-up the catalysts more quickly, and can sustain bed temperatures of ∼450°C, whereas the baseline case will cool down the catalysts when above ∼350°C. LIVC and CDA promote a better heat transfer rate at bed temperature above 150°C for 1.5 g/hp-hr BSNOx compared with the highest heat transfer rate with conventional valve profiles using delayed SOI. Both LIVC and CDA can keep catalyst bed temperature of ∼550°C and LIVC has lower fuel cost.

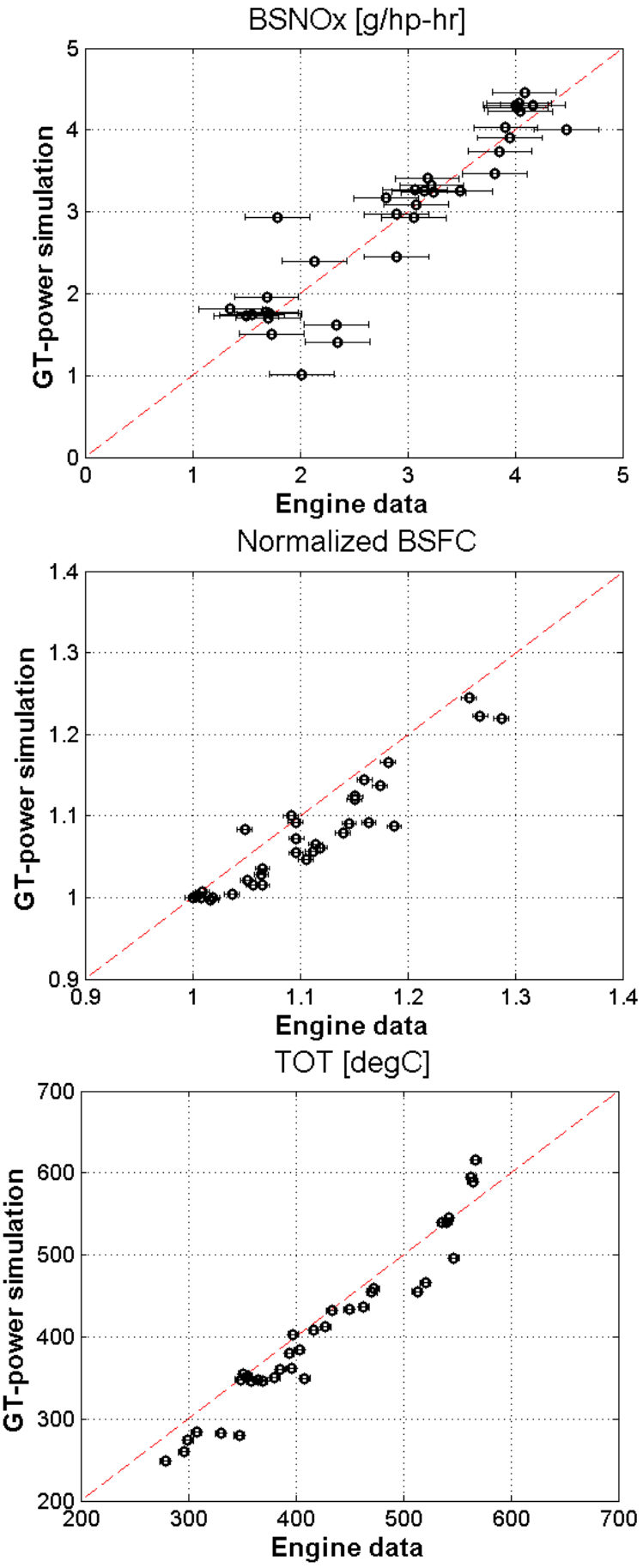

Figure 4.26. GT-power and Engine data comparison.

5. SIMULATION EXPLORATION OF MILLER CYCLE WITH ELEVATED GCR

Elevated geometric compression ratio (GCR) typically leads to better thermal efficiency, however, the application is constrained by physical limits such as peak cylinder pressure (PCP) and turbine inlet temperature (TIT), particularly at, or near, rated condition. Miller cycling reduces the amount of effective compression which is a promising method to enable the engine running on the torque curve without violating mechanical constraints. Miler cycling can improve the BSNOx/fuel consumption trade-off by allowing early combustion event. In addition, the reduction in the effective compression ratio can enable the use of higher GCR, even at the rated engine condition. This chapter explores both potential benefit of Miller cycling with elevated GCR. Five operating conditions were selected and analyzed using simulation method as shown in Fig. 5.1.

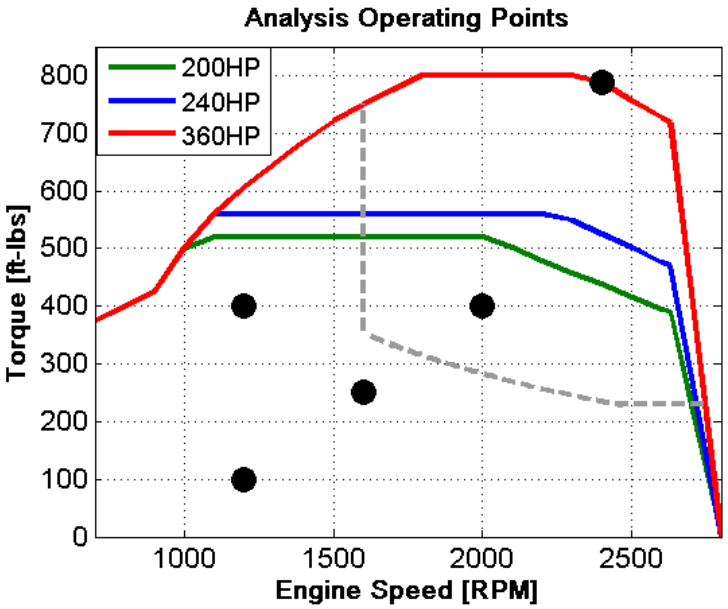

Figure 5.1. Operating conditions selected for Miller cycling at elevated GCR analysis.

5.1 Miller Cycling with Variable GCR

The stock geometric compression ratio of the engine is 16.9. Higher GCR were investigated to explore thermal efficiency and emission control of a diesel engine that also includes the ability to modulate IVC via EIVC or LIVC.

5.1.1 GCR 16.9, 20 and 23

GCR 16.9, 20 and 23 were selected to analyze fuel economy at 1200 RPM and 400 ft-lbf operating condition. Figure 5.2 shows that BSFC decreases as GCR increases through BSNOx between 4 g/hp-h and 10 g/hp-h. The highest GCR of 23 reduces the fuel consumption by 3% and 1.5% compared with the baseline (GCR of 16.9) at 4 g/hp-hr and 8 g/hp-hr BSNOx separately.

The brake thermal efficiency (Fig. 5.3) increases with high GCR, which is consistent with the BSFC results (Fig. 5.2). The BTE improvement is the result of higher closed cycle efficiency (Fig. 5.4) due to centralized heat release profiles with high GCR (Fig. 5.5) for three points picked at 3.9 g/hp-h BSNOx on trade-off curve (Fig. 5.2). Moreover the piston work increases with higher expansion ratio, which also results in higher closed cycle efficiency.

The open cycle efficiency (Fig. 5.6) has little variation with variable GCR. Theoretically mechanical efficiency decreases as GCR increases because of higher friction losses associated with elevated in-cylinder pressure. Chen-Flynn model is used to capture this effect in Eq. (5.1). The friction mean effective pressure (FMEP) is related with peak cylinder pressure (PCP) and mean piston speed (which is constant at a certain engine speed). Elevated GCR realized by reducing clearance volume at top of the cylinders does not influence the motion of piston. The FMEP is dominated by PCP in this simulation which is a reasonable approximation. Elevated GCR has slightly higher friction losses due to higher PCP resulting in a decrease of mechanical efficiency as shown in Fig. 5.7. The model captures the effect of elevate GCR as GCR16.9 has higher mechanical efficiency than GCR20 and GCR23.

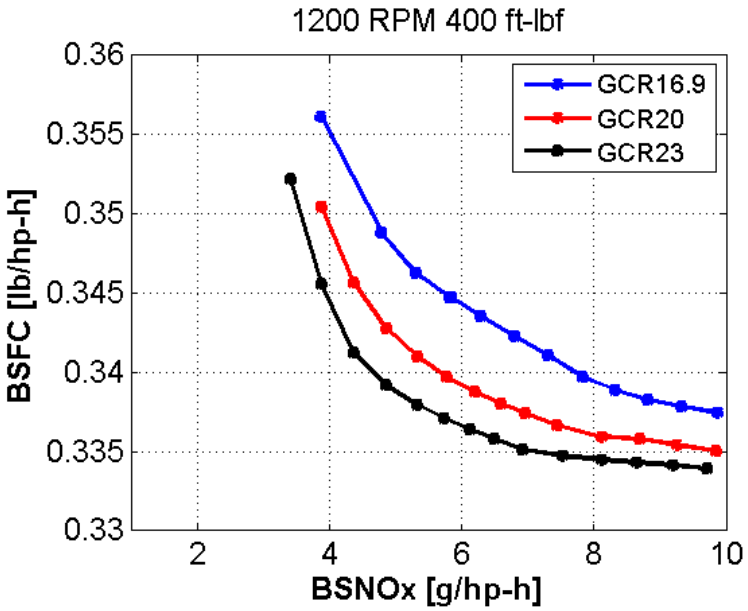

Figure 5.2. GCR varying BSFC vs BSNOx trade-off.

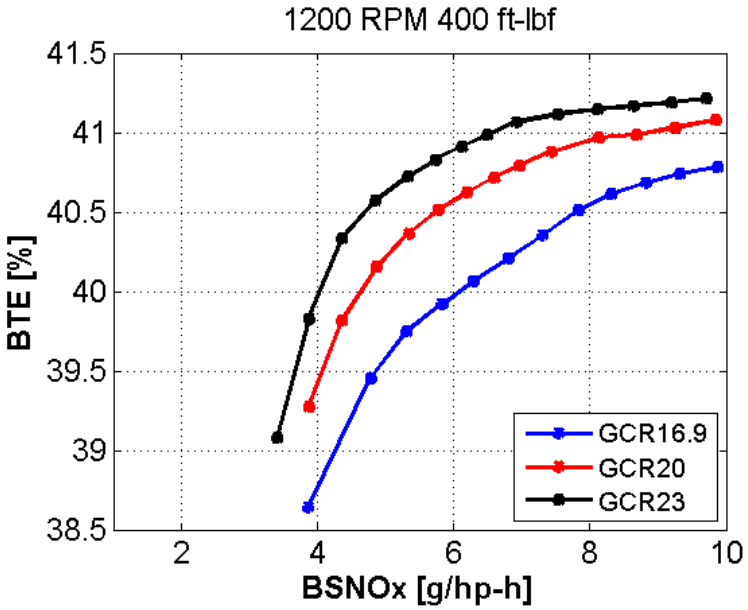

Figure 5.3. GCR varying BTE.

$$\text{FMEP} = A + B \times (\text{PCP}) + C(\text{mean piston speed}) + D(\text{mean piston speed})^2, \tag{5.1}$$

A B C D are coefficients.

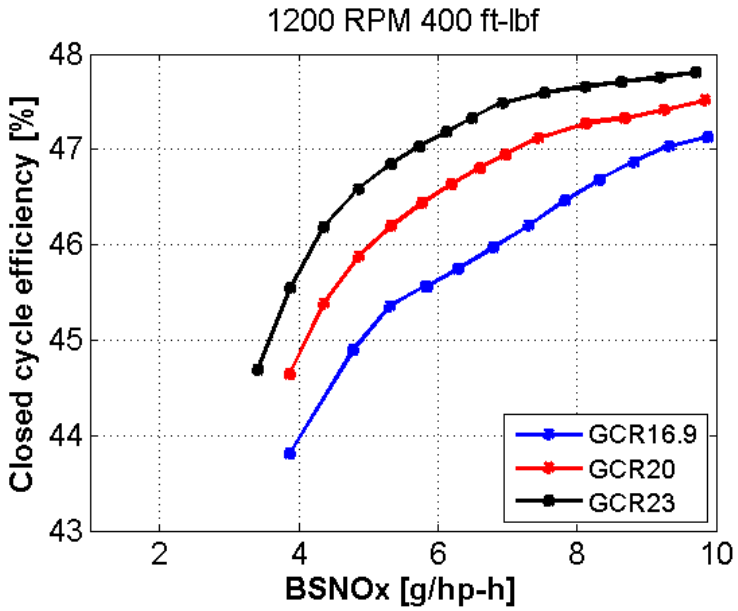

Figure 5.4. GCR varying closed cycle efficiency.

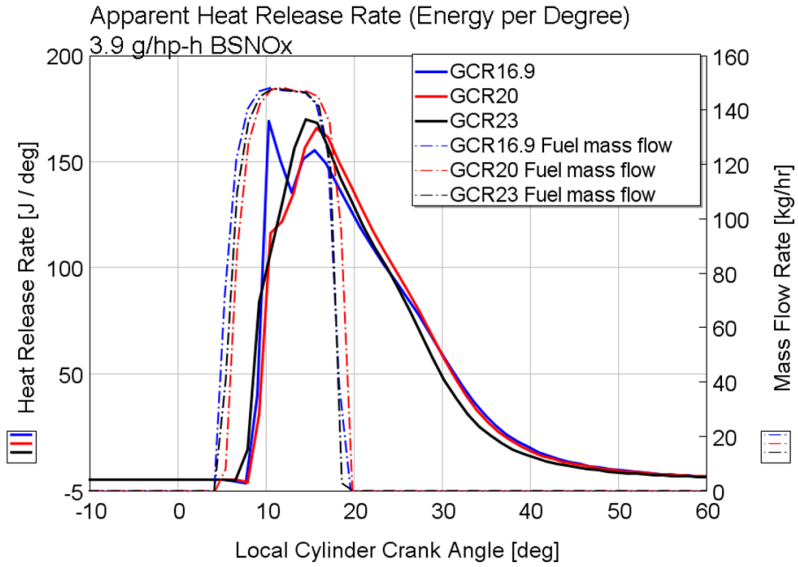

Figure 5.5. GCR varying heat release rate.

Together, the balance in increased closed cycle efficiency, similar open cycle efficiency and reduced mechanical efficiency results in higher BTE and better fuel econ-

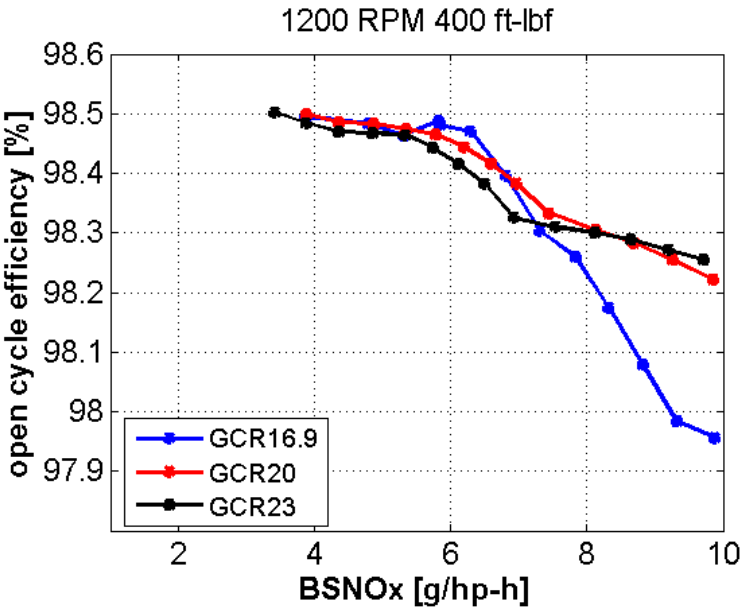

Figure 5.6. GCR varying open cycle efficiency.

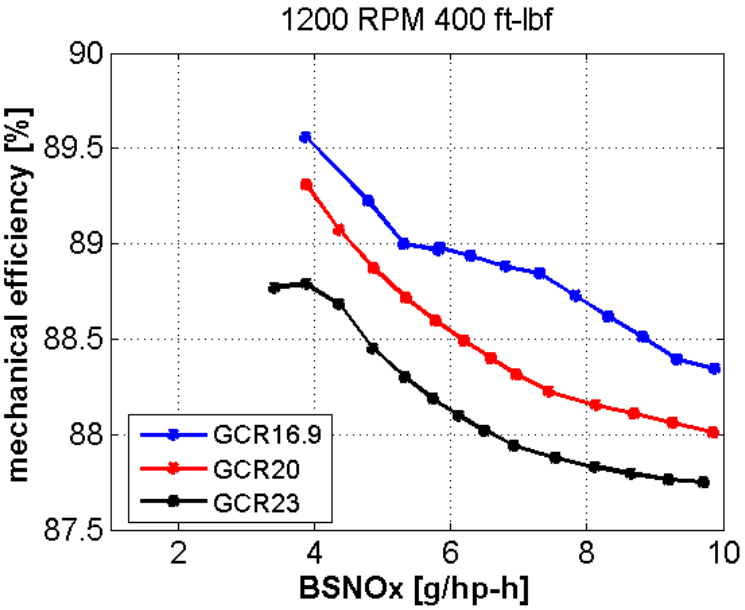

Figure 5.7. GCR varying mechanical efficiency.

omy with elevated GCR. The best scenario is GCR of 23, which increases BTE by 1.2% at 3.9 g/hp-h BSNOx.

5.1.2 Miller Cycling with Variable IVC Timing

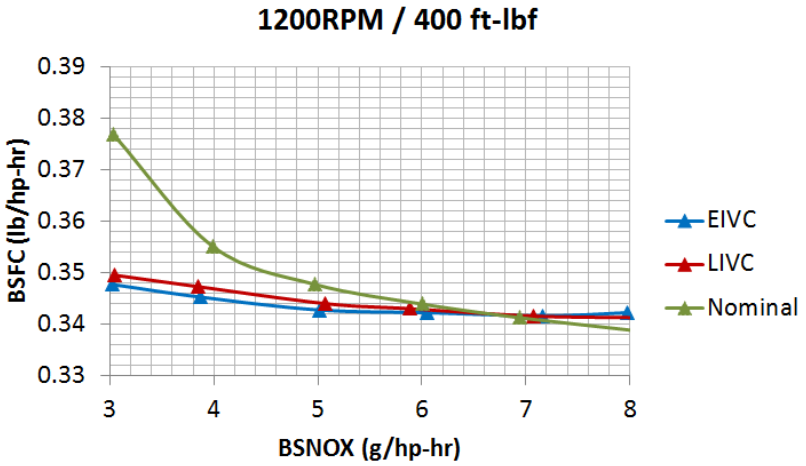

Figure 5.8. Miller cycling BSFC vs BSNOx trade-off curves.

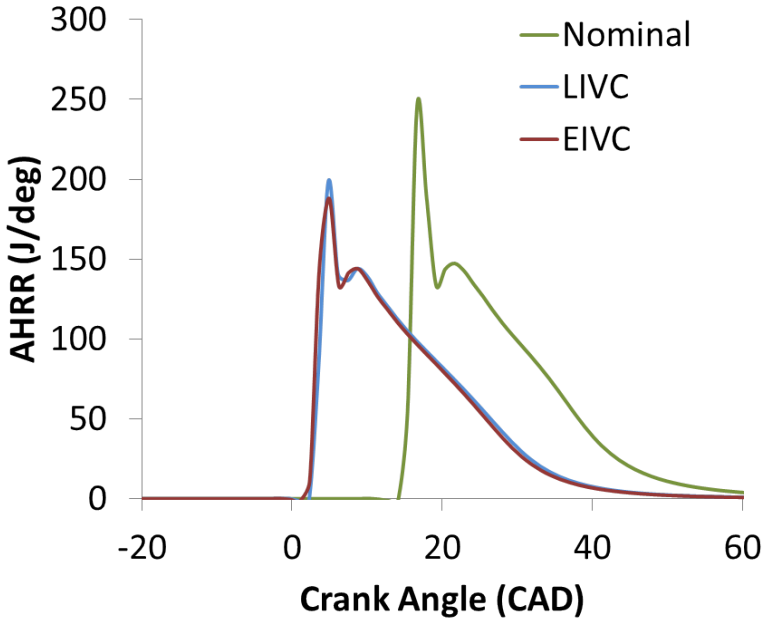

Figure 5.9. Miller cycling heat release at 3 g/hp-h BSNOx.

Miller cycling reduces NOx with lower piston-motion induced compression which decreases in-cylinder temperature (a BSNOx reducer), allowing earlier heat release (which decreases BSFC) at same BSNOx.

Figure 5.8 shows three BSFC and BSNOx trade-off curves corresponding to "EIVC", "LIVC" and the nominal case with conventional IVC timing. Miller cycling via EIVC/LIVC reduces the ECR resulting in lower in-cylinder pressure and temperature. The reduced temperature decreases NOx formation rate, thus the amount of NOx produced in the combustion process. Miller cycling, without increase NOx emissions, enables earlier combustion timing strategy to improve the closed cycle efficiency. EIVC/LIVC is able to advance the heat release profile closer to TDC than the nominal case (Fig. 5.9) at 3 g/hp-h BSNOx. Moreover, the reduced in-cylinder pressure and temperature will help elevated GCRs meet with physical constraints at high load conditions.

5.1.3 Variable IVC Timing at High GCR

The optimization of BSFC at certain BSNOx levels were performed for three GCRs separately at the 1200 RPM and 400 ft-lbf operating condition, as shown in Table 5.1. The table details the optimized range for each independent variables including IVC timing and other production actuators to control the air handling and fuel injection systems. The nominal IVC timing is 565 CAD and varies between 520 CAD and 620 CAD. EIVC and LIVC are optimized separately to avoid multiple optimal results in the design of experiment. The fuel injection timing (SOI) is optimized near the top dead center (TDC) where fuel energy is mostly efficient in generating power.

Cases with GCR at 16.9 (Fig. 5.10) provides the baseline for a fair comparison among different GCRs. As expected, BSFC decreases as GCR increases from 16.9 to 20 and 23 at a fixed BSNOx. Longer expansion ratio associated with high GCR increases the piston work reducing the fuel consumption. EIVC has slightly better BSFC/NOx trade-off compared with LIVC at both GCR20 and GCR23 as EIVC is more efficient in reducing NOx. LIVC increases the temperature of charged air as hot residual gases are pushed back into the intake manifold. The temperature increase of charged air results in higher NOx emission. EIVC/LIVC reduces the lowest achievable

Table 5.1. Optimized Parameters of Variable IVC Timing at Elevated GCR.

Parameter Name	Unit	**GCR16.9**	**GCR20**	**GCR23**
EIVC	ATDC	565	520 – 556	520 – 551
LIVC	ATDC	565	578 – 620	578 – 620
ECR		17.6	18.5 – 20.7	21.2 – 23.8
VGT Closed	%	0 (full open) – 61	13 – 58	6 – 61
Main SOI	ATDC	-3.1 – 2.8	-2.5 – -0.6	-1.5 – 0.8
Rail Pressure	bar	700 – 762	700 – 991	700 – 1154

BSNOx ∼2 g/hp-hr with reduced ECR. The best BSFC/NOx trade-off in these cases is EIVC with highest GCR23 which increases BSFC by 5% (per Fig. 5.10) and BTE by 2% (per Fig. 5.11) compared with the baseline (GCR16.9) at 3.9 g/hp-hr BSNOx.

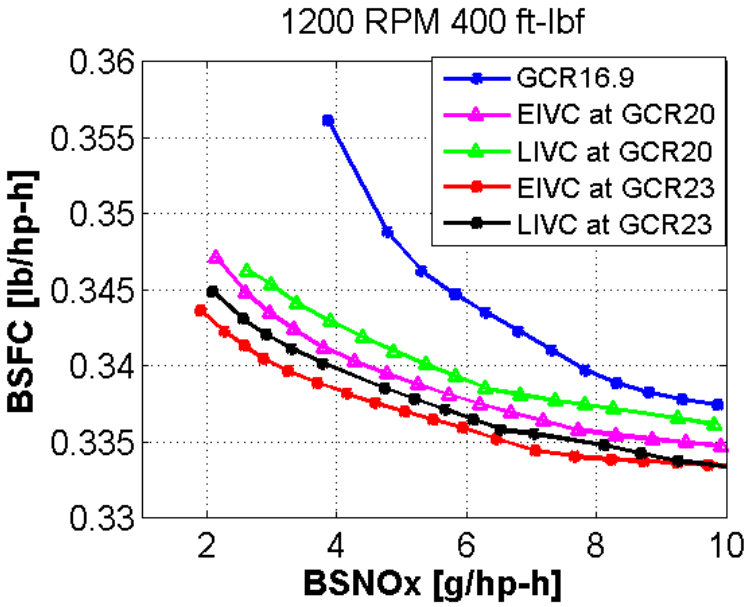

Figure 5.10. BSFC vs BSNOx trade-off of variable IVC timing at elevated GCR.

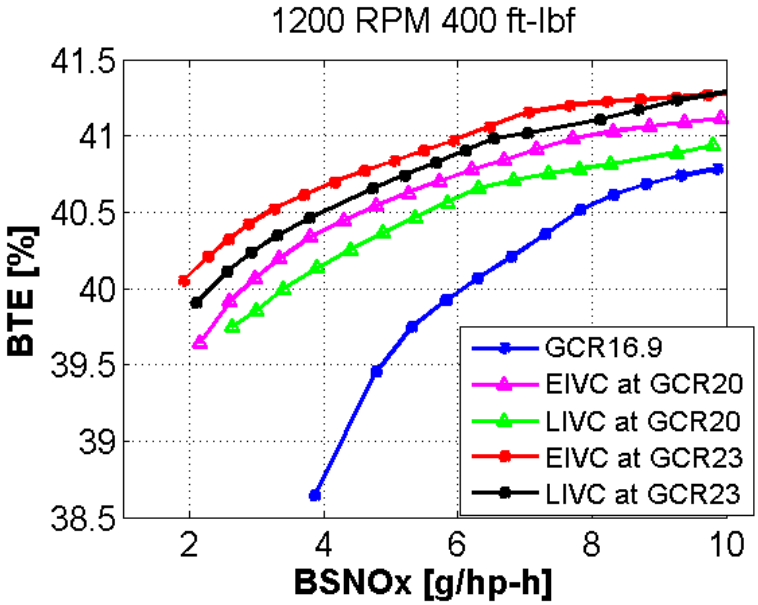

Figure 5.11. BTE of variable IVC timing at elevated GCR.

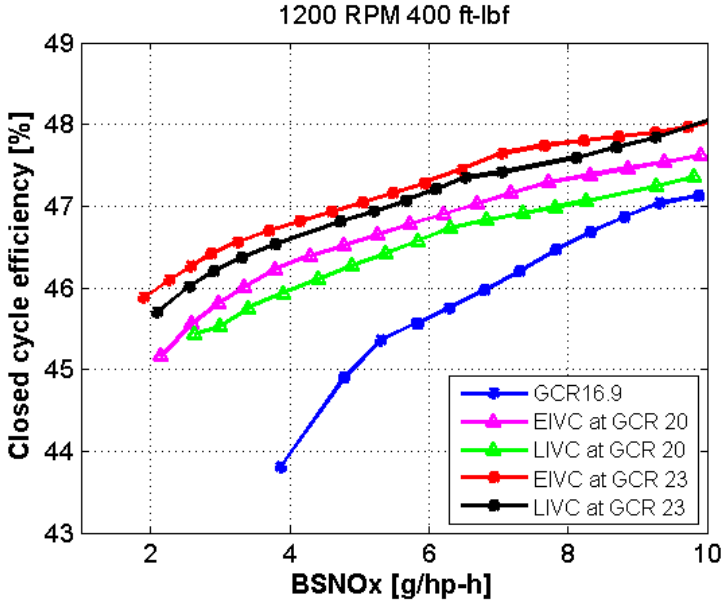

Figure 5.12. Variable IVC timing at high GCR closed cycle efficiency.

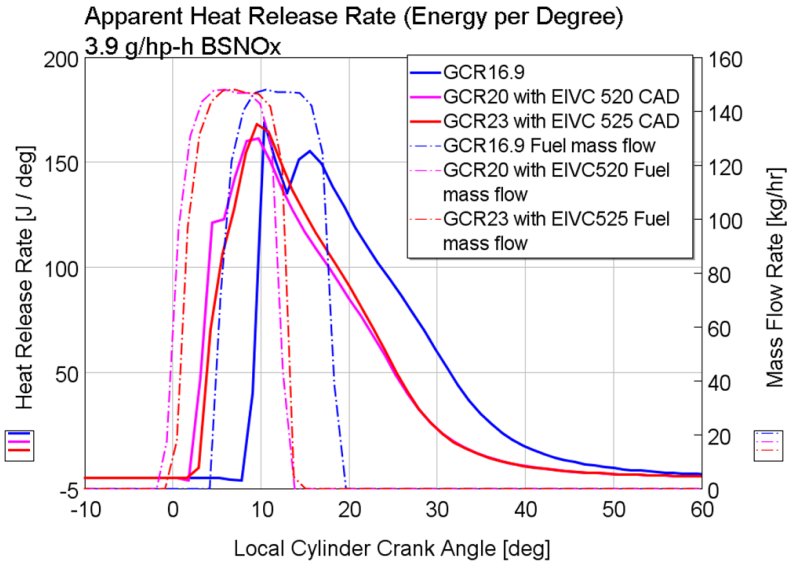

Figure 5.13. Variable IVC timing at high GCR heat release rate.

The improvement of BSFC and BTE is mainly due to increased closed cycle efficiency with elevated GCR as shown in Fig. 5.12. Closed cycle efficiency increases with elevated GCR and Miller cycling due to early and centralized heat release. Miller cycling (EIVC/LIVC) reduces NOx via a reduced ECR allowing an earlier heat release closer to TDC (Fig. 5.13) resulting in higher closed cycle efficiency. Higher GCR increases piston work via longer expansion ratio also resulting in higher closed cycle efficiency. EIVC with GCR23 has the highest closed cycle efficiency (Fig. 5.12) corresponding to the highest BTE (Fig. 5.11) among the five scenarios.

Open cycle efficiency has little variation among cases explored at this operating condition as shown in Fig. 5.14. The similar open cycle efficiencies are the result of optimized gas exchange process. For instance, VGT is squeezed to boost air flow compensating the reduced air flow with Miller cycling. Mechanical efficiency decreases with elevated GCR as shown in Fig. 5.15. Together the increased closed cycle efficiency (Fig. 5.12) and lower mechanical efficiency (Fig. 5.15) result in higher BTE with Miller cycling at elevated GCR.

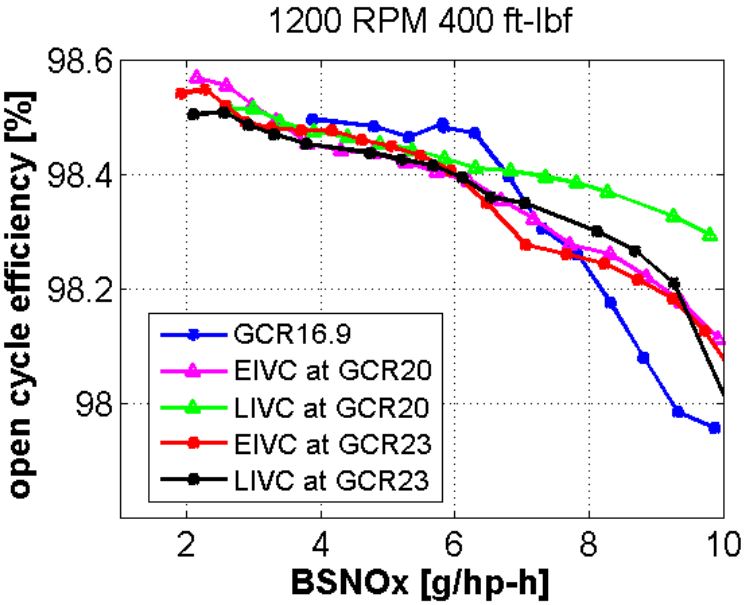

Figure 5.14. Variable IVC timing at high GCR open cycle efficiency.

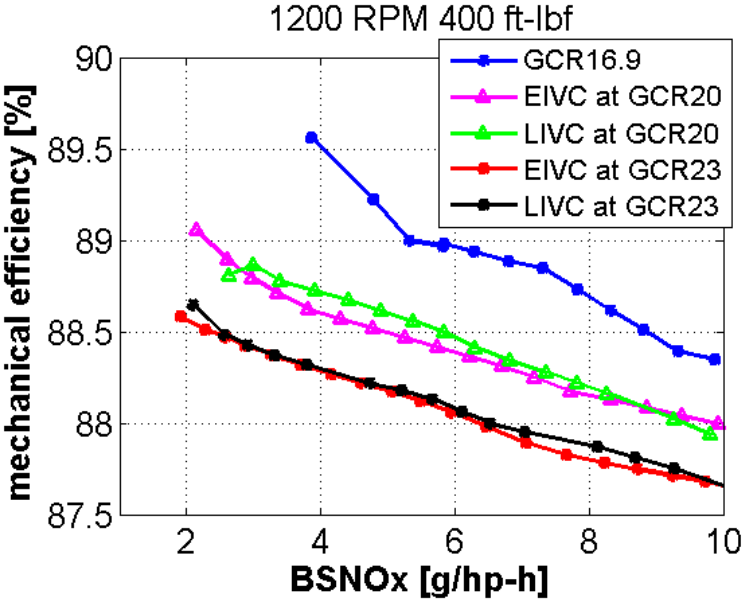

Figure 5.15. Variable IVC timing at high GCR mechanical efficiency.

5.1.4 EIVC and LIVC

Miller cycling is realized by advancing or retarding the IVC timing to reduce ECR. Although both EIVC and LIVC can effectively reduce ECR lowering NOx emission, LIVC is not as efficient as EIVC in NOx control perspective due to higher charged gas temperatures which increase the NOx formation rate.

Effective compression ratio is defined as the effective volume at intake valve closure over clearance volume when the piston reaches the top dead center position as shown in Eq. (5.2). This pressure based ECR calculation takes into account the piston-motion induced compression. The corresponding ECRs at difference IVC timing between 520 CAD and 620 CAD are shown in Fig. 5.16. The peak ECR is 24 at nominal IVC, 565 CAD. EIVC advances IVC by 45 degrees (to 520 CAD) reducing ECR to 20.6. LIVC delays IVC by 45 CAD (to 610 CAD) reduces ECR to 22. The results demonstrate that EIVC is more effective in reducing ECR with same distance from the nominal IVC compared with LIVC.

$$ECR = \frac{V_{ivceff}}{V_{tdc}}. \tag{5.2}$$

EIVC/LIVC reduces the temperature and pressure before combustion occurrs as shown in Fig. 5.17 and 5.18, resulting in lower NOx emission as the formation rate of NOx is strongly related with the combustion temperature. LIVC has slightly higher temperature compared with EIVC due to the back flow into the intake manifold. LIVC delayed the IVC timing allowing part of trapped air flow back into the intake manifold. This back flow is relatively hot compared with fresh air due to hot residual gases included from last combustion event and heat absorption from the cylinder wall. The phenomenon results in relatively higher charged air temperature with LIVC compared with EIVC, which is less efficient in NOx reduction.

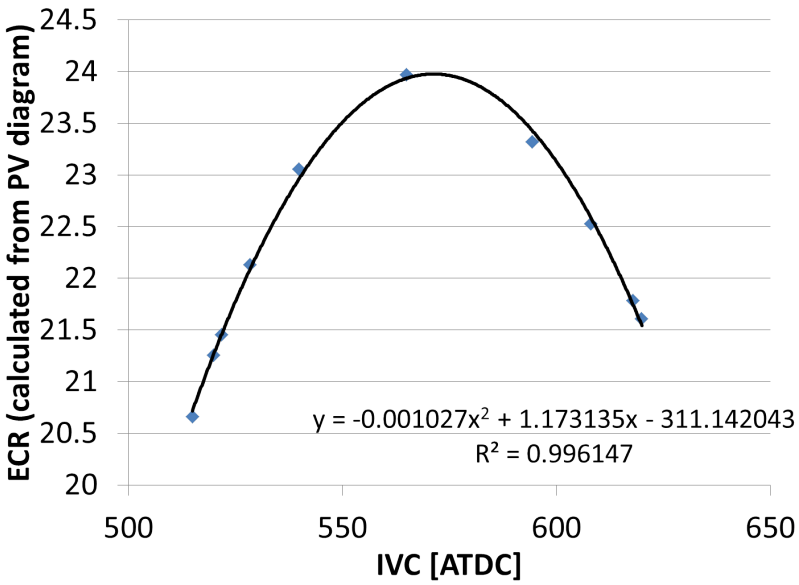

Figure 5.16. Effective compression ratio of variable IVC timing (GCR = 23).

5.2 EIVC at Elevated GCR

As the best scenario for Miller cycling with elevated GCR is EIVC and GCR23, more operating conditions were investigated for better fuel economy including 1600 RPM/250 ft-lbf, 1200 RPM/100 ft-lbf and 2000 RPM/400 ft-lbf.

5.2.1 1600RPM 250ft-lbf

GCR16.9 shows the baseline of BSFC/NOx trade-off at 1600 RPM/250 ft-lbf as shown in Fig. 5.19. It uses EGR as a method to reduce NOx and is able to achieve almost zero emissions. Elevated GCR at 23 decreases the fuel consumption by 1% with either EGR or EIVC. The minimum NOx with EIVC and elevated GCR is close to 2 g/hp-hr, which is not as effective as EGR in NOx reduction perspective. The usage of both EGR and EIVC slightly improves the BSFC/NOx trade-off compared with using single function only.

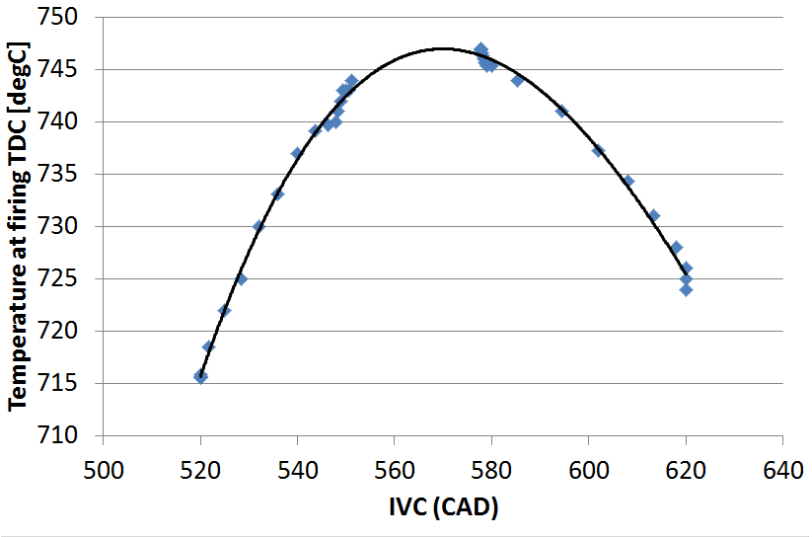

Figure 5.17. Temperature at firing TDC of variable IVC timing (GCR = 23).

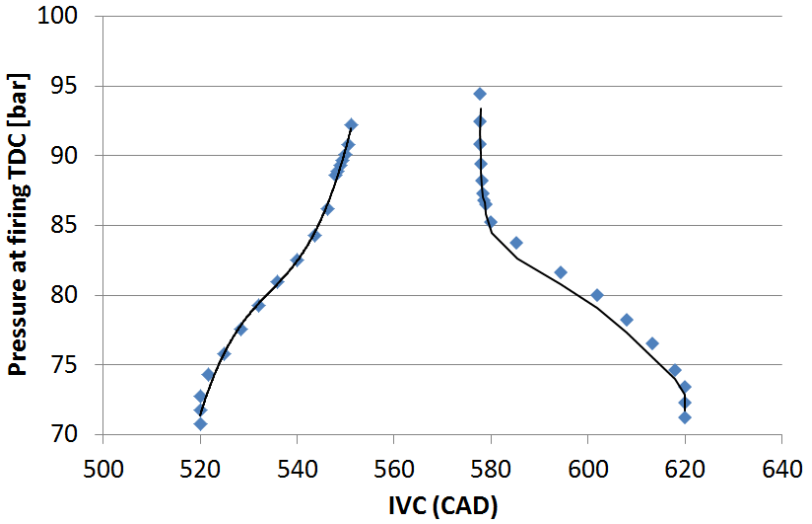

Figure 5.18. Pressure at firing TDC of variable IVC timing (GCR = 23).

Cycle efficiencies are analyzed using four points selected at ~2.5 g/hp-hr BSNOx (per Table 5.2) from four BSFC/NOx trade-off curves (Fig. 5.19). The columns in order shows the "baseline (GCR16.9)", "EGR at GCR 23", "EIVC at GCR23" and "EGR + EIVC at GCR 23". The rows represent the optimized independent variables and results.

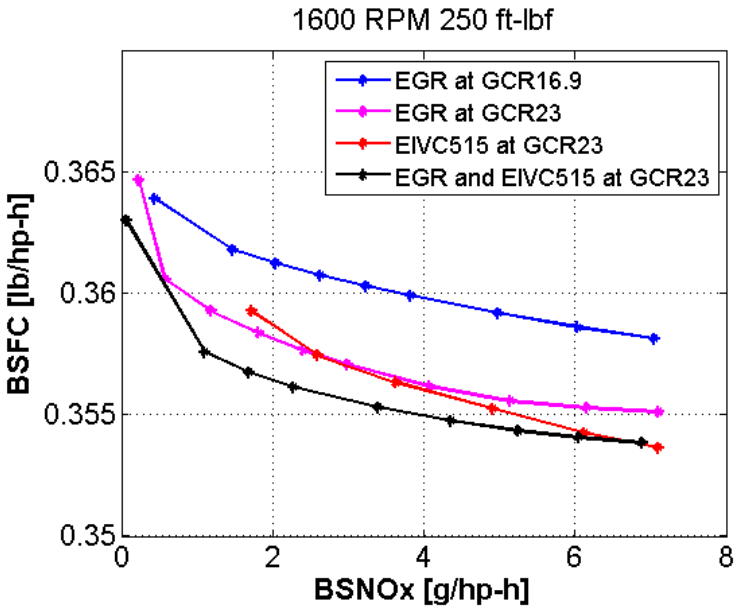

Figure 5.19. 1600 RPM / 250 ft-lbf BSFC vs BSNOx trade-off curve.

Elevated GCR with EGR increases BTE by 0.3% (corresponding to an 1% BSFC decrease). The BTE improvement is mainly from increased closed cycle efficiency. The "EGR at GCR23" case (the second column in Table 5.2) has increased closed cycle efficiency (due to elevated GCR), same open cycle efficiency and decreased mechanical efficiency (due to elevated in-cylinder pressure with GCR23) compared with the baseline (the first column in Table 5.2). Together these changes result in higher BTE and BSFC.

Instead of EGR, EIVC reduces NOx emission resulting in a BTE increase of 0.3% (corresponding to an 1% BSFC decrease), which is very similar as the EGR case at GCR23. EIVC reduces the effective compression lowering peak cylinder pressure and friction losses resulting in higher mechanical efficiency compared with the EGR case. However, lower in-cylinder pressure offsets the benefit of elevated GCR in reduced closed cycle efficiency. The balance between mechanical efficiency and closed cycle efficiency result in the same BTE using EGR or EIVC at elevated GCR(second and third column in Table 5.2).

Table 5.2. Optimization Results at 1600 RPM / 250 ft-lbf.

Parameter	Unit	Parameter Value			
GCR	-	16.9	23	23	23
IVC	CAD	565	565	515	515
EGR	%	18.5	17.2	0	10.0
VGT Closed	%	48.5	43.7	18.2	33.8
Pilot SOI	ATDC	-12.6	-8.7	-11.5	-9.5
Main SOI	ATDC	-2.8	1.1	-1.7	0.3
Post SOI	ATDC	11.5	15.4	12.5	14.6
Rail Pressure	bar	1700	1700	759	1700
BSFC	lb/hp-h	0.361	0.358	0.357	0.356
BSNOx	g/hp-hr	2.6	2.4	2.6	2.3
BTE	%	38.2	38.5	38.5	38.6
Closed Cycle Efficiency	%	48.4	49.3	48.8	49.0
Open Cycle Efficiency	%	96.3	96.3	96.4	96.5
Mechanical Efficiency	%	81.8	81.2	81.8	81.7
Air Fuel Ratio	-	25.8	26.2	25.9	23.1
Charge Flow	g/s	110	108.52	89	88

The combination of EGR and EIVC further improves BTE by 0.1% (fourth column in Table 5.2) at elevated GCR. The open cycle efficiency slightly improved compared with the baseline case due to reduced air flow. The closed cycle and mechanical efficiency is between EIVC and EGR cases. Together these changes result in a small improvement of thermal efficiency.

5.2.2 1200RPM 100ft-lbf

A low load operating condition is selected at 1200 RPM/100 ft-lbf with BSNOx around 8 g/hp-hr for conventional operation. This is a no EGR operating condition with single injection pulse. EIVC at elevated GCR slightly improves the BSFC/NOx trade-off as shown in Fig. 5.20.

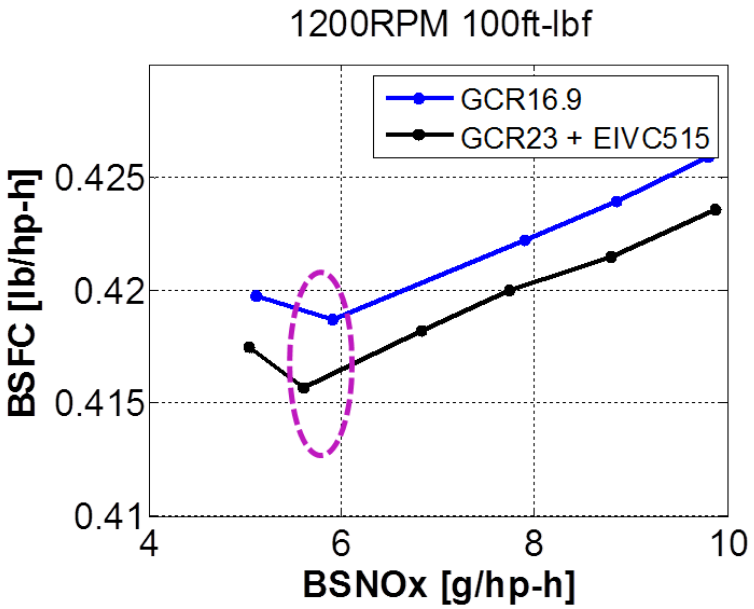

Figure 5.20. 1200 RPM / 100 ft-lbf BSFC vs BSNOx trade-off curve.

Cycle efficiencies are analyzed using two points selected around 6 g/hp-hr BSNOx from Fig. 5.20 as shown in Table 5.3. The columns in order shows the baseline at "GCR16.9" and "EIVC at GCR23". The rows represent the optimized independent variables and results.

EIVC with elevated GCR increases BTE by 0.2% (corresponding to 0.7% decrease of BSFC). Closed cycle efficiency increases with elevated GCR although the start of injection (main SOI) is slightly delayed for NOx reduction besides reduced ECR with EIVC. The open cycle efficiency is very similar between these two cases. Mechanical efficiency slightly reduces with elevated GCR. Together these changes result in little

Table 5.3. Optimization Results at 1200 RPM / 100 ft-lbf.

Parameter Name	Unit	Parameter Value	
GCR	-	16.9	23
IVC	CAD	565	515
EGR	%	0	0
VGT Closed	%	0 (full open)	26.4
Main SOI	ATDC	3.1	4.6
Rail Pressure	bar	1800	1800
BSFC	lb/hp-h	0.419	0.416
BSNOx	g/hp-h	5.9	5.6
BTE	%	32.9	33.1
Closed Cycle Efficiency	%	49.9	50.5
Open Cycle Efficiency	%	95.8	95.9
Mechanical Efficiency	%	68.8	68.3
Air Fuel Ratio	-	62.6	54.6
Charge Flow	g/s	75	65

improvement in BTE and BSFC. In addition the excess oxygen and higher air to fuel ratio lead to relatively higher BSNOx at this low load condition.

5.2.3 2000RPM 400ft-lbf

Another operating condition was selected and investigated at high speed and high load condition (2000 RPM/400 ft-lbf, with EGR usage). Miller cycling with elevated GCR23 improves BSFC at BSNOx below 4 g/hp-hr as shown in Fig. 5.21. The increase of fuel consumption at higher NOx levels is mainly due to decreased turbine and compressor efficiencies. The AFR is relatively lower at high load condition which required squeezed VGT to drive enough air for combustion. The more closed VGT

results in lower turbine and compressor efficiencies. This phenomenon is more obvious at high NOx levels increasing the fuel consumptions.

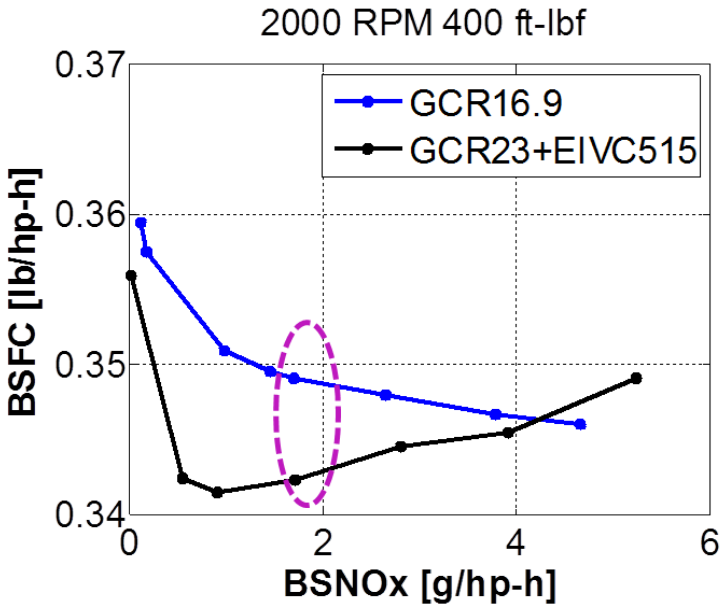

Figure 5.21. 2000 RPM / 400 ft-lbf BSFC vs BSNOx trade-off curve.

Cycle efficiencies are analyzed using selected two cases ~2 g/hp-hr BSNOx as shown in Table 5.4. The columns in order shows the baseline with "GCR16.9" and "EIVC at GCR23". The rows represent the optimized independent variables and results. EIVC with elevated GCR increases BTE by 0.8% (corresponding to a 2% reduction in BSFC). The elevated GCR increases closed cycle efficiency and decreases mechanical efficiency due to higher in-cylinder pressure. The turbo efficiency with EIVC decreases from 52% to 47% as the VGT closed from 37.8 % to 66.6% resulting in lower open cycle efficiency. Together the increased closed cycle efficiency balances the decrease of open cycle and mechanical efficiencies resulting in higher BTE.

In summary, Miller cycling with elevated GCR 23 brings 0.2% - 0.8% BTE benefit (corresponding to a 0.7% - 2% decrease in BSFC) at three operating conditions without increasing NOx emission. Miller cycling with elevated GCR 23 outperforms

Table 5.4. Optimization Results at 2000 RPM / 400 ft-lbf.

Parameter Name	Unit	Parameter Value	
GCR	-	16.9	23
IVC	CAD	565	515
EGR	%	16.7	13.7
VGT Closed	%	37.8	66.6
Pilot SOI	ATDC	-12.6	-12.6
Main SOI	ATDC	-7.0	-4.4
Post SOI	ATDC	19.3	19.3
Rail Pressure	bar	1702	1800
BSFC	lb/hp-h	0.349	0.341
BSNOx	g/hp-h	2.0	1.9
BTE	%	39.5	40.3
Closed Cycle Efficiency	%	48.1	50
Open Cycle Efficiency	%	96.0	95.2
Mechanical Efficiency	%	85.5	84.7
Air Fuel Ratio	-	21.0	20.9
Turbo Efficiency	%	52	47
Charge Flow	g/s	169	158

conventional operation at no-EGR conditions. As a BSNOx reducer, Miller cycling is approximately equivalent to EGR in BSFC/NOx trade-off.

5.3 Rated Point Analysis with Elevated GCR

Elevated GCR improves fuel economy and BTE without increasing NOx emissions, however, the challenge of operating at maximum power conditions is critical. The

rated condition (maximum 360 horsepower at 2400 RPM and 788 ft-lbf) was analyzed with elevated GCR enabled by Miller cycling.

5.3.1 Elevated GCR at Rated Condition

A design of experiment was performed at GCR23 with independent variables (including EGR, VGT closed%, SOI and rail pressure) varying in a wide range to find the possible solution satisfying the physical constraints (Miller cycling not involved). The physical constraints of current engine are shown in Table 2.2. Peak cylinder pressure (PCP) and turbine inlet temperature (TIT) are the key constraints preventing the engine running at higher speed, torque and GCR. Figure 5.22 shows the DOE results with elevated GCR and PCP is above 2500 psi for all the cases. It indicates that current engine setup is not feasible to run at GCR23 and rated condition. It is not a surprising conclusion as the engine is designed for GCR close to 17.

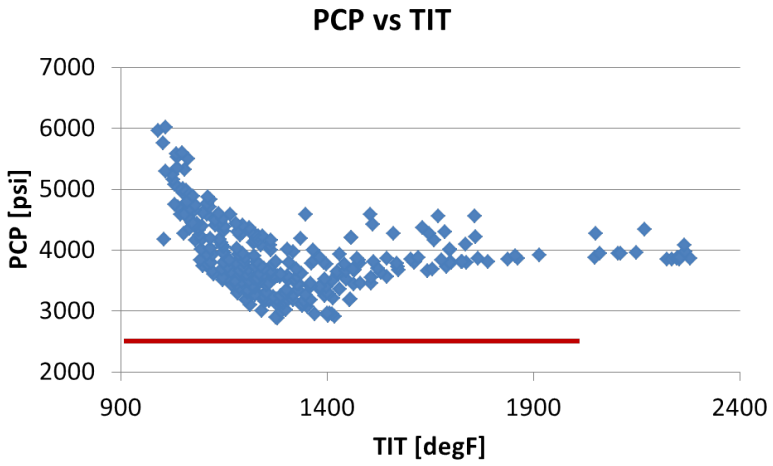

Figure 5.22. 2400 RPM / 788 ft-lbf PCP limit at GCR = 23.

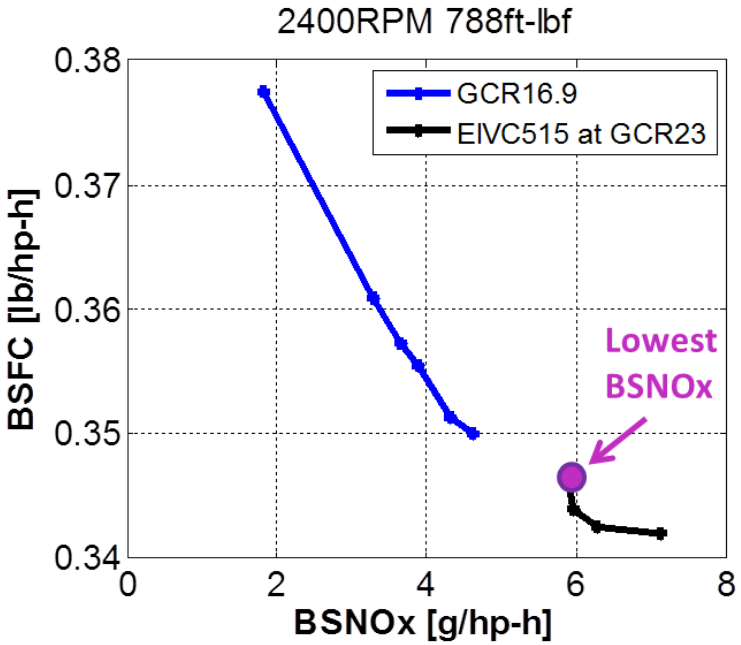

Figure 5.23. 2400 RPM / 788 ft-lbf BSFC vs BSNOx trade-off curve.

5.3.2 Miller Cycling with Elevated GCR

Miller cycling is used to enable rated engine operation with a GCR of 23. EIVC with elevated GCR achieves 6 g/hp-hr BSNOx with little fuel economy benefit as shown in Fig. 5.23. Two cases with similar BSFC are selected for detailed analysis as shown in Table 5.5.

The first column in Table 5.5 shows the baseline result with GCR16.9 and the second column corresponds to EIVC with elevated GCR. Both of these cases satisfy all the physical constraints. EIVC reduces NOx via lower ECR 18.6 (reduced from 24) which is still higher than the baseline. It results in relatively higher NOx emission at 5.9 g/hp-hr. Further advancing IVC could reduce NOx emission but it cannot satisfy TIT constraint (will be discussed in the next section). EIVC with EGR has also been tested at elevated GCR as previous results revealed that EGR is more effective in reducing NOx. However this strategy breaks one or more engine constraints due to an AFR close to stoichiometric.

Table 5.5. Results at 2400 RPM / 788 ft-lbf.

Parameter Name	Unit	Nominal	Elevated GCR
GCR	-	16.9	23
IVC	CAD	565	515
ECR	-	17.6	18.6
EGR	%	14.8	0
VGT Closed	%	20	40
Main SOI	ATDC	-10	-3.0
Post SOI	ATDC	31.8	38.8
Rail Pressure	bar	1800	1800
BSFC	lb/hp-h	0.350	0.346
BSNOx	g/hp-hr	4.6	5.9
BTE	%	39.3	39.7
Closed Cycle Efficiency	%	46.2	46.6
Open Cycle Efficiency	%	94.6	94.8
Mechanical Efficiency	%	90.0	90.0
Air Fuel Ratio	-	19.0	20.6
Charge Flow	g/s	346	322
Peak Cylinder Pressure (PCP)	psi	2469	2495
Turbine Inlet Temperature (TIT)	°F	1321	1337
Turbine Inlet Pressure	psi	40.2	47
Maximum Turbine Speed	kRPM	108	117
Compressor Outlet Temperature	°F	375	424

Closed cycle efficiency increases with elevated GCR as well as open cycle efficiency as shown in Table 5.5. The increase of open cycle efficiency is due to reduced charge flow with lower ECR. Mechanical efficiency is the same because EIVC decreases in-cylinder pressure results in same PCP right below 2500 psi as the baseline. In general

the engine is enabled to run without violating PCP and TIT limits and the BTE is improved by 0.4 % corresponding to a 1% decrease of BSFC.

5.3.3 PCP and TIT Limits

The optimized solutions of EIVC with elevated GCR are limited to high NOx due to PCP and TIT constraints. Two actuator sweeps (VGT and fuel injection timing (SOI) sweep) were performed to assist the analysis. A VGT sweep is performed with rail pressure maximized at 1800 bar and SOI fixed at -3 ATDC. The dot in Fig. 5.24 and Fig. 5.25 corresponds to the lowest BSNOx case with EIVC at GCR23 in Fig. 5.23.

PCP (Fig. 5.24) is 2495 psi right below 2500 psi limit (per Table 2.2). PCP increases with closing the VGT driving more air into the cylinders. Contrarily PCP decreases as VGT is less squeezed reducing the air flow. It results in lower AFR (Fig. 5.25) closer to stoichiometric condition for diesel fuel combustion. Lower AFR increases the combustion temperature resulting in higher TIT exceeding the physical constraint. Generally AFR below 20 could result in TIT higher than 1350 °F at rated condition. Above all, VGT closed% is constrained between 35% to 40% to keep both PCP and TIT within the limits.

The results of another sweep indicate that SOI is limited between -4 ATDC and -3 ATDC to keep PCP and TIT under physical constraint as shown in Fig. 5.26 and Fig. 5.27. Rail pressure is fixed at 1800 bar and VGT is 40% closed in this SOI sweep. The dot corresponds to the lowest achievable BSNOx using EIVC at elevated GCR (per Fig. 5.23). TIT is 1337 psi right below 1350 °F as shown in Fig. 5.26. TIT increases with delayed SOI as more fuel energy is left in the exhaust gases. Advancing SOI closer to TDC reduces TIT as more piston work generated per fuel energy. However heat release towards TDC (aggressive combustion) increases in-cylinder pressure and peak pressure as shown in Fig. 5.27. The constraints of PCP and TIT limit SOI between -4 ATDC and -3 ATDC at rated condition with EIVC and elevated GCR.

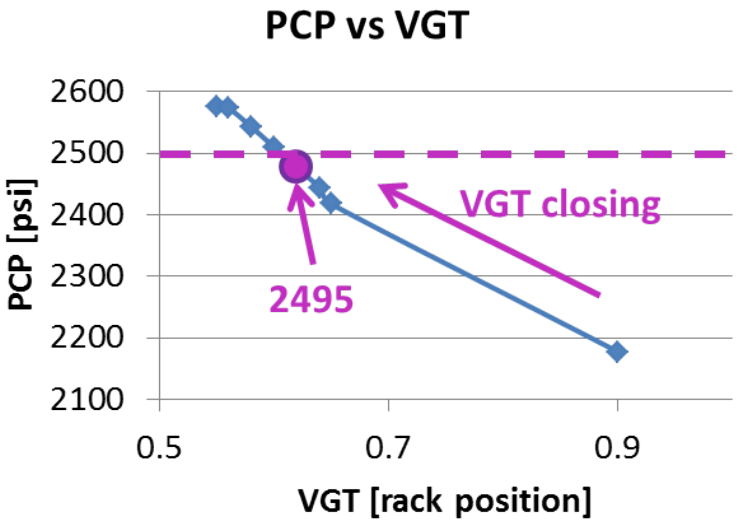

Figure 5.24. 2400 RPM / 788 ft-lbf VGT sweep in EIVC with GCR = 23.

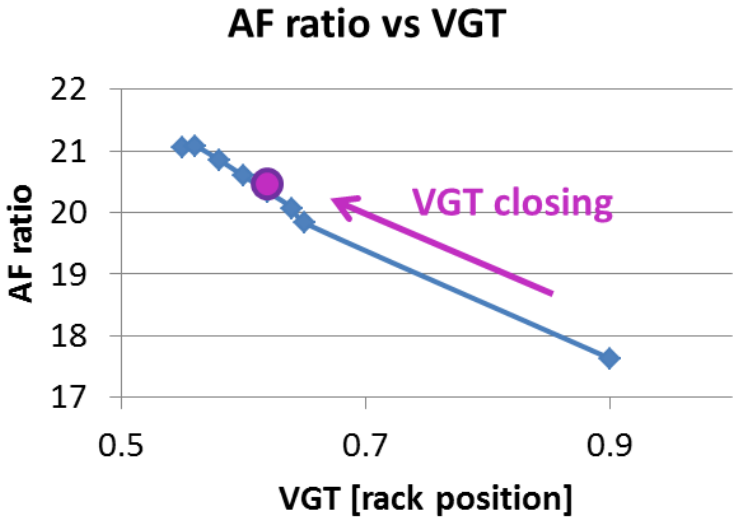

Figure 5.25. 2400 RPM / 788 ft-lbf AF ratio vs VGT.

The sweep of engine actuators demonstrate the limited solution using EIVC with elevated GCR at rated condition due to physical constraints.

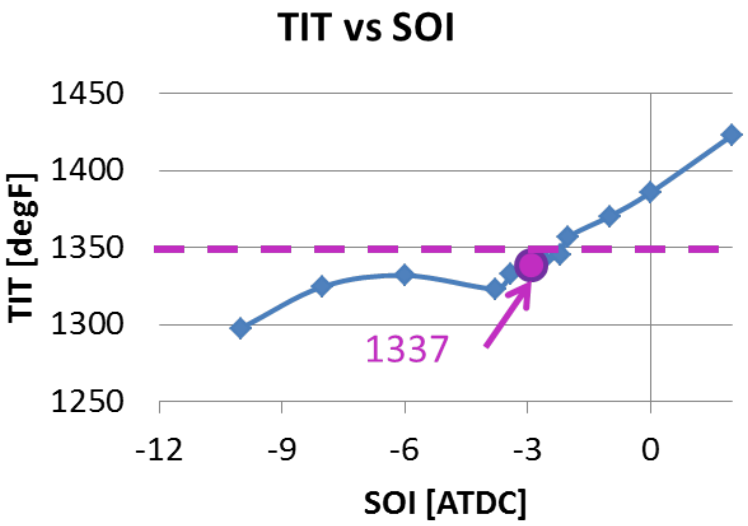

Figure 5.26. 2400 RPM / 788 ft-lbf TIT vs SOI.

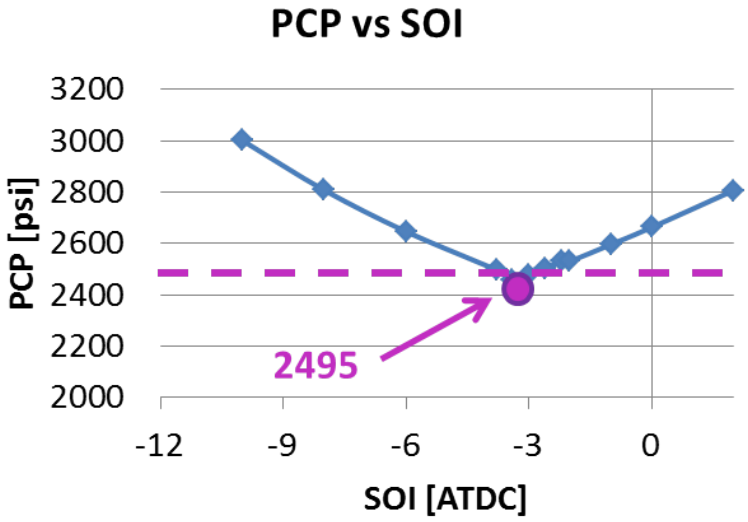

Figure 5.27. 2400 RPM / 788 ft-lbf SOI sweep in EIVC with GCR = 23.

5.3.4 Variable IVC

IVC timing is also limited around 515 CAD to keep engine running without violating the physical constraints. Fig. 5.28 demonstrates optimized results with EIVC

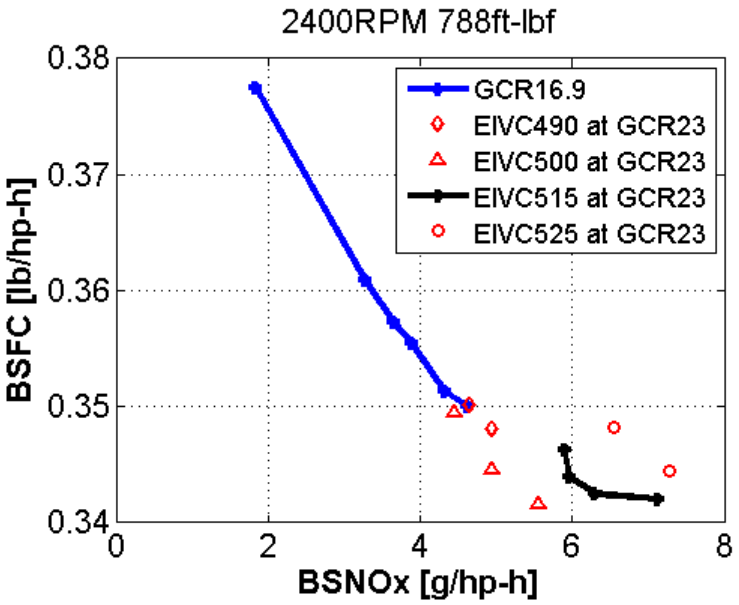

Figure 5.28. 2400 RPM / 788 ft-lbf variable IVC.

varying from 490 to 525 CAD. EIVC 490 CAD and 500 CAD lower PCP with reduced ECR but the compressor outlet temperature is 524 °F exceeding the physical constraint at 450 °F (Table 2.2). EIVC 490 CAD also violates the turbo speed limit as VGT is overly squeezed to back up the charge flow. Retarded IVC (EIVC 525) was also investigated at elevated GCR (per Fig. 5.28). It does not improve the BSFC/NOx trade-off due to less Miller cycling benefit. It hardly satisfies the physical constraints as ECR is higher resulting in higher NOx emission.

Above all, conventional engine actuators and IVC timing are limited in a small range in order to keep physical constraints not violated. It indicates that elevated GCR at 23 may be aggressive for current engine set-up. The suggestion would be to reduce GCR below 23 a little to ensure the engine constraints not violated while achieving a more reasonable NOx level. If GCR 23 is preferred for higher thermal efficiency, an update of hardware will be needed to relax physical constraints or the rated condition will need to be redefined to a lower power level.

5.4 Summary

This chapter investigated the benefit utilizing Miller cycling at elevated GCR on a modern diesel engine equipped with variable valve actuation system for fuel economy and emission reduction considerations. BSFC vs BSNOx trade-offs were obtained using experiment validated model and constrained optimization at five operating conditions. Miller cycling does not improve efficiency at moderate loads when cooled EGR is available. Miller cycling can allow higher GCR operation at rated condition, enabling GCRs at low-moderate loads for efficiency improvement.

6. SUMMARY

Advanced thermodynamic strategies were investigated to improve fuel economy, emission control and thermal management. The analytical and experimental work focused on unloaded idle, loaded idle and cruise conditions to find the optimal solution with flexible valve-train. Model based analysis explored the possibility and benefit of Miller cycling with elevated geometric compression ratio at five operating conditions.

CDA and valve-train flexibility were investigated to improve thermal management on a diesel engine at unloaded and loaded idle conditions. These results would be useful in the thermal management of aftertreatment system as the efficiencies of DOC, DPF and SCR are heavily temperature dependent and generally require temperatures between 250°C and 450°C to provide required performance. Specifically the lowest exhaust gas temperature required to activate SCR is 200°C to avoid urea deposits. CDA enables a 64°C increase in TOT (to 180°C) with only 3% fuel consumption increase compared with the most efficient no-CDA operation at unloaded idle (800 RPM, 0.26bar BMEP). Valve-train flexibility enables TOT ∼200°C with no fuel economy penalties by combining CDA with intake/exhaust valve based throttling and EIVC. CDA with valve throttling, LIVC and iEGR maximizes TOT up to 260°C. CDA enables TOT to 308°C with 39% lower fuel consumption than that achieved with no-CDA case at loaded idle (800 RPM, 2.5 bar BMEP). This corresponds to an 118°C TOT increase and nearly no fuel penalty compared with the most efficient no-CDA operation. CDA coupled with over-closed VGT and delayed fuel injection maximizes TOT up to 390°C at loaded idle.

Strategies using flexible valve actuation (I-EGR, LIVC and CDA) were investigated to optimize fuel economy (BSFC) and exhaust temperature (TOT) at three NOx levels at cruise condition (1200 RPM, 7.58 bar BMEP). I-EGR, LIVC and CDA bring no benefit in fuel economy over conventional valve profiles as efficiency maxi-

mized at a "highway cruise" condition. Conventional operation increases TOT from 350°C to 450°C with delayed SOI resulting in a 23% increase of fuel consumption. iEGR via re-induction or NVO reduces the fuel consumption by 10% at same TOT due to lower total heat losses and AFR. iEGR via re-induction and NVO will warm-up the catalysts more quickly, and can sustain bed temperatures of ∼450°C, whereas the baseline case will cool down the catalysts when above ∼350°C. LIVC increase TOT up to 550°C with 5% less fuel used compared with conventional valve profiles at 450°C. CDA further maximizes TOT above 550°C with additional 3% fuel used due to lower AFR. LIVC and CDA promote a better heat transfer rate at bed temperature above 150°C for 1.5 g/hp-hr BSNOx compared with the highest heat transfer rate with conventional valve profiles using delayed SOI. Both LIVC and CDA can keep catalyst bed temperature of ∼550°C and LIVC has lower fuel cost.

Miller cycling with elevated geometric compression ratio was investigated for fuel economy and emission reduction using a experimentally validated model. Fuel economy and NOx trade-offs were obtained through optimizations at five operating conditions. Miller cycling reduces piston-motion induced compression which allows advanced combustion to improve thermal efficiency. Elevated GCR generates more power and increases brake thermal efficiency due to longer expansion and higher closed cycle efficiency. Miller cycling enables engine operating at rated condition (maximum power) with elevated GCR although the solutions are still quite limited. It also allows the usage of elevated GCR at low-moderate loads for efficiency improvement. EIVC with GCR of 23 reduces fuel consumption by 0.7%∼5% corresponding to 0.1%∼2% increase of BTE at medium speed and low-moderate load conditions.

REFERENCES

REFERENCES

[1] Mojghan Naseri, Raymond Conway, and Howard Hess et al. Development of Emission Control Systems to Enable High NOx Conversion on Heavy Duty Diesel Engines. Technical report, SAE Technical Paper 2014-01-1525, 2014.

[2] Xianjun Hou, Yi Ma, Fuming Peng, Fuwu Yan and Xianan Zhang. Research on Temperature Characteristics of DPF Regeneration Technology Based on Catalytic Combustion of Fuel Injection. In *Power and Energy Engineering Conference (APPEEC), 2010 Asia-Pacific*, pages 1–4. IEEE, 2010.

[3] Donald Stanton, Stephen Charlton and Phani Vajapeyazula. Diesel Engine Technologies Enabling Powertrain Optimization to meet US Greenhouse Gas Emission. Technical report, SAE Technical Paper 2013-23-0094, 2013.

[4] Jeffrey Seger, Long-Kung Hwang and Josh Shao. System Engineering Approach for the Design of a Low Carbon, Fuel Efficient, Diesel Engine Powertrains for Commercial Vehicles. Technical report, SAE Technical Paper 2011-01-2189, 2011.

[5] Donald W Stanton. Systematic Development of Highly Efficient and Clean Engines to Meet Future Commercial Vehicle Greenhouse Gas Regulations. *Diesel Engine*, 2013:05–16, 2013.

[6] Qianfan (Harry) Xin. Overview of Diesel Engine Applications for Engine System Design-Part 2: General Performance Characteristics. Technical report, SAE Technical Paper 2011-01-2179, 2011.

[7] Harald Fessler and Marco Genova . An electro-hydraulic lost motion VVA system for a 3.0 liter diesel engine. *SAE transactions*, 113(3):1639–1649, 2004.

[8] S. Trajkovic, A. Milosavljevic, P. Tunestal and B. Johansson . FPGA controlled pneumatic variable valve actuation. *SAE Technical Paper 2006-01-0041*, 2006.

[9] Anders Widd, Rolf Johansson and Patrick Borgqvist et al. Investigating Mode Switch from SI to HCCI using Early Intake Valve Closing and Negative Valve Overlap. Technical report, SAE Technical Paper 2011-01-1775, 2011.

[10] Patrick Borgqvist, Per Tunestal and Johansson. Investigation and Comparison of Residual Gas Enhanced HCCI using Trapping (NVO HCCI) or Rebreathing of Residual Gases. Technical report, SAE Technical Paper 2011-01-1772, 2011.

[11] Tobias Joelsson, Rixin Yu and Johan Sjoholm et al. Effects of Negative Valve Overlap on the Auto-ignition Process of Lean Ethanol/Air Mixture in HCCI-Engines. Technical report, SAE Technical Paper 2010-01-2235, 2010.

[12] Gregory M. Shaver, Mathew J. Roelle, J. Christian Gerdes. Modeling cycle-to-cycle dynamics and mode transition of HCCI engines with variable valve actuation. *Control Engineering Practice*, 14:213–222, 2006.

[13] Gregory M. Shaver, J. Christian Gerdes and Mathew J. Roelle et al. Dynamic Modeling of Residual-Affected Homogeneous Charge Compression Ignition Engines with Variable Valve Actuation. *Journal of Dynamic Systems, Measurement, and Control*, 127:374, 2005.

[14] G. M. Shaver, M. J. Roelle and P. A. Caton et al. A physical-based approach to the control of homogeneous charge compression ignition engines with variable valve actuation. *International Journal of Engine Research*, 6:361–375, 2005.

[15] Peter A Dittrich, Frank Peter, Gerd Huber and Michael Kuehn. Thermodynamic Potentials of a Fully Variable Valve Actuation System for Passenger-Car Diesel Engines. *SAE transactions 2010-01-1199*, 2010.

[16] HCCI operation of a passenger car DI diesel engine with an adjustable valve train, author=Helmantel, Arjan and Denbratt, Ingemar. In *Presented at SAE 2006 World Congress, Detroit, MI, USA, April 2006*, 2006.

[17] R. Kitabatake, A. Minato, N. Inukai, and N. Shimazaki . Simultaneous Improvement of Fuel Consumption and Exhaust Emissions on a Multi-Cylinder Camless Engine. *SAE Int. J. Engines 4(1):1225-1234*, 2011.

[18] S. Zhong, G. Jin, M. Wyszynski and H. Xu. Promotive Effect of Diesel Fuel on Gasoline HCCI Engine Operated with Negative Valve Overlap (NVO). *SAE Technical Paper 2006-01-0633*, 2006.

[19] Mark Stabinsky, William Albertson, Jim Tuttle and others. Active fuel management technology: hardware development on a 2007 GM 3.9 L V-6 OHV SI engine. *SAE Technical Paper 2007-01-1292*, 2007.

[20] K. J. Douglas, N. Milovanovic, J. W. G. Turner and D. Blundell. Fuel Economy Improvement Using Combined CAI and Cylinder Deactivation (CDA)-An Initial Study. *SAE Technical Paper 2005-01-0110*, 2005.

[21] Kevin Dean Edwards, Robert M Wagner and Thomas E Briggs . Investigating potential light-duty efficiency improvements through simulation of turbocompounding and waste-heat recovery systems. Technical report, Oak Ridge National Laboratory (ORNL); National Transportation Research Center, 2010.

[22] Michael Ralph Foster, Matthew G Foster and Kenneth S Price . Engine cylinder deactivation to improve the performance of exhaust emission control systems, 2005. US Patent 6,904,752.

[23] Chih Wu, Paul V. Puzinauskas, Jung S Tsai. Performance analysis and optimization of a supercharged Miller cycle otto engine. *Applied Thermal Engineering*, 23:511–521, 2003.

[24] Yaodong Wang Lin Lin, Anthony P. Roskilly et al. An analytic study of applying Miller cycle to reduce NOx emission from petrol engine. *Applied Thermal Engineering*, 27:1779–1789, 2007.

[25] Jiann-Chang Lin and Shuhn-Shyurng Hou. Performance analysis of an air-standard Miller cycle with considerations of heat loss as a percentage of fuel's energy, friction and variable specific heats of working fluid. *International Journal of Thermal Sciences*, 47:182–191, 2008.

[26] Rahim Ebrahimi. Performance analysis of an irreversible Miller cycle with considerations of relative air-fuel ratio and stroke length. *Applied Mathmatical Modelling*, 36:4073–4079, 2012.

[27] Sebastian Gehrke, Dávid Kovács, Peter Eilts, Alexander Rempel and Peter Eckert. Investigation of VVA-Based Exhaust Management Strategies by Means of a HD Single Cylinder Research Engine and Rapid Prototyping Systems. *SAE International Journal of Commercial Vehicles*, 6(1):47–61, 2013.

[28] Y. Murata, J. Kusaka, Y. Daisho et al. Miller- PCCI combustion in an HSDI diesel engine with VVT. *SAE Technical Paper 2008-01-0644*, 2008.

[29] Jiamei Deng and Richard Stobart. BSFC investigation using variable valve timing in a heavy duty diesel engine. *SAE Technical Paper 2009-01-1525*, 2009.

[30] G. B. Parvate-Patil, H. Hong and and B. Gordon. Analysis of variable valve timing events and their effects on single cylinder diesel engine. *SAE transactions*, 113(3):1510–1519, 2004.

[31] William De Ojeda. Effect of variable valve timing on diesel combustion characteristics. Technical report, SAE Technical Paper 2010-01-1124, 2010.

[32] B. Yang and P. Keller. Analysis of Diesel Engine Emissions Reduction by Late Intake Valve Close and VTG Turbocharger Using 1-D Simulation. *SAE Technical Paper 2008-01-2444*, 2008.

[33] A. Munnannur, S. Kong and R. Reitz. Performance Optimization of Diesel Engines with Variable Intake Valve Timing Via Genetic Algorithms. *SAE Technical Paper 2005-01-0374*, 2005.

[34] Y. Murata, J. Kusaka, M. Odaka, Y. Daisho et al. Achievement of Medium Engine Speed and Load Premixed Diesel Combustion with Variable Valve Timing. *SAE Technical Paper 2006-01-0203*, 2006.

[35] W. Su, Y. Lu, W. Yu et al. High Density-Low Temperature Combustion in Diesel Engine Based on Technologies of Variable Boost Pressure and Intake Valve Timing. *SAE Technical Paper 2009-01-1911*, 2009.

[36] Xin He, Russell P Durrett and Zongxuan Sun. Late intake valve closing as an emissions control strategy at tier 2 bin 5 engine-out NOx level. *SAE International Journal of Engines*, 1(1):427–443, 2009.

[37] D. Gurney, J. Mitcalf, M. Warth, S. Schneider et al. Integrated Simulation, Analysis and Testing of a Variable Valve Train for Passenger Car Diesel Engines. *SAE Technical Paper 2012-01-0829*, 2012.

[38] John B Heywood. *Internal combustion engine fundamentals*, volume 930. Mcgraw-hill New York, 1988.

[39] Amjad Shaik, N. Shenbaga Vinayaga Moorthi and R Rudramoorthy. Variable compression ratio engine: a future power plant for automobiles - an overview. *Proceedings of the Institution of Mechanical Engineers, Part D: Journal of Automobile Engineering*, 221:1159–1168, 2007.

[40] A. Parker and J. Scalzo. Exploring the advantages of variable compression ratio in internal combustion engines by using engine performance simulations. In *SAE 2011 World Congress and Exhibition*, page 1. SAE International, 2011.

[41] Alberto Boretti and Joseph Scalzo. Exploring the Advantages of Atkinson Effects in Variable Compression Ratio Turbo GDI Engines. Technical report, SAE Technical Paper 2011-01-0367, 2011.

[42] Frank Stefan Will and Dylan Mayson. Combustion Simulations for a Self Controlling Variable Compression Ratio Connecting Rod. Technical report, SAE Technical Paper 2012-01-1154, 2012.

[43] Yiliang Zhu, Richard Stobart and Jiamei Deng. Analysis of the Impact on Diesel Engine Fuel Economy and Emissions by Variable Compression Ratio Using GT-power Simultation. Technical report, SAE Technical Paper 2010-01-1113, 2010.

[44] Daisuke Akihisa and Sawada Daisaku. Research on improving thermal efficiency through variable super-high expansion ratio cycle. Technical report, SAE Technical Paper 2010-01-0174, 2010.

[45] Federico Millo, Marco Gianoglio Bernardi and Diego Delneri. Computational analysis of internal and external EGR strategies combined with Miller cycle concept for a two stage turbocharged medium speed marine diesel engine. Technical report, SAE Technical Paper 2011-01-1142, 2011.

[46] Erik Doosje, , Frank Willems, Rik Baert and Martin Van Dijk. Experimental study into a hybrid PCCI/CI concept for next-generation heavy-duty diesel engines. *SAE transaction 2012-01-1114*.

[47] Karla Stricker, Lyle Kocher, Ed Koeberlein, Dan Van Alstine and Gregory M Shaver. Estimation of effective compression ratio for engines utilizing flexible intake valve actuation. *Proceedings of the Institution of Mechanical Engineers, Part D: Journal of Automobile Engineering*, 226(8):1001–1015, 2012.

[48] R. Modiyani, L. Kocher, D Van Alstine, E. Koeberlein, K. Stricker, P. Meckl and G. Shaver. Effect of intake valve closure modulation on effective compression ratio and gas exchange in turbocharged multi-cylinder engines utilizing EGR. *International Journal of Engine Research*, 12(6):617–631, 2011.

[49] Lyle Kocher, Ed Koeberlein, D. Van Alstine, Karla Stricker and Greg Shaver. Physically based volumetric efficiency model for diesel engines utilizing variable intake valve actuation. *International Journal of Engine Research*, 13(2):169–184, 2012.

[50] C. Tai, T. Tsao, N. Schrn and M. Levin. Increasing Torque Output from a Turbodiesel with Camless Valvetrain. *SAE Technical Paper 2002-01-1108*, 2002.

[51] Gamma Tech. GT-POWER, User's Manual and Tutorial, GT-SUITE Version 7.2, 2011.

[52] Daniel Van Alstine, Lyle Kocher, Ed Koeberlein, Karla Stricker and Gregory M Shaver. Control-oriented PCCI combustion timing model for a diesel engine utilizing flexible intake valve modulation and high EGR levels. In *American Control Conference (ACC), 2012*, pages 2060–2065. IEEE, 2012.

[53] Frank P Incropera. *Fundamentals of heat and mass transfer*. John Wiley & Sons, 2011.

VITA

VITA

EDUCATION:

Purdue University, West Lafayette, Indiana:

Ph.D. in Mechanical Engineering, December 2014

Beihang University, Beijing, China:

M.S. in Power Machinery and Engineering, March 2011

Beijing University of Technology, Beijing, China:

B.E. in Energy and Thermal Engineering, July 2008

EMPLOYMENT EXPERIENCE:

Purdue University, Herrick Laboratories: Graduate Research Assistant, August 2011 - January 2014.

Purdue University, Mechanical Engineering: Lambert Teaching Fellow, January 2014 - May 2014.